RNA-based therapies for dysferlinopathies

Inaugural-Dissertation
to obtain the academic degree
Doctor rerum naturalium (Dr. rer. nat.)
submitted to the
Department of Biology, Chemistry and Pharmacy
of Freie Universität Berlin
and
in cotutelle to the
Ecole Doctorale 515 "Complexité du vivant"
of Université Pierre et Marie Curie Paris
by

Susanne Philippi

from Wuppertal, Germany

2014

The experimental work presented in this thesis was conducted under the supervision of Luis Garcia, PhD DR1 at the Institute of Myology, 105 Boulevard de l'Hôpital, 75012 Paris, France (15.09.2010 - 30.03.2013) (and for a short period after the relocation of the laboratory at the UFR des sciences de la santé Simone Veil, Université de Versailles Saint-Quentin-en-Yvelines, 2 Avenue de la Source de la Bièvre, 78180 Montigny-le-Bretonneux, France (01.04.2014 - 30.06.2014)),

and under the supervision of Prof. Dr. med. Simone Spuler at the Experimental and Clinical Research Center - a collaboration between the Max Delbrück Center for Molecular Medicine and the Charité, Lindenberger Weg 80, 13125 Berlin, Germany (15.04.2010 - 14.09.2010 and 01.07.2014 - 30.04.2014)

Thesis director Université Pierre et Marie Curie Paris:	Luis Garcia PhD, DR1
Thesis director Freie Universität Berlin:	Prof. Dr. med. Simone Spuler
Representative Université Pierre et Marie Curie Paris:	Denis Furling PhD, DR2
Reviewer Freie Universität Berlin:	Prof. Dr. rer. nat. Florian Heyd
External Reviewer:	Isabelle Marty PhD, DR2
External Reviewer:	François-Jérome Authier MD, PU-PH
Date of defense: 25.09.2014	

To Margareta and Joachim

Contents

CONTENTS

List of Figures

LIST OF FIGURES

1 Preamble

Loss-of-function mutations of the *DYSF* gene result in muscular dystrophies of different disease phenotypes the majority of which manifests as Limb girdle muscular dystrophy 2B and Miyoshi myopathy 1. Unfortunately, gene-replacement therapy is not suitable for the treatment of these diseases as over-expression of *DYSF* has been shown to induce progressive myopathy in the murine animal model. Alternatively, the modification of the *cis*-splicing process of the *DYSF* precursor-mRNA (pre-mRNA) is thought a promising strategy for the *in situ* correction of mutated *DYSF*, as it leaves its transcription regulation unmodified and does not induce over-expression.

In the presented thesis, my goal was to develop two strategies of *DYSF* pre-mRNA *cis*-splicing modification: (i) spliceosome-mediated pre-mRNA *trans*-splicing (SmaRT) by an engineered pre-mRNA *trans*-splicing molecule (PTM) and (ii) antisense oligonucleotide (AON)-induced excision of *DYSF* exon 32 from *DYSF* pre-mRNA. Preliminary to the establishment of the RNA-therapeutic approaches, I analysed four cell lines of immortalized myoblasts derived from muscle biopsies of dysferlinopathy patients in respect of their differentiation potential compared to a primary human myoblast cell line and tested their eligibility as a read-out tool of dysferlin protein repair by performing laser-mediated membrane wounding assays on myotubes.

To induce SmaRT, the PTM has to bind to intron internal sequence of a chosen target intron preceding the mRNA portion to be replaced in a gene's pre-mRNA to be able to interfere into the *cis*-splicing process by providing strong splicing signals. To design an efficient *DYSF trans*-splicing strategy, I focussed on the determination of a suitable target intron in the *DYSF* pre-mRNA. In an initial screening, I targeted four different introns that were characterized by disparately strong splicing signals by PTMs in human immortalized dyferlinopathy myoblasts. To localize PTMs at the respective target introns, two different antisense sequences complementary to the target intron sequence to either localize the PTM in close proximity of the intron internal 5'splice site or to mask the intron internal 3'splice site were tested. The *cis*-splicing process of target introns encoding weak splicing signals was more susceptible to manipulation by a PTM then of strongly defined introns. The antisense sequence localizing the PTM in 5'splice site proximity and thus close to the active spliceosomal U1 snRNP during the splicing process most efficiently induced pre-mRNA *trans*-splicing. PTMs which had induced *trans*-splicing in human myoblasts were tested *in vivo*, as the murine counterparts of the human target introns reflected the same qualities regarding their splicing signals. I designed antisense sequences complementary to the murine target introns (mPTMs) and by recombinant adeno-associated virus vectors mPTMs were delivered via intramuscular injection into *tibialis anterior* skeletal muscles in wild-type and *DYSF-/-* mice. The

injection of mPTMs led to moderate levels of dysferlin protein rescue in the *DYSF-/-* mouse model.

The second strategy of RNA-based therapy was AON-induced excision of *DYSF* exon 32. This approach was based on the knowledge that a naturally occurring *DYSF* exon 32-excision led to mild LGMD2B in a patient who was ambulant until high age. To induce excision of *DYSF* exon 32, I applied AONs of the tricyclo-DNA (tcDNA-AON) backbone chemistry. I designed AON sequences masking putative exon internal splice enhancer motifs or the splice site sequences framing the exon. I tested tcDNA-AONs in human immortalized dysferlin-deficient myoblasts harbouring a STOP mutation in *DYSF* exon 32 next to a *DYSF* null-allele. Two of the exon internally binding AONs induced dysferlin protein rescue in dysferlin-deficient immortalized human myoblasts. TcDNA-AONs complementary to the murine *DYSF* exon 32 sequence were tested in wild-type mice and AONs masking putative exon internal splice enhancer sequences were shown to induce exon 32 excision most efficiently *in vivo* as well.

2 Introduction

2.1 Spliceosome-mediated splicing of precursor-mRNA

2.1.1 Precursor-mRNA *cis*-splicing

In higher eukaryotes the ribonucleic acid (RNA) polymerase II transcribes precursor-messenger RNA (pre-mRNA) from genes encoded by chromosomal deoxyribonucleic acid (DNA). The pre-mRNA comprises non-coding sequences, so-called introns and coding sequences, so-called exons (Crick, 1979), besides other sequence portions encoding post-transcriptional signalling, the most prominent the so-called 5' and 3' untranslated region (UTR) and the polyadenylation-signal (poly(A)-signal) that are involved in providing stability to the mature messenger RNA (mRNA) and in translation initiation and regulation. The pre-mRNA is processed in the nucleus of the cell into the mature mRNA and is subsequently exported to the cytoplasm for translation into the amino acid sequence of a protein. One part of the processing is the excision of introns from between exons within the pre-mRNA molecule, the so-called *cis*-splicing. *Cis*-splicing of an intron is performed by the spliceosome, which assembles from uridine-rich small nuclear ribonucleoproteins (U snRNP) on the intron internal sequence of the pre-mRNA and directs two consecutive transesterification reactions (Padgett et al., 1984) (Fig. 2.1). snRNPs are complexes of small nuclear RNA (snRNA), snRNP-specific Sm-proteins and common proteins (Lerner and Steitz, 1979; Branlant et al., 1982) that interact among themselves, with other proteins and the pre-mRNA by RNA-RNA, RNA-protein and protein-protein interaction. Two spliceosomes have been identified in higher eukaryotes, the
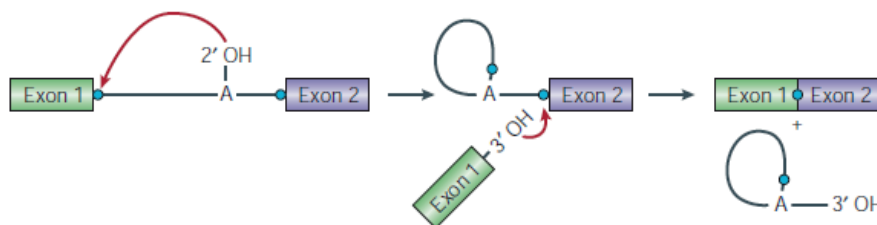
Figure 2.1: Pre-mRNA *cis*-splicing occurs by two consecutive transesterification reactions. The 2'hydroxyl-group exposed from the conserved adenosine of the branch point sequence attacks the phosphodiesterbond between the 5'splice site and upstream exon by the first nucleophilic attack. The disengaged upstream exon attacks the phosphodiesterbond between 3'splice site and downstream exon in the second nucleophilic attack. The two exons are connected and the intron is excised as a lariat structure. Figure from Patel and Steitz (2003).
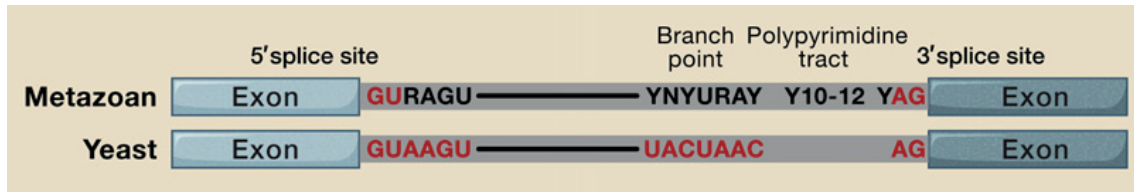
Figure 2.2: Metazoan and yeast conserved 5' and 3'splice sites, branch point sequence and poly-pyrimidine tract sequence composition. Figure from Wahl et al. (2009).
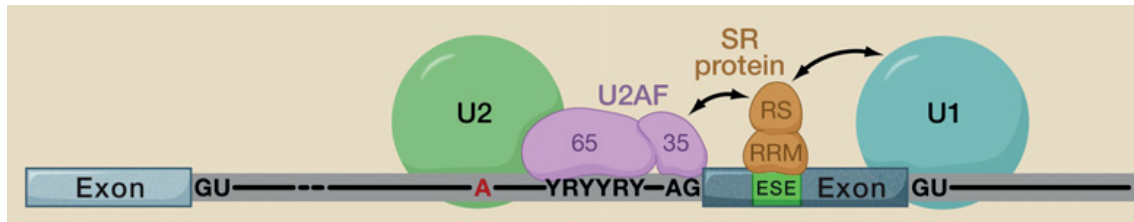
Figure 2.3: Definition of the exon-intron boundary by so-called exon definition, the recognition of the 3' and 5'splice site surrounding an exon by U2AF, U2 snRNP and U1 snRNP within a unit directed by ESE binding splicing factors, for example of the SR-protein family. Firgure from Wahl et al. (2009).

major and the minor spliceosome that both comprise five U snRNPs (reviewed in Tarn and Steitz, 1997). The majority of eukaryotic pre-mRNAs is processed by the major spliceosome comprising the U1, U2, U4, U5 and U6 snRNP. The minor spliceosome, assembled of U11, U12, U4atac, U6atac and U5 snRNP, splices so-called U12-introns (Wahl et al., 2009; Patel and Steitz, 2003). In the here presented work, I focussed on the manipulation of *cis*-splicing of so-called U2-introns spliced by the major spliceosome.

A crucial event during *cis*-splicing is the initial recognition of the intron internal 5' and 3'splice sites by the U1 and U2 snRNPs, respectively (Reed, 1996). The portion of the 5' and 3' splice site that in metazoan U2-introns is truly highly conserved consists of the dinucleotide GT (guanosine, thymidine) at the 5'splice site and the dinucleotide AG (adenosine, guanosine) at the 3'splice site preceded by a pyrimidine, i.e. cytidine or thymidine (in RNA uridine) (Burge et al., 1999) (Fig. 2.2). Upstream of the 3'splice site metazoan introns encode a poly-pyrimidine tract whose length and intron internal position is disparately conserved (Schwartz et al., 2008). Further, the branch point encodes the conserved adenosine surrounded by a less conserved sequence composition (Schwartz et al., 2008). The recognition of the 3' and 5' splice site in metazoan pre-mRNA is further regulated by exon splice enhancers (ESE) and exon splice silencers (ESS), which are conserved sequence motifs within the exon to which splicing factors of the SR-protein (serine/arginine-rich proteins) family and heterogenous nuclear RNPs (hnRNP) bind (Smith and Valcárcel, 2000). This concept, referred to as exon definition, is the primary mode of intron-exon junction recognition in metazoan pre-mRNA, where relatively short exons are generally surrounded by long introns (Berget, 1995) (Fig. 2.3). Apart from exon definition, the concept of intron definition, wherein the intron is initially recognized as a unit within the pre-mRNA, exists. Intron definition takes place on short introns and is the main recognition mode in lower eukaryotes like yeast (Abovich et al., 1994).

For the assembly of the major spliceosome on the intron the U1snRNP, supported by SR-

proteins, recognizes and binds the intron internal 5'splice site (Staknis and Reed, 1994) (Fig. 2.4). The recognition of the 3' splice site region is initiated by the U2 auxiliary factors 35 and 65 (U2AF35 and U2AF65). U2AF35 directly binds the 3'splice site (Wu et al., 1999) and the poly-pyrimidine tract is recognized by the U2AF65 (Zamore et al., 1992). Pre-mRNA-binding of both U2AFs is regulated by SR-proteins (Graveley et al., 2001). Upstream of the poly-pyrimidine tract lies the branch point sequence that encoding the highly conserved adenosine nucleotide and is initially recognized by the splicing factor 1/mammalian branchpoint bridging protein (SF1/mBBP) (Arning et al., 1996; Berglund et al., 1997) which interacts with U2AF65. The SF1/mBBP is replaced by the U2 snRNP that together with other splicing factors leads to the exposition of the 2'hydroxyl-group of the conserved adenosine base. The first transesterification reaction takes place between the adenine 2'hydroxyl-group and the phosphodiesterbond at the 5'splice site of the intron and thereby frees the upstream exon (Padgett et al., 1984). The tri-complex of U4, U5 and U6 snRNPs facilitates the juxtaposition of the two exons. By the second transesterification reaction between the 3'hydroxyl-group of the upstream exon and the phosphodiesterbond of the intronic 3'splice site the two exons are linked together.

2.1.2   Precursor-mRNA *trans*-splicing

Trans-splicing, the process of splicing two exons from separate pre-mRNA molecules together, like *cis*-splicing also occurs endogenously. Two different modes of natural *trans*-splicing can be differentiated, the spliced leader (SL) *trans*-splicing, which involves an SL RNA encoding the 5'exon and 5'splice site and the genic *trans*-splicing, which connects exons of two different pre-mRNAs (Lasda and Blumenthal, 2011).

SL *trans*-splicing is known to occur in nemathodes, trypanosomes and also in primitive chordates and has been mainly investigated in *Trypanosoma brucei* and in *Caenorhabditis elegans* (*c.elegans*), wherein all pre-mRNAs and ~70% of pre-mRNAs, respectively are SL *trans*-spliced (Blumenthal, 2012; Preußer et al., 2012). The SL RNA exists as snRNP representing the paired U1 snRNP and intron 5'splice site during *cis*-splicing (Djikeng et al., 2001). The so-called outron which is the 5' end of an mRNA that comprises no intact 5'splice site serves as the inititation signal for SL *trans*-splicing and is spliced together with the SL (Conrad et al., 1995). The exact function of the SL is not known, but has been postulated to comprise translation initiation as it presents the 5'end of the processed mRNA (Blumenthal, 2012). In general, SL *trans*-splicing provides regulation of gene expression from poly-cystronic pre-mRNAs in providing the intact 5'end for the maturation of the encoded open reading frames (Blumenthal, 2012). Like *cis*-splicing, the SL *trans*-splicing process occurs by the two consecutive transesterification reactions and involves spliceosomal U2, U4 and U6 snRNP (Tschudi and Ullu, 1990), wherein instead of the intron-lariat a Y-shaped intron structure is formed. Expression of *c.elegans* SL RNA in COS cells has led to *trans*-splicing with an artificial 3'acceptor sequence showing that the *trans*-splicing mechanism can be mediated in the mammalian organism (Bruzik and Maniatis, 1992).

Genic *trans*-splicing among artificially expressed mammalian pre-mRNAs has been detected *in vitro*. The efficiency of the process was reported to depend on the degree of complementarity
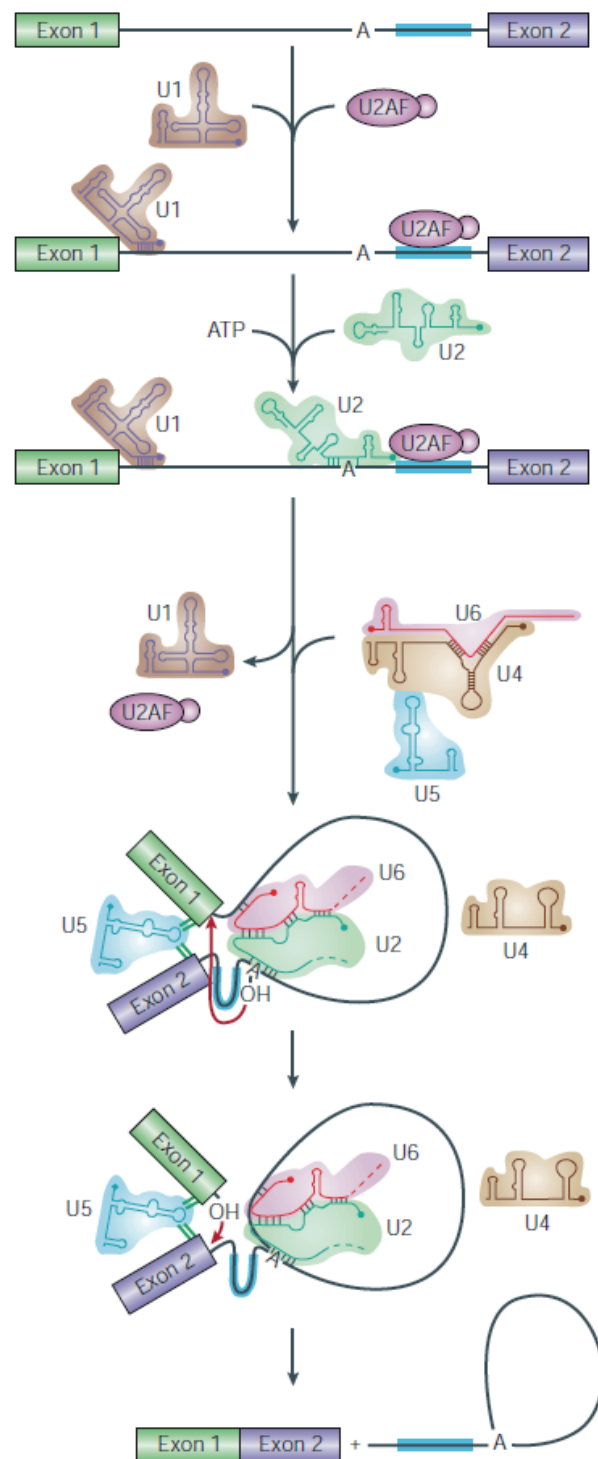
Figure 2.4: Assembly of the spliceosomal U snRNPs of the major spliceosome on the pre-mRNA intron for *cis*-splicing by two consecutive transesterifications. Figure from Patel and Steitz (2003).

between overlapping sequences of the two transcripts (Konarska et al., 1985; Solnick, 1985). Naturally occuring genic *trans*-splicing events among endogenous pre-mRNAs of mammalian genes have been detected on sequence level in several cases (Vellard et al., 1992; Shimizu and Honjo, 1993; Breen and Ashcroft, 1997; Caudevilla et al., 1998), but the *trans*-splicing mechanism for the combination between two separate mammalian pre-mRNA molecules has not been identified.

2.2 Mutation of the dysferlin gene causes muscular dystrophy

2.2.1 The dysferlin gene

The dysferlin (*DYSF*) gene encodes an approximately 7 kilobase (kb) long mRNA and has been mapped to the human chromosome 2p13 (Liu et al., 1998; Bashir et al., 1998). The human and murine *DYSF* (*mDYSF*) genes show sequence similarity above 90% (Vafiadaki et al., 2001). In human tissue, *DYSF* mRNA is ubiquitously expressed, whereas a particularly high abundance was shown in skeletal muscle tissue, next to heart and placenta (Liu et al., 1998; Bashir et al., 1998). In brain compartments putamen, temporal lobe, frontal lobe and occipital lobe a short isoform of approximately 4kb was identified at high expression levels and relatively high expression of the full-length transcript of 7kb was presented in medulla tissue (Bashir et al., 1998). The distinct coding structure of the short isoform present in brain has not yet been described any further. Besides 55 canonical exons encoded by the full-length transcript (Aoki et al., 2001) alternative splicing of four exons, the alternative exon v1, 5a, 17 and 40a, has been described (Pramono et al., 2006, 2009). Transcribed by an alternative promotor within the human canonical *DYSF* intron 1, the alternative exon v1 is to 85% homologue to the murine *DYSF* exon 1 and leads to the transcription of human *DYSF-v1* transcript at the size of ~7kb. *DYSF-v1* encodes a protein comprising an alternative version of the dysferlin C2A domain and is suggested to interact calcium-independently with membrane phospholipids in plasma membrane repair, which is distinct from the calcium-dependent interaction assumed for the *DYSF* encoded dysferlin protein (Fuson et al., 2014). Together the four alternative exons were shown to give rise to 14 alternative in frame *DYSF* transcripts. In skeletal muscle approximately 18% of total *DYSF* pre-mRNA is spliced as *DYSF-v1* transcript. The Leiden Muscular Dystrophy pages (http://www.dmd.nl/) currently register two mutations in the promotor region of the alternative exon v1 which both have been reported in four cases. The alternative splicing of the exons 5a, 17 or 40a was detected at rates below 7% in skeletal muscle. Mutations from the alternatively spliced exons 5a and 40a were excluded in a small cohort of dysferlinopathy patients (Krahn et al., 2010a). Pramono et al. (2009) further showed that in human blood ~11% of *DYSF* pre-mRNA is spliced as *DYSF-v1* transcript, whereas *DYSF* transcript lacking exon 17 was present at ~44% and *DYSF* including both exon 5a and 40a was present at ~18% of total *DYSF* in blood, suggesting a more important role for alternative *DYSF* transcripts apart from *DYSF-v1* outside of skeletal muscle.
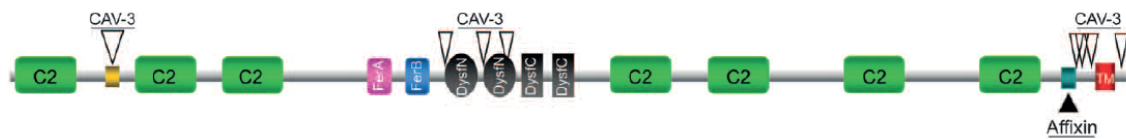
Figure 2.5: Dysferlin, a member of the ferlin protein family comprises seven tandem C2 domains and a transmembrane domain (TM), which both are the characteristic features of ferlins (N-terminus is left, C-terminus right). Interaction sites with Caveolin3 (CAV-3) and Affixin have been identified. FerA, FerB and Dysf domains are yet of unknown function. Figure from Glover and Brown (2007).

2.2.2 Structure and localization of the dysferlin protein

The dysferlin protein encoded by canonical *DYSF* and *mDYSF* transcripts comprises 237kDa. Dysfelin has been shown to be ubiquitiously expressed in rodents with particularly high expression in skeletal muscle, heart and kidney (Anderson et al., 1999). In human tissue, dysferlin is expressed in skeletal muscle, heart and particularly strong in placenta (Anderson et al., 1999; Vandré et al., 2007). The short mRNA transcript detected in brain compartments is not translated (Anderson et al., 1999). In human and rodent skeletal muscle, dysferlin localizes to the plasma membrane of myofibres, the so-called sarcolemma (Anderson et al., 1999; Bansal et al., 2003) and to the t-tubule system (Ampong et al., 2005; Klinge et al., 2010), the deep invagination of the sarcolemma into the muscle cell that mediates its depolarization. Dysferlin was as well reported to be expressed in muscle stem cells (De Luna et al., 2004), also referred to as satellite cells, and in peripheral blood monocytes (Ho et al., 2002). In determined muscle precursor cells, the myoblasts, dysferlin expression is reported to be very weak or absent, whereas the protein is robustly expressed in cultured differentiated multi-nucleated muscle cells, so-called myotubes, wherein it localizes to the plasma membrane, the t-tubuli system and to intracellular membrane compartments (Doherty et al., 2005; Klinge et al., 2007). Dysferlin comprises seven tandem C2 domains and a c-terminal transmembrane domain (Fig. 2.5), the two characteristic features of members of the ferlin protein family (Therrien et al., 2006). Besides the C2 domains DysF, FerI, FerA and FerB domains were identified, that are disparately present in ferlins and are yet of unknown function (Lek et al., 2010). In human, six ferlins are known to be expressed, wherein only dysferlin, myoferlin and otoferlin have been investigated further. Apart from dysferlin, a human disease phenotype has only been attributed to otoferlin (Yasunaga et al., 1999), which has been shown to be indispensable for exocytosis at the auditory ribbon synapse (Roux et al., 2006).

C2 domains were investigated deeply in synaptotagmins where they are known to mediate calcium-dependent and -independent interaction with membrane phospholipids and other proteins involved in membrane fusion events (reviewed in Südhof and Rizo, 1996). The C2 domains of the dysferlin protein were investigated for their calcium-sensitivity and their capability to interact with membrane phospholipids revealing that the n-terminal C2A domain interacts with membrane phospholipids and phosphatidylinositides in a calcium-dependent manner *in vitro* (Davis et al., 2002). The C2A domain has recently been investigated further in direct comparison with its alternative C2Av1 domain translated from the alternatively spliced exon v1 of the *DYSFv1* isoform.

In contrast to C2A, C2Av1 most likely interacts with phospholipids calcium-independently (Fuson et al., 2014). Both full-lengths protein isoforms locate predominantly to the plasma membrane and have been hypothesized to act in membrane fusion processes via their ability for highly flexible conformational changes. The six remaining dysferlin C2 domains interact weakly with phosphatidylserine, some of them calcium-independently and not at all with phosphatidylinositides. They have further been characterized by investigating the localisation of dysferlin proteins lacking differential combinations of 6 of the 7 C2 domains (Klinge et al., 2007). Location to the t-tubule system in myotubes was abrogated by lack of either the three or four most n-terminally (C2A, B, C and D) or the three or four most c-terminally located C2 domains (C2D, E, F and G) together with the transmembrane domain. The result due to the lack of the n-terminal C2 domains is especially noteworthy, since a mini-dysferlin protein carrying the two c-terminal C2F and G domains and the transmembrane domain only, has been shown to rescue membrane repair in otherwise dysferlin-deficient myofibres (Krahn et al., 2010b). The capability to interact with membrane phospholipids via its C2A domain was as well shown for myoferlin, a dysferlin homologue with 74% amino acid sequence similarity as well expressed in skeletal muscle (Davis et al., 2002; Doherty et al., 2005). Myoferlin overexpression rescues the membrane repair defect in dysferlin-deficient myofibres (Lostal et al., 2012).

2.2.3 Dysferlin is implictated in plasma membrane repair and in the innate immune response

Due to the finding that laser-mediated membrane wounding in myofibres of dysferlin-deficient mice (*DYSF-/-*) leads to disrupted sarcolemma repair, dysferlin is known to be required for the functional membrane repair mechanism (Bansal et al., 2003) (Fig.2.6). This finding has been verified in a second dysferlin-deficient mouse model as well displaying late-onset progressive skeletal muscular dystrophy as manifests mainly in dysferlinopathies (Krahn et al., 2010b; Lostal et al., 2010). A subsarcolemmal accumulation of large vacuoles was detected at the site of membrane injury in *DYSF-/-* mice (Bansal et al., 2003) and at the site of membrane leasions in human muscle fibres (Selcen et al., 2001). Based on the finding that the first identified ferlin, the *c. elegans* homolog *fer-1* is essential for the fusion of large membranous organelles with the spermatid plasma membrane during spermatogenesis (Achanzar and Ward, 1997), dysferlin was assumed to mediate calcium-activated membrane vesicle fusion during plasma membrane repair. The calcium-activated formation of a patch formed from intracellular membrane vesicles subsequently recruited to the sarcolemma injury site was postulated as a general cellular response to plasma membrane injury (McNeil and Steinhardt, 2003), after intracellular membrane had been shown to be essential for the rapid calcium-dependent resealing of membrane injuries in sea urchin eggs, fibroblasts and neurons (McNeil et al., 2003) (Fig. 2.7).

Several interaction partners of dysferlin protein have been identified and hypothesized to co-act with dysferlin in sarcolemma repair. Dysferlin was shown to interact with the membrane lipid-binding proteins Annexin A1 and A2, and Annexin A1 is, like dysferlin, detected at the site of membrane injury (Lennon et al., 2003; Marg et al., 2012). The protein Annexin A1 is as well
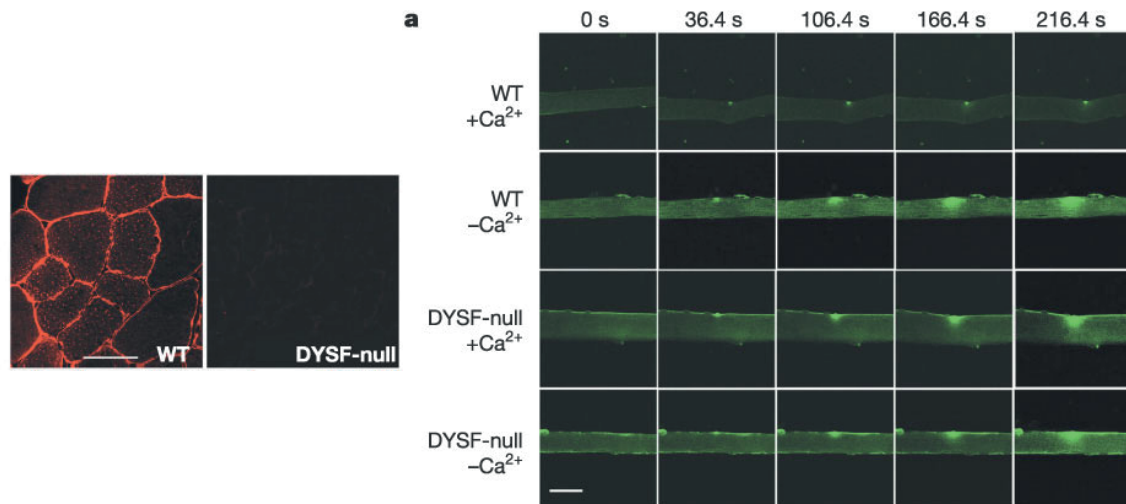
Figure 2.6: Sarcolemma repair is defect in dysferlin-deficient muscle fibres from the *DYSF-/-* mouse model. No dysferlin has been detected at the membranes of muscle fibres as depicted in the transversal section of *DYSF-/- tibiales anterior* skeletal muscle. Laser-mediated membrane wounding has been shown to lead to influx of the fluorescent F1-43 dye into dysferlin-deficient muscle fibres from the *DYSF-/-* model (DYSF-null) due to defect sarcolemma resealing, which occurs in wild-type muscle fibres after wounding (WT) leading to no influx of the fluorescent dye. The process is calcium-dependent. Figures fromBansal et al. (2003).

known to bind membrane phospholipids due to calcium-dependent activation (McNeil et al., 2006) and Annexin A2 was shown to be involved in cellular exocytosis of large membraneous vesicles (Lorusso et al., 2006). In the zebrafish model, dysferlin knock-out also causes myopathy and dysferlin recruites Annexin A1 and A2 homologs to the site of muscle membrane injury (Roostalu and Strähle, 2012). Another interaction partner of dysferlin is the muscle-specific tripartite motif family protein (TRIM72) Mitsugumin53 (MG53) (Cai et al., 2009a; Matsuda et al., 2012). MG53-deficient mice as well display defect sarcolemma repair (Cai et al., 2009a). Vesicles comprising MG53 were recruited to membrane injury sites in response to celullar calcium-influx. MG53 was shown to interact with caveolin3, next to dysferlin and was thus hypothesized to orchestrate the repair machinery at the injury site (Cai et al., 2009b). Caveolin3 which is the prinicipal component of functional membrane invaginations in the sarcolemma, so-called caveolae and a regulator of sarcolemma integrity (Gazzerro et al., 2010) as well interacts with dysferlin (Matsuda et al., 2001). It plays a role in the intracellular localisation of dysferlin (Hernández-Deviez et al., 2006) and was as well hypothezised to be involved in membrane repair (Cai et al., 2009b). Caveolin3 was recently shown not to locate directly at membrane injury sites (Marg et al., 2012; Lek et al., 2013).

Besides investigation in muscle cells, dysferlins role in membrane repair has been investigated in sea urchin embryos. The sea urchin dysferlin homologue acts calcium-triggered as well and mediates an intercellular signal among neighbouring embryonic cells that is assumed to lead to ATP-release due to membrane injury (Covian-Nares et al., 2010). In human myofibres, the ATPase EDH2 (Eps15 homology (EH)-domain-containing protein 2) has been shown to translocate to the site of injury long after the induction of the injury (Marg et al., 2012). Even though many interaction partners of dysferlin are determined and have been implicated in intracellular membrane
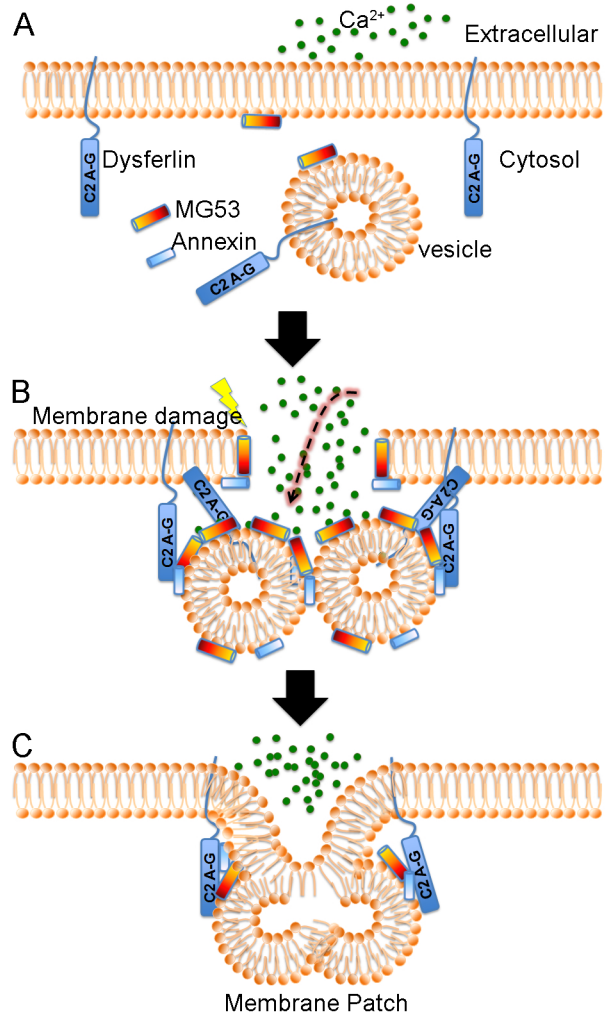
Figure 2.7: Dysferlin is assumed to particicpate in calcium-activated plasma membrane repair by a patch of intracellular vesicles forming to seal the injury site together with MG53 and Annexin. Figure from Han (2011).

vesicle recruitment and plasma membrane fusion, the precise function of dysferlin together with it interaction partners in these processes has not been defined.

Furthermore, dysferlin has been implicated in the regulation of the innate cell-mediated immune response in skeletal muscle. In dysferlin-deficient human skeletal muscle, membrane complement attack complex deposits were found on nonnecrotic fibres (Spuler and Engel, 1998; Selcen et al., 2001) and CD4- and CD8-positive cells and macrophages were determined highly abundant in endomysial and perivascular infiltrate from dysferlinopathy patients (Gallardo et al., 2001). The downregulation of the complement cascade inhibitor decay-accelerating factor (DAF)/CD55 in human and murine dysferlin-deficient skeletal muscle fibres and the resulting expression of membrane attack complex (MAC) complement component C5b9 on nonnecrotic fibres was reported (Wenzel et al., 2005). *In vitro* the C5b9-expressing nonnecrotic fibres were more susceptible to lysis induced via the complement cascade, which was suggested as the cause of fibre damage in dysferlin-deficient muscle. The implication of dysferlin with the complement cascade was further corroborated by the finding that a double knock-out mouse model of the complement cascade component C3 and the dysferlin protein exhibited attenuation of muscle dystrophy (Han et al., 2010).

In monocytes, cell adhesion during human monocyte differentiation was shown to be impaired at dysferlin-deficiency (De Morrée et al., 2013). The additional detection of increased motility in dysferlin-deficient macrophages in connection with decreased cell adhesion in monocytes was suggested to explain stronger infiltration into the muscle cell (De Morrée et al., 2013). This was assumed before due to the detection of MHC class 1 cell surface receptors in human dysferlin-deficient skeletal muscle and in muscle of the dysferlin-deficient mouse model SJL (Nagaraju et al., 2008). In contrast to these findings, it has been shown that muscle of dysferlin-deficient SJL mice (backcrossed to C57Bl/10) shows an excessively high number of immature fibres following induced injury, indicative of slow regeneration. Further, the neutrophil emission after muscle injury was greatly reduced compared to wild-type mice, which was suggested to cause attenuated monocyte recruitment and delayed switch of macrophages to the repair mode (Chiu et al., 2009).

2.2.4 Dysferlinopathies

Mutations in the *DYSF* gene are reported to cause two major muscular dystrophy (MD) phenotypes, the limb girdle muscular dystrophy type 2B (LGMD2B) (Bashir et al., 1998) and Miyoshi myopathy 1 (MMD1) (Liu et al., 1998). Distal anterior compartment myopathy (DMAT) was attributed to *DYSF* mutations as well (Bashir et al., 1998; Illa et al., 2001). In typical LGMD2B, shoulder and pelvic girdle muscle (Mahjneh et al., 1996) and in MMD1 posterior distal muscle of the lower limb show inflammation and progressive dystrophy resulting in atrophy (Miyoshi et al., 1986). Both disease phenotypes lead to elevated serum creatine kinase (CK) levels, a signature of muscle dystrophy by the release of CK from the damaged muscle cells. The mean onset age ranges between the 2nd to 3rd decade of life, even though deviations have been reported with the latest reported onset being at the age of 73 years (Klinge et al., 2008). In general LGMD2B and MMD1 progress slowly, whereas DMAT is reported to occur by rapid disease progression (Illa et al., 2001).
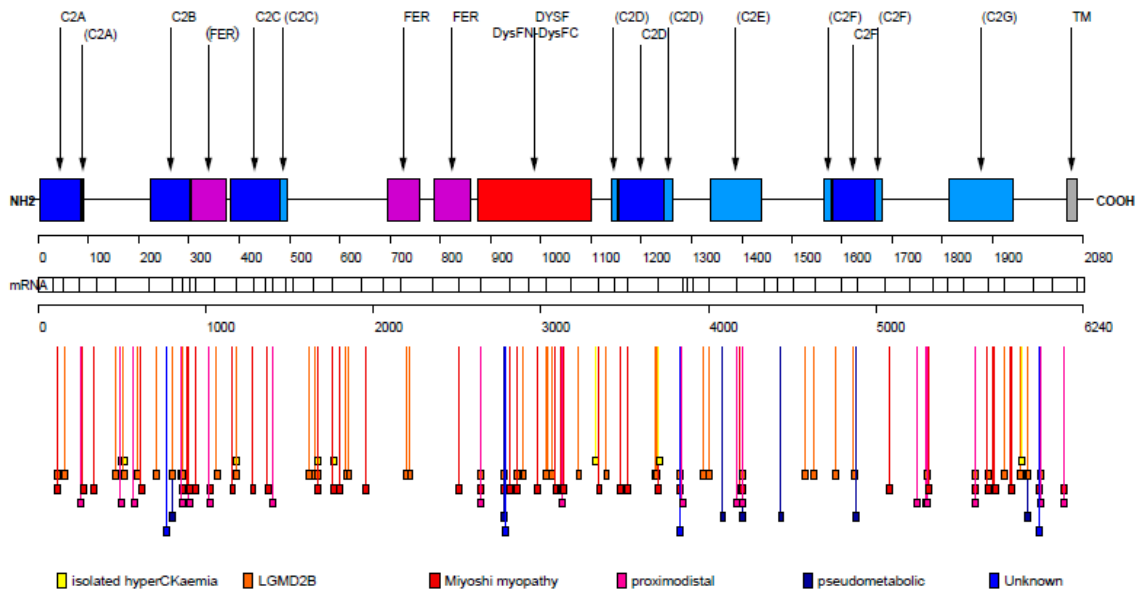
Figure 2.8: Disease-causing mutations in the *DYSF* gene leading to different muscular dystrophy phenotypes are spread over the entire open-reading frame of the gene. Figure from Krahn et al. (2009).

A relation between the age of onset and the severeness of the *DYSF* mutations reflected by the detectable dysferlin protein amount was reported, suggesting earlier disease onset caused by more fiercly reduced dysferlin protein levels (Guglieri et al., 2008a).

Besides the classical clinical phenotypes *DYSF* mutations have been identified in patients that presented painful distal limb swelling with no signs of muscular dystrophy or atrophy that were described as the "pseudometabolic", in patients with disease onset in proximal and distal limb muscle that has been described as "proximodistal" phenotype and in asymptomatic patients that exclusively presented an increased serum CK level, the so-called "isolated hyperCKemia" (Nguyen et al., 2007; Okahashi et al., 2008).

Additional involvement of the heart next to the described skeletal muscle phenotypes was reported in two cases of LGMD2B in the form of dilated cardiomyopathy (Wenzel et al., 2007) that was also described for one case to occur in connection with diffuse hypokinesia (Kuru et al., 2004).

The analysis of the mutations in European-African dysferlinopathy patient cohorts displayed that sequence variations causing the two major disease phenotypes, LGMD2B or MMD1, as well as the isolated hyperCKemia, proximodistal and pseudometabolic phenotypes, are spread over the entire *DYSF* gene sequence and do not coincide in a "mutational hot spot" (Nguyen et al., 2007; Guglieri et al., 2008a; Krahn et al., 2009) (Fig. 2.8). This was as well found in a study investigating a Japanese cohort of MMD1 diagnosed patients (Takahashi et al., 2003). These studies further highlight that a particular mutation or mutation type can neither be attributed as predominant to the two major disease phenotypes, nor to the observed isolated hyperCKemia, proximodistal or pseudometabolic phenotypes (Nguyen et al., 2007; Krahn et al., 2009). That phenotype-classification of *DYSF* mutations remains impossible is further reflected by the fact that identical mutations have been reported as the cause of both LGMD2B and MMD1 (Weiler et al., 1999; Illarioshkin et al., 2000).

13
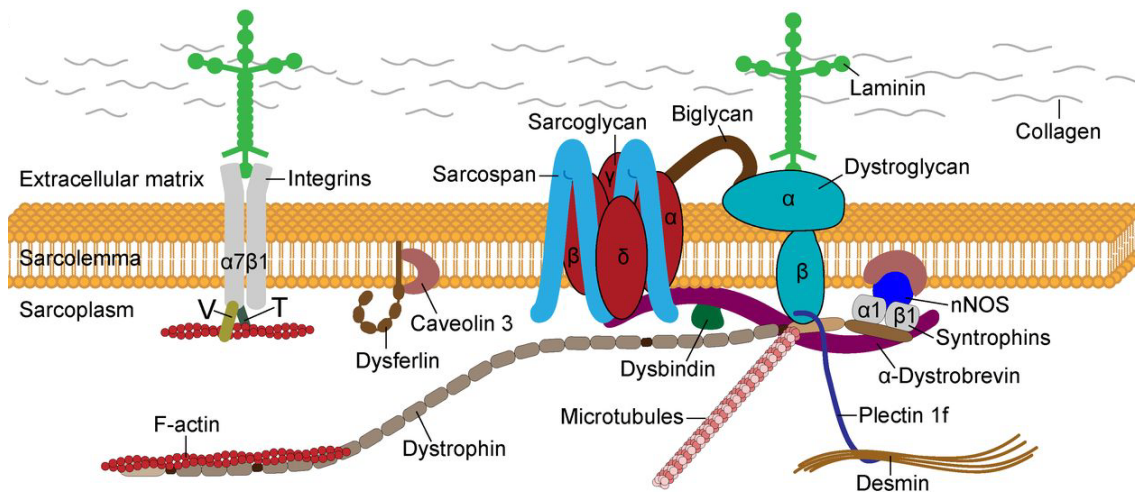
Figure 2.9: Proteins located at the sarcolemma of skeletal muscle which are involved in muscular dystrophies. Dysferlin does not interact witht the dystrophin associated-glycoprotein complex, but is known to interact with Caveolin3. Its seven C2 domains loom into the cytoplasm. Figure from Rahimov and Kunkel (2013).

The two major disease phenotypes LGMD2B and MMD1 fall into the category of orphan diseases, which in Europe are defined by the prevalence of less than 5 affected per 10000 individuals (http://ec.europa.eu/health/rare_diseases/policy/index_en.htm) and in the USA by less than 7.5 affected per 10000 individuals (http://rarediseases.info.nih.gov/gard/browse-by-first-letter/). LGMD2B and MMD1 are reported to the orphanet database with a prevalence of 1-9 per 1 million individuals, whereas DMAT is reported with an estimated prevalence of <1 per 1 million individuals (http://www.or
pha.net/consor/cgi-bin/index.php?lng=EN). In Europe, LGMD2B has been reported more prevalent in southern than in northern European countries (Nguyen et al., 2007; reviewed in Guglieri et al., 2008b). The Jain Foundation, a privately funded non-profit foundation initiated by the Indian-American Jain family has recorded dysferlinopathy cases worldwide with the highest prevalence registered in the USA and India, followed by the People's Republic of China and the United Kingdom of Great Britain (http://www.jain-foundation.org/patient-physician-resources/patient-registration\). The influence of the foundations geographical origin might be reflected by these data.

Dysferlinopathies are MDs that do not affect the transmembrane dystrophin associated-glycoprotein complex (DGC) that is unfunctional in recessive x-chromosome-linked Duchenne muscular dystrophy (DMD) and partly unfunctional in milder Becker muscular dystrophy (BMD) which are with 1-9 cases per 100000 individuals the most prevalent MDs during early childhood caused by mutations in the dystrophin (*DMD*) gene (Koenig et al., 1987; Hoffman et al., 1987). Disruption of the DGC, which in healthy muscle is essential to maintain muscle fibre integrity by connecting the basal lamina with the cytoskeleton of the muscle cell (Petrof et al., 1993), was initially assumed the general cause for MDs (reviewed in Worton, 1995) (Fig. 2.9). Mutation of other components of the DGC, like the sarcoglycans-γ, -α, -β and –δ cause different LGMDs namely the LGMD2C, D, E

and F, respectively. LGMD2I and LGMD2K affect the functionality of the DGC indirectly caused by mutations in genes encoding glycosyltransferases Fukutin-related protein and O-Mannosyl transferase-1. Like LGMD2B they belong to the category of LGMDs of type 2 (LGMD2) that are inherited autosomal recessively besides the group of autosomal dominantly inherited LGMDs of type 1 (LGMD1). The five remaining of the presently 12 appointed LGMD2s, caused by mutation of the genes encoding Calpain3 (LGMD2A), Theletonin (LGMD2G), TRIM32 (LGMD2H), Titin (LGMD2J) and Anoctamin5 (LGMD2L) protein, like dysferlin do not affect the DGC (reviewed in Guglieri et al., 2008b; Bolduc et al., 2010).

Dysferlinopathies were assumed to belong to a group of MDs caused by disrupted preservation of membrane integrity by defect membrane repair next to the group of MDs destabilizing membrane integrity due the defect DGC (Piccolo et al., 2000). The assumption of this new group of MDs was initially reinforced by the finding that plasma membrane repair is as well disrupted in fibroblasts from patients showing LGMD2B- and MMD1-like disease phenotypes due to mutations in the anoctamin5 gene (Jaiswal et al., 2007) that were recently appointed LGMD2L and MMD3 (Bolduc et al., 2010). As recently shown, rescue of membrane repair in murine muscle fibres does not infer the cure of dysferlinopathy as dystrophic features were retained in muscles that show efficient membrane repair capacity (Krahn et al., 2010b; Lostal et al., 2012). The disease symptomes diagnosed due to *DYSF* mutation obviously cannot be attributed exclusively to the deficiency of membrane repair in muscle fibres. The complex heterogeneity of LGMDs is expanded by the fact that genes primarily causing one type of LGMD were shown as secondary mutations in another LGMD. In cases of LGMD2B secondary mutation of the gene encoding Calpain3 that is as well mutated in LGMD2A (Richard et al., 1995) occurs (Guglieri et al., 2008a). Further, mutations in the Caveolin3 encoding gene that lead to LGMD1C (Minetti et al., 1998) have been identified together with *DYSF* mutations and were attributed to aberrant cytoplasmatic localisation of the dysferlin protein (Hernández-Deviez et al., 2006; Lo et al., 2008).

2.2.5 Therapeutic approaches for dysferlinopathies

There is no available cure for dysferlinopathies yet. Only a single therapeutic approach that led to a significant increase in dysferlin protein levels in *in vitro* experiments was tested in a clinical trial in patients carrying a single heterozygous mutation in the DYSF gene. De Luna et al. (2012) have found the dysferlin promoter region to comprise a vitamin D3 response element and have shown that application of the steroid hormone 1-α,25-Dihydroxyvitamin D3 to human dysferlin deficient monocytes and myotubes induces an increase in dyfserlin expression. They further showed that dysferlin upregulation was additionally mediated by activation of the MAPK/ERK pathway. After a one year treatment dysferlin expression was significantly increased in patient monocytes, but did not lead to reversion of elevated serum CK levels or muscle dystrophic signs.

Lostal et al. (2010) have shown the feasibility of full-length dysferlin protein expression from the concatamerized 5' and 3'moiety of the *DYSF* mRNA transcribed from two simoultaneously provided rAAVs. The full-length dysferlin expression was detected at a moderate level and no clinical trial has followed the study yet.
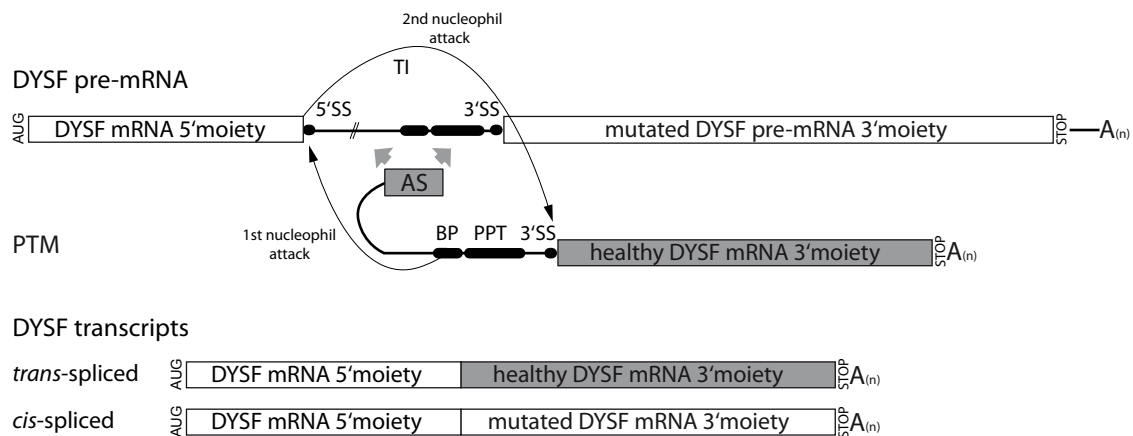
Figure 2.10: Mechanims of therapeutical *trans*-splicing at the example of *DYSF* pre-mRNA by a 3'replacement pre-mRNA *trans*-splicing molecule (PTM). The PTM comprises an antisense sequence (AS) for its localisation to the target intron (TI), and a splicing domain comprising splicing signals: branch point (bp), poly-pyrimidine tract (PPT) and 3'splice site (3'SS). In case of *trans*-splicing, the PTM conducts the first nucleophil attack on the TI 5'SS and in the second nucleophil attack the free upstream exon subsequently interacts with the 3'SS of the PTM splicing domain resulting in the *trans*-spliced *DYSF* transcript.

2.3 RNA-based therapies modifying precursor-mRNA *cis*-splicing

The *cis*-splicing process of the pre-mRNA of a gene is an attractive target for the repair of monogenic mutations encoded by genomic DNA. The transcriptional regulation of the gene, mediated in numerous ways by the respective promoter region to determine its spatio-temporal expression, remains unmodified as it has already occurred when pre-mRNA transcription is initiated. This is crucial for genes whose overexpression, occuring in classic gene therapy by tissue-specific expression of extra-chromosomal complementary DNA (cDNA), is cytotoxic. Further, the repair of dominant negative mutations on the pre-mRNA level can reduce translation of the opposing protein.

2.3.1 Spliceosome-mediated pre-mRNA *trans*-splicing by a pre-mRNA *trans*-splicing molecule

An approach of *cis*-splicing manipulation for the repair of disease-causing mutations identified on various locations in the pre-mRNA of a gene is spliceosome-mediated pre-mRNA *trans*-splicing (SMaRT) by an engineered pre-mRNA *trans*-splicing molecule (PTM) (Puttaraju et al., 1999) (Fig. 2.10). By SMaRT either the 3' or the 5'portion of a pre-mRNA can be replaced by a mutation-free mRNA sequence (Puttaraju et al., 1999; Mansfield et al., 2003). To manipulate the *cis*-splicing process, the PTM is localized to the site of the splicing process by its binding domain, an antisense sequence that is complementary to a region of the so-called target intron (TI), the intron that precedes the pre-mRNA portion to be replaced. Besides the binding domain, the PTM comprises a splicing domain and a coding domain. The coding domain encodes the mRNA sequence replacing the 3' or 5' portion of the pre-mRNA. The splicing domain encodes consensus splicing sequences of the 3'splice site region, the branch point sequence, the poly-pyrimidine

tract and the conserved 3'splice site sequence for a 3'replacing PTM, or the conserved splicing signals of a 5'splice site for a 5'replacement PTM. The aim is to provoke splicing factors and U snRNPs of the spliceosome to assemble on the splicing domain of the PTM instead of the splicing motifs in the target intron of the pre-mRNA. In this case, the two transesterification reactions proceeding during *cis*-splicing will proceed between the pre-mRNA and the PTM (2.10). The 2'hydroxyl-group of the conserved adenosine encoded by the branch point of the PTM will attack the phosphodiesterbond at the 5'splice site of the target intron to free the upstream exon in the targeted pre-mRNA. The 3'hydroxyl-group of the disengaged upstream exon subsequently attacks the phosphodiester bond at the 3'splice site junction with the first exon of the PTM coding domain to connect the 5'portion of the pre-mRNA and the 3'mRNA sequence of the PTM coding domain. thus forming a *trans*-spliced transcript. The disengaged upstream exon can as well interact with the 3'splice site of the pre-mRNA, resulting in a *cis*-spliced mRNA trasncript.

In yet realized 3'mRNA replacement approaches (Puttaraju et al., 1999; Mansfield et al., 2000; Chao et al., 2003; Coady et al., 2007, 2008; Coady and Lorson, 2010; Rodriguez-Martin et al., 2005, 2009; Avale et al., 2013; Lorain et al., 2010, 2013), the focus was laid on the validation of a functional PTM design (Fig. 2.11).The PTM localisation to the target intron by its binding domain has been shown to be essential for the specificity of the *trans*-splicing reaction. PTMs lacking the binding domain were detected to cause unspecific *trans*-splicing reactions that were assumed to be due to interactions of other PTM parts with pre-mRNA (Puttaraju et al., 1999; Kikumori et al., 2001; Rodriguez-Martin et al., 2005). Further, the length of the binding domain has been shown to be determinative for the specificity of the process. Liu et al. (2002) designed PTMs comprising binding domains of more than ~20 nucleotides (nt), at 72 and 134 nt and have no longer detected unspecific *trans*-splicing products. PTM designs in following feasible strategies, where a protein product translated from the *trans*-spliced mRNA transcript was detected, had been adapted to this finding and were performed with binding domains at the length of 125 nt to ~150 nt (Chao et al., 2003; Coady et al., 2007, 2008; Coady and Lorson, 2010; Rodriguez-Martin et al., 2005, 2009; Avale et al., 2013; Lorain et al., 2010, 2013). The sequence motifs in the splicing domain were identical in all these functional PTMs: the poly-pyrimidine tract (ppt) and the dinucleotide AG of the 3'splice site which are recognized by the U2AF65 and U2AF35 splicing auxiliary factors, respectively (Zamore et al., 1992; Wu et al., 1999) and the highly conserved UACUAAC *Saccharomyces cerevisiae* branch point sequence, which recruits SF1/mBBP and U2 snRNP (Parker et al., 1987; Berglund et al., 1997). The branch point sequence, the ppt and the 3'splice site have been tested for their necessity in PTM-mediated *trans*-splicing by omitting them singly and in differential combinations and were all shown to be essential for the process (Fig. 2.11). The spacer sequence which connects the PTM binding domain with the splicing domain was shown to be essential for the PTM to facilitate *trans*-splicing by Puttaraju et al. (1999) and was adopted with a length of 30 nt and the almost identical sequence composition proposed by Mansfield et al. (2000) in subsequently following approaches.

Besides the advantage of manipulating at the pre-mRNA level, in view of the transcriptional regulation of a gene, this technology allows to preserve the full-length transcript and therefore the full-length protein product of a gene. The exclusion of exon or intron internal sequence harbouring

	binding domain (bd)	spacer (sp)	branch point (bp)	poly-pyrimid. tract (ppt)	3'SS	PTM controls /modifications
Puttaraju M, 1999	18nt	30nt	TACTAAC	16nt	CAG	-bd; -sp; -bp, ppt, 3'SS; -ppt, 3'SS safety span
Mansfield SG, 2000	23nt	30nt	TACTAAC	18nt	CAG	safety span
Kikumori T, 2001	18nt	30nt	TACTAAC	14nt	CAG	-bd; -3'SS
Liu X, 2002	72nt 134nt	30nt	TACTAAC	18nt	CAG	–
Chao H, 2003*	125nt	30nt	TACTAAC	17nt	CAG	-3'SS; -bd,sp,bp,ppt,3'SS
Coady T, 2007 2008 & 2010*	~130nt	30nt	TACTAAG	16nt	CAG	–
Rodriguez T, 2005 & 2009; Avale ME 2013*	125nt	30nt	TACTAAC	17nt	CAG	-bd -bd, sp, ppt, 3'SS
Lorain S, 2013*	150nt	30nt	TACTAAC	20nt	CAG	-sp, bp, ppt, 3'SS

Figure 2.11: Design of PTMs that induced efficient *trans*-splicing in previous studies. Length of spacer sequence (sp) and poly-pyrimidine tract (ppt) and composition of branch point (bp) and 3'splice site (3'SS) are depicted. Differential domains or combinations of domains have been excluded in PTM controls to test their necessity for the process. PTMs comprising a so-called safety span, a partly complementary sequence protecting the splicing domain of spliceosome assembly prior its localisation, have been designed, but led to less inefficient *trans*-splicing. Studies marked with * showed the protein product of the *trans*-spliced transcript.

disease-causing variants by AON-mediated *cis*-splicing modification presumes that the respective portion or domain encoded by the suspended coding sequence is dispensable for the function of the encoded protein. This is not determined for mutation-harbouring domains of most proteins that are involved in monogenic diseases. Furthermore, SmaRT allows the repair of genes encoded by large open-reading frames by replacing portions of them, as was performed for the dsytrophin *(DMD)* gene (Lorain et al., 2010, 2013), the cystic fibrosis transmembrane conductance regulator (*CFTR*) gene (Mansfield et al., 2000; Liu et al., 2002, 2005), the coagulation factor 8 (*F8*) gene (Chao et al., 2003) or the microtubule-associated protein tau (*tau*) gene (Rodriguez-Martin et al., 2005, 2009; Avale et al., 2013) that would not be eligible for full-length expression by classic replacement gene therapy due to the packaging limit of the universal rAAV delivery technology.

2.3.2 Antisense-oligonucleotide mediated *cis*-splicing modification

The most widely established mode of therapeutic pre-mRNA *cis*-splicing modification is the use of antisense-oligonucleotides (AON) to induce the excision (Mann et al., 2001) or inclusion of exon internal sequence (reviewed in Singh and Cooper, 2012). AONs are oligonucleotides of 15 to 20 nucleotides in length which are complementary to regions encoding splicing signals in the pre-mRNA whose *cis*-splicing is to be manipulated. The manipulation takes place by masking exon or intron internal splicing signals via the binding of the AON to the pre-mRNA thus inhibiting the recognition of the splicing motifs by splicing factors or spliceosome subunits.

Controversial aspects of AON-induced *cis*-splicing modification are the choice of backbone
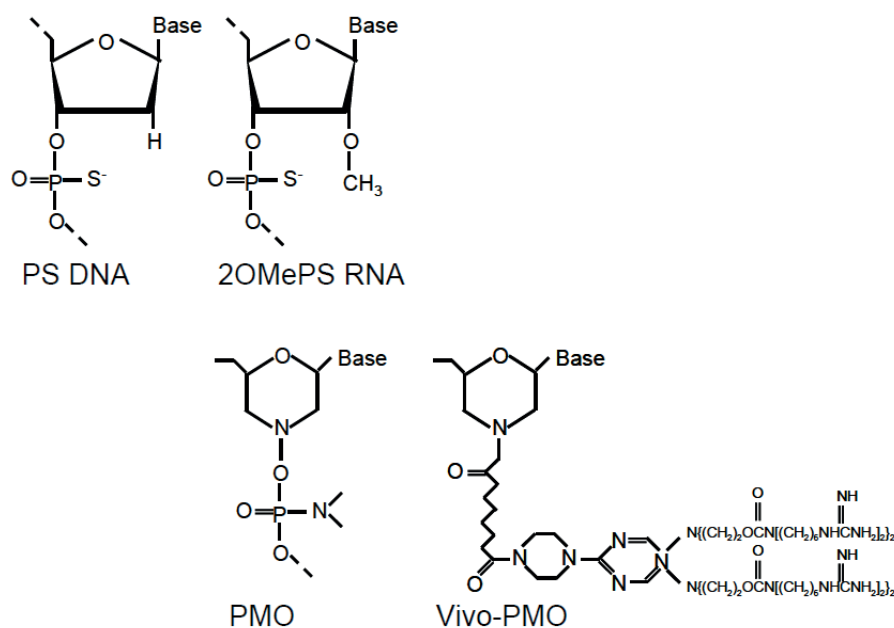
Figure 2.12: Backbone chemistries used in *in vivo* models and clinical trials for AON-mediated pre-mRNA *cis*-splicing modification. Depicted are phsophorothioate (PS)-DNA, 2'O-methyl-phosphorothioate (2OMePS)-RNA, phosphoroamidate morpholino (PMO) and dendrimeric octaguanidine-conjugated phosphoroamidate morpholino (vivo-PMO). Figure modified from Verhaart IEC and Aartsma-Rus AM, Neuromuscular Disorders, AON-Mediated Exon Skipping for Duchenne Muscular Dystrophy.

chemistry of the AON and the mode of AON-delivery into the nucleus of the cell. Backbone chemistry modifications, in comparison to the endogenous RNA- or DNA-backbone, were developed to increase binding affinity to the pre-mRNA target molecule, to increase the *in vivo*-stability of the AON molecule as well as to facilitate more efficient passing of the celullar membrane lipid-bilayer (Fig. 2.12). The replacement of one of the non-bridging phosphate oxygen atoms in the RNA- or DNA-backbone by a sulphur atom in phsophorothioate (PS)-backbones increased AON stability towards nuclease degradation while susceptibility to ribonuclease H (RNAse H) degradation was not eliminated, whereas the 2'O-methyl-addition of the nucleoside ring eliminated susceptibility of AONs to RNAse H degradation (reviewed in Bennett and Swayze, 2010). The phosphoroamidate (PMO)-backbone is as well not susceptible to RNAse H degradation (reviewed in Chan et al., 2006).

The toxicologically best investigated backbone chemistries are the PS-, the 2'O-methyl modified PS (2OMePS)- and the PMO-backbone chemistries as the largest number of clinical trials has been conducted employing them (reviewed in Bennett and Swayze, 2010; Goemans et al., 2011; Cirak et al., 2011). The PS-backbone has been associated with adverse effects at high doses due to non-specific protein binding, which conversely also has been described to facilitate enhanced cellular uptake (reviewed in Chan et al., 2006). The PMO-backbone modified by a membrane-penetrating dendrimeric octaguanidine-moiety, the so-called vivo-PMO-backbone (Fig. 2.12) led to increased AON-effectiveness compared to the unconjugated PMO-backbone (Wu et al., 2011).

The expression of an AON as the part of a stable cellular snRNA is a technology to direct AONs straight to the localisation of pre-mRNA splicing in the nucleus (Gorman et al., 1998), which *in*

vitro has been delivered into the cell by retrovirus vectors (De Angelis et al., 2002) and *in vivo* by recombinant adeno-associated virus (rAAV, chapter 2.3.3) vectors (Goyenvalle et al., 2004; Denti et al., 2006).

The establishment of an AON-mediated RNA-based therapy is usually limited to the repair of a small group of mutations within one exon or a single disease-cause within exon or surrounding introns that in some diseases, like for example in spinal muscular atrophy (Lefebvre et al., 1995), manifest as a disease-causing genotype affecting many individuals. Multiple-exon skipping approaches mediated by the simultaneous application of a mixture of multiple AONs are a concept to repair a larger group of mutations and thus to address a larger cohort of individuals affected by a monogenic disease that does not manifest in a single mutational hot spot (Béroud et al., 2007). A successful multiple-exon skipping approach has been reported by the simultaneous application of 10 vivo-PMO-backbone AONs to simultaneously skip *DMD* exons 45 to 55 (Aoki et al., 2012).

2.3.3 Recombinant adeno-associated virus as a delivery tool of RNA-therapies

Recombinant adeno-associated virus (rAAV) vectors are based on the viral genome of adeno-associated virus (AAV). AAV is a single stranded DNA virus of the *Parvoviridae* family of the genus *Dependovirus*. Its genome has the size of 4.7 kb (Xiao et al., 1999a) and encodes the *rep* and *cap* genes, wherein the *rep* gene encodes proteins necessary for viral replication and the *cap* gene encodes the VP1, VP2 and VP3 proteins that together form the viral capsid (reviewed in Muzyczka, 1992). The open-reading frames of these two genes are framed by inverted terminal repeats (ITR), palindromic sequences that are essential for the regulation of the replication and packing process of the viral genome (McLaughlin et al., 1988). As a *Dependovirus* rAAV requires genes of a so-called helper virus, the adenovirus or herpes virus, for its replication and the assembly of the viral particle (Berns and Giraud, 1995). In rAAV that are used for transgene delivery in gene therapy, the *rep* and *cap* open-reading frames are replaced by the transgene expression cassette, comprising a promoter, the transgene and a poly(A)-signal. For production of rAAV particles, performed in packaging cell-lines by transfection with plasmids expressing the *cap* and *rep* genes in *trans,* an adenovirus-free helper plasmid encoding a mini-adenovirus genome, which is incapable of producing infectious AAV, has been devloped to facilitate the assembly of rAAV particles (Xiao et al., 1998).

Twelve serotypes of AAV (AAV1-12) occuring in primates are presently identified (Rutledge et al., 1998; Xiao et al., 1999a; Schmidt et al., 2008), which differ in their capsid protein composition leading to differential tropisms for vertabrate tissue types. The AAV serotypes 1, 6, and 8 have been shown to efficiently transduce murine skeletal muscle in *in vivo* experiments (Chao et al., 2000; Wang et al., 2005; Blankinship et al., 2006). For gene delivery, transgenes are most commonly integrated between the ITR sequence of the AAV2 genome, which can facilitate packaging with capsid proteins of other serotypes chosen according to the identified tropism of the targeted tissue (Rabinowitz et al., 2002), leading to so-called pseudotyped rAAV. For intramuscular delivery of the PTM expression cassettes in the *in vivo* experiments in this study, rAAV2/1 vector particles were produced (chapter 4.6), i.e. the transgenes were integrated between AAV2-genome ITRs packaged
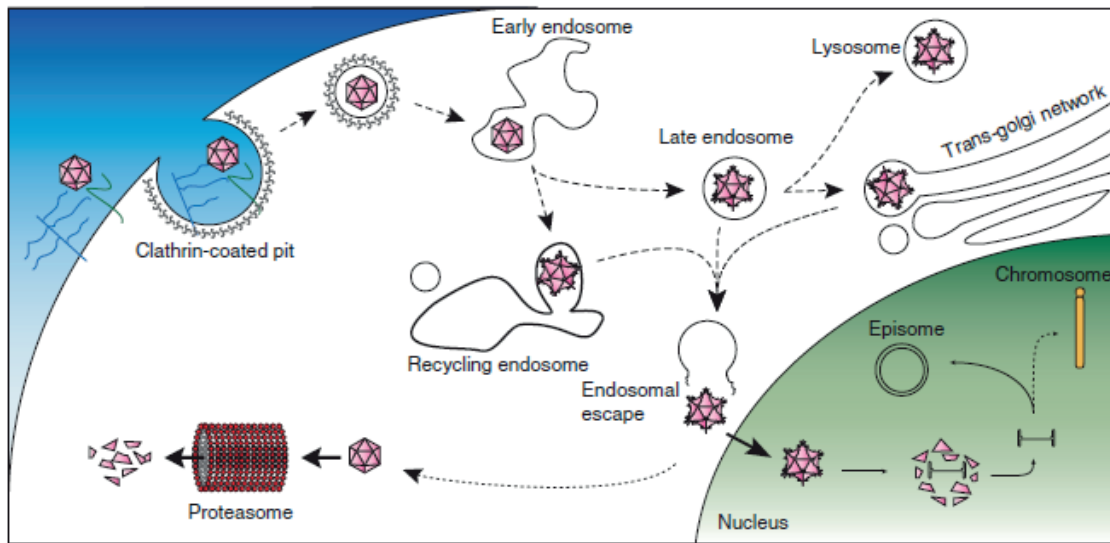
Figure 2.13: Model of recombinant adeno-associated virus (rAAV) entry into the cell and nucleus. rAAV particles enter the cell by receptor-mediated endocytosis and are assumed to be processed by the endosome to become able to enter the nucleus. Assumably, they are decoated inside the nucleus, where the single-stranded rAAV genome is replicated into a double-stranded genome creating an episome. Part of the cytoplasmatic rAAV particles are thought to be degraded by the cytoplasmic proteasome. A very rare event is the chromosomal integration of rAAV genomes. Figure from Schultz and Chamberlain (2008).

into the AAV1-serotype capsid, known for its high tropism to skeletal muscle (Chao et al., 2000).

The cell entry of rAAV occurs by receptor-mediated endocytosis via clathrin-coated pits (Bartlett et al., 2000) (Fig. 2.13), which for AAV1 has been determined to occur via N-linked sialic acids functioning as AAV1 attachment receptors in different cell types (Wu et al., 2006). rAAV particles that have entered the cell are assumed to be processed by the endosome, which has been determined to play an important role for nuclear rAAV entry by the finding that direct injection of rAAV into the nucleus or cytoplasm led to less efficient transgene expression (reviewed in Ding et al., 2005). The rAAV is thought to be released from the endosome in the cytoplasm and the uncoating of the viral genome most likely takes place in the nucleus (Seisenberger et al., 2001). A portion of cytoplasmatic rAAV has been shown to be degraded by the proteasome before entering the nucleus (Douar et al., 2001). Inside the nucleus, the single stranded rAAV genome is processed into a double-stranded rAAV genome by a yet unknown mechanism and concatamerizes into an episome (reviewed in Schultz and Chamberlain, 2008). It has been shown that in murine skeletal muscle the majority of rAAV exists as a double stranded episome in the nucleus from which the transgene is transcribed (Schnepp et al., 2003). These episomes were shown to persist in a quiescent tissue like muscle for several years (Rivera et al., 2005; Penaud-Budloo et al., 2008) allowing the enduring expression of the transgene.

Controversial aspects for the use of rAAV in gene therapy in animal models and human are the provocation of innate and humoral immune response by the AAV capsid proteins and rare unspecific genomic integration. In murine animal models the humoral immune response by neutralizing antibodies against the AAV capsid proteins have led to very low transduction

efficiencies following a first efficient administration of AAV1-, AAV2- and AAV5-encapsidated vectors by intramuscular injection (Xiao et al., 1999a; Chirmule et al., 2000; Riviere et al., 2006). Innate cell-mediated immune response has been detected to act against the AAV2 capsid after injection into murine muscle, but not against the AAV1 capsid that lack the VP3 heparan sulfate proteoglycan–binding motif identified immunogenic in the AAV2 capsid in mice (Vandenberghe et al., 2006; Lorain et al., 2008). In the dog animal model the first application by intramuscular injection raised innate immune response against AAV1, 2, 6, 8 and 9 and in human humoral and innate immune response against AAV1 and 2 capsid proteins (reviewed in Wang et al., 2011). In the analyses of human sera the innate titre of neutralizing antibody (NAB) against AAV1 was significantly lower than NAB-titre against AAV2 (Xiao et al., 1999a).

In the presence of the Rep protein rAAV, like AAV, (Kotin et al., 1990) can stably integrate into human chromosome 19 (Samulski et al., 1991) at the myosin-binding subunit 85 open-reading-frame. The unspecific chromosomal integration of rAAV has been shown to occur at a negligible percentage in murine muscle (Schnepp et al., 2003), but is known to possibly occur by non-homologous recombination at sites of chromosomal breakage or sites that are susceptible to breakage (Inagaki et al., 2007). Strategies to facilitate targeted chromosomal integration of rAAV by homologous recombination for targeted stable integration of transgenes are under development (reviewed in Vasileva and Jessberger, 2005).

2.4   RNA-based therapies for dysferlinopathies

2.4.1   3' mRNA replacement of the dysferlin pre-mRNA by spliceosome-mediated pre-mRNA *trans*-splicing

In the presented work, I established replacement of the 3'moiety of the *DYSF* pre-mRNA by spliceosome-mediated 3'mRNA *trans*-splicing (SmaRT) employing engineered pre-mRNA *trans*-splicing molecules (PTM). The replacement of a large portion of the *DYSF* pre-mRNA was considered a suitable therapeutic approach for dysferlinopathies for several reasons. Mutations in the *DYSF* gene do not agglomerate in a mutational "hot spot", but spread over the entire open-reading frame of the gene (chapter 2.2.4), which rendered a therapeutic approach possibly facilitating the repair of a large portion of the open-reading frame by a single functional molecule desirable. Neither the precise function of the dysferlin protein, nor of single identified domains of the protein have yet been determined precisely (chapter 2.2.2 and 2.2.3). Therefore the SmaRT approach represented a securely feasible therapeutic approach regarding a possible application in patients, as it maintains the full-length dysferlin protein with unrestrained functionality. This intention was corroborated by the finding that a mini-dysferlin protein in murine dysferlin-deficient skeletal muscle has not led to the recovery of dystrophic muscle histology, albeit it induced rescue of the membrane repair mechanism attributed to the dysferlin protein (Krahn et al., 2010b). Another strategy to recover a full-length protein would be the classic gene therapeutic approach of gene replacement therapy by extrachromosomal expression of full-length cDNA under a tissue-specific promoter, by which the disregulation of the endogenous transcription regulation of the gene cannot

be avoided. The *DYSF* gene is encoded by an open-reading frame of ~6.5kb which makes efficient cDNA expression facilitated by delivery of a single rAAV vector impossible due to the rAAV-genome packaging limit (chapter 2.3.3). Further, the sensitive transcriptional regulation of the *DYSF* gene has been shown to be crucial for the proper functioning of the protein. The overexpression of human dysferlin protein in murine animal models caused progressive muscular dystrophy leading to kyphosis, irregular gait and loss of muscle mass and strength (Glover et al., 2010), which are more severe symptoms then observed in dysferlinopathies (chapter 2.2.4).

In the here presented establishment of the SmaRT approach for the *DYSF* gene, the focus was laid on the identification of a pre-mRNA target intron most susceptible for *trans*-splicing by a PTM. In an initial *in vitro* screening, four target introns in the human *DYSF* pre-mRNA harbouring different qualities in terms of 3'splice site strength and size were targeted by PTMs in human immortalized myoblasts (IM DYSF4, chapter 3.1.1). To determine the optimal localisation of the PTM for *cis*-splicing manipulation, each target intron was targeted by two different binding domains, localising the PTM either in close proximity of the target intron 5'splice site or masking the intron internal 3'splice site (Fig. 2.10). The design of the PTMs in respect of binding domain length, branch point sequence, poly-pyrimidine tract and 3'splice site was adopted from previous functional approaches (Puttaraju et al., 1999; Mansfield et al., 2000; Lorain et al., 2013). *Cis*-splicing of target introns harbouring weak 3'splice sites was succefully manipulated by addressing the intron in 5'splie site proximity and led to *trans*-splicing of endogenous *DYSF* pre-mRNA into a *trans*-spliced *DYSF* mRNA transcript. The *in vivo* application of the functional PTMs was performed in wild-type *C57Bl/6* mice and in the *DYSF-/-* mouse model, harbouring a deletion of exon 53 and 54 in the *mDYSF* open-reading frame (Bansal et al., 2003) to exclude any effect of mutations in the direct sequence-surrounding of the target intron on the *trans*-splicing process. Two of the functional PTMs induced dysferlin protein rescue in *DYSF-/-* mice at moderate levels. The mRNA region replaced by these PTMs (PTM 2.1: exon 32-55 and PTM 3.1: exon 36-55) covers the *DYSF* sequence for which 144 variations leading to dysferlin protein alteration have been reported to date (http://www.dmd.nl/).

2.4.2 Exon skipping of dysferlin exon 32

The *DYSF* gene does not encode a protein of modular structure, as for example the *DMD* gene does, in which the excision of particular exons is eligible without confinement of dystrophin protein function (Lu et al., 2003; Goyenvalle et al., 2004; Aoki et al., 2010). Despite this and the scattered arrangement of disease-causing mutations in the *DYSF* open reading frame, an exon skipping approach using tri-cyclo DNA antisense-oligonucleotides (AONs) for the excision of *DYSF* exon 32 was pursued. It has been shown that *DYSF* mRNA lacking exon 32, which encodes part of the dysferlin C2D domain, encodes a dysferlin protein functional to a degree, to cause very mild dysferlinopathy symptoms in patient wich remained ambulant until the age of 70 years (Sinnreich et al., 2006). This patient was the carrier of a heterozygous compound *DYSF* mutation, wherein the precise excision of *DYSF* exon 32 was encoded by only one allele, next to a *DYSF* null-allele. The feasibility of exon 32 excision from *DYSF* pre-mRNA was shown before employing 20mers of
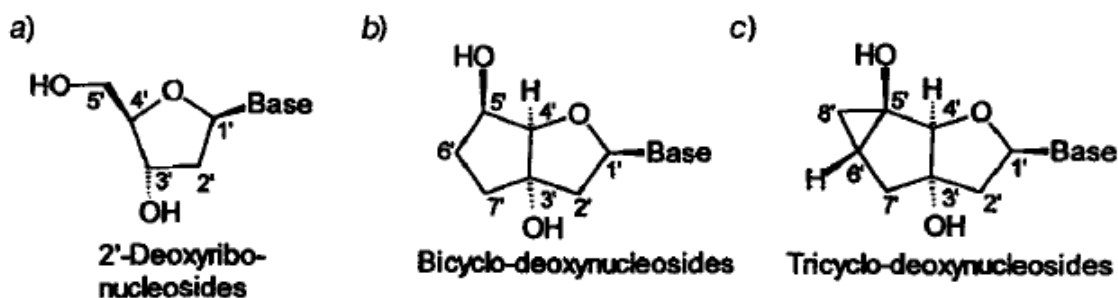
Figure 2.14: Conformational structures of 2'deoxyribonucleosides present in DNA and the DNA-analogs bicyclo-deoxynucleosides and tricyclo-deoxynucleosides. Figure from Steffens and Leumann (1997).

2'OMePS-RNA AONs and lentivirus-delivered AONs masking exon internal ESE sequences of *DYSF* exon 32 in human myoblasts (Wein et al., 2010). The protein rescue by exon 32 excision was not yet shown in this approach and consequently no further functional studies of a dysferlin-Δ32 protein were conducted yet.

In the present work, the feasibility of 15mer tri-cyclo DNA-AONs (tcDNA-AON) for the excision of *DYSF* exon 32 was investigated as a possible future amelioration of the previous exon 32 skipping approch regarding the toxicological features of the AON backbone chemistry by using a DNA-backbone lacking the sulphur-addition (chapter 2.3.2) and employing shorter AON molecules. Tri-cyclo DNA (tcDNA) is a DNA analogue that has been synthesized by the addition of a cyclopropane unit to a bi-cyclodeoxynucleoside (Fig. 2.14). Bi-cyclodeoxynucleosides comprise the addition of an ehtylen-bridge between the C(3') and the C(5') centers of the deoxyribonucleoside found in DNA (Tarköy et al., 1993). The double nucleoside structure of bicyclo-deoxynucleosides was aimed at to mimic the naturally occurring highly stable two nucleoside-structure of the DNA double helix to facilitate stable Watson-Crick base-pairing with a complementary oligonucleotide. The addition of a cyclopropane unit to the bi-cyclodeoxynucleoside at C(5') and C(6') further enhanced structural rigidity in an oligonucleotide chain and was also expected to enhance cellular uptake of molecule chains due to its hydrophobicity-increasing effect (Steffens and Leumann, 1997). The resulting tcDNA oligonucleotides were investigated for their AON functionality since tcDNA-RNA duplexes exhibited high thermostability (Renneberg and Leumann, 2002a) and they emerged to be stable in serum and insusceptible to RNase H degradation (Renneberg et al., 2002). Future pharmaco-toxicological investigations of the tc-DNA backbone will give more insight into this aspect relevant for its application in human.

Here I focussed on the design of 15mer AON sequences which efficiently induce *DYSF* exon 32 excision. Different tc-DNA AONs complementary to the human *DYSF* exon 32 sequence were tested *in vitro* in an immortalized human control (IM WT3, 2.5) and a dysferlin-deficient (IM DYSF5) myoblast line. AONs targeting putative exon internal splice enhancer-motifs were found to lead to most efficient exon 32 excision and to induce dysferlin protein rescue in IM DYSF5. Tc-DNA AONs complementary to the murine *DYSF* sequence (mAON) were tested by intramuscular injection in wild-type *C57BL/6* mice and tcDNA-mAONs targeting putative exon internal splice enhancer sequences were as well found to induce exon 32 excision most efficiently. Presently, eight

diferent variations of *DYSF* exon 32 leading to protein alteration have been reported to occur in either heterozygous or homozyogous state in total 37 cases (http://www.dmd.nl/; Wein et al., 2010).

2.5 Immortalisation of dysferlin-deficient human patient myoblasts

The access to primary human myoblasts from biopsies of patients with disease-causing *DYSF* mutations is limited. Due to excessive fibrosis, these muscle biopsies often contain only very few myogenic cells and are highly intermingled with connective tissue cells like fibroblasts and adipocytes. Additionally, primary human myoblasts in culture show a limited proliferative potential and undergo changes that are linked to replicative senescence (Bigot et al., 2008). To circumvent these limitations immortalized human myoblast lines were generated of primary human myoblasts harbouring different disease-causing mutations by retroviral transduction with cDNAs of telomerase (*hTERT*) and cyclin-dependent kinase 4 (*CDK-4*) (Zhu et al., 2007; Mamchaoui et al., 2011). *hTERT* overexpression overcomes the progressive erosion of telomeres occuring due to cell division and the overexpression of *CDK-4* blocks the induction of the p16-mediated cellular stress-pathway (Zhu et al., 2007). After their immortalization these cell lines showed a prolonged proliferation and differentiation capacity compared to primary human myoblasts *in vitro* and could succesfully be transplanted into regenerating muscle *in vivo (Mamchaoui et al., 2011)*.

Preliminary to the establishment of the RNA-based therapeutic approaches, I analysed four different dysferlinopathy patient myoblasts lines (IM DYSF1, IM DYSF2, IM DYSF3 and IM DYSF4) that were immortalized by stable *hTERT-* and *cdk-4-* transduction within a collaboration with the laboratory of Vincent Mouly (Institute of Myology, Paris). I subsequently used these cell lines to test the developed therapeutical approaches in a tissue-specific *in vitro* model.

To investigate the differentiaion potential of IM DYSF myoblasts into multi-nucleated myotubes, I analysed the expression of structural proteins indicating differentiation in muscle cells and compared them to the differentiation of myoblasts from a primary human control myoblast culture. Further, the laser-mediated membrane wounding assay established by Bansal et al. (2003) to detect defectiveness of membrane resealing due to dysferlin deficiency, was performed on myotubes derived from the IM DYSF myoblasts lines to determine whether these cell lines presented a read-out tool for dysferlin rescue by therapeutic *DYSF* repair approaches.

3 Results

3.1 Immortalized dysferlinopathy patient myoblasts

3.1.1 Immortalized dysferlinopathy patient myoblasts differentiate into multi-nucleated muscle cells

Stable immortalized myoblast lines (IM DYSF1, IM DYSF2, IM DYSF3 and IM DYSF4) were generated from primary human dysferlinopathy patient myoblasts (DYSF1, DYSF2, DYSF3 and DYSF4) carrying different mutations in the *DYSF* gene that lead to the expression of missense dysferlin protein (DYSF1 and DYSF2) or the complete absence of dysferlin protein (DYSF3 and DYSF4) (Fig. 3.1) (Wenzel et al., 2006; Philippi et al., 2012). The immortalization of primary myoblasts was performed in the laboratory of Vincent Mouly (Institute of Myology, Paris) by stable integration of *CdK4* and *hTERT* cDNAs via lentiviral transduction (Zhu et al., 2007; Mamchaoui et al., 2011). Selected clones were returned to the laboratory and analysed for their myogenicity and differentiation potential. An immortalized control cell line (IM WT3) generated from the biopsy of a healthy individual was analysed in parallel. By immuncytochemistry against the muscle specific intermediate filament desmin all immortalized cell lines were shown to be purely myogenic, i.e. free of connective tissue cells such as fibroblasts and adipocytes (Fig. 3.2). All immortalized cell lines were further analyzed for their differentiation degree be detection of the muscle specific isoform of the actin-binding protein alpha-actinin and the muscle specific contractile protein myosin heavy chain. The striated staining pattern for both proteins indicating Z-lines showed that myoblasts properly differentiated into multi-nucleated myotubes (Fig. 3.2). As further indicators of a proper differentiation, expression of the muscle specific isoform of

Immortalized myoblast line	Nucleotide change	Exon	Intron	Allelic state	RNA change	Protein change	Mutation first described in
IM DYSF1	c.4022T>C	38		homozygous	r.4022u>c	p.L1341P missense	Wenzel K, 2006
IM DYSF2	c.855+1delG		8	heterozygous	5'SS mut. mRNA decay		Wenzel K, 2006
	c.895G>A	9		heterozygous	r.895g>a	p.G299R missense	
IM DYSF3	c.1448C>A	16		heterozygous	r.1448c>a	p.S483X nonsense	Wenzel K, 2006
	c.*107T>A	3'UTR		heterozygous	r.*107u>a mRNA decay		
IM DYSF4	c.2810+2T>A		26	homozygous	5'SS mut. mRNA decay		-

Figure 3.1: Primary myoblasts from biopsies of identified dysferlinopathy patients were immortalized to IM DYSF1, IM DYSF2, IM DYSF3 and IM DYSF4 myoblast cell lines.
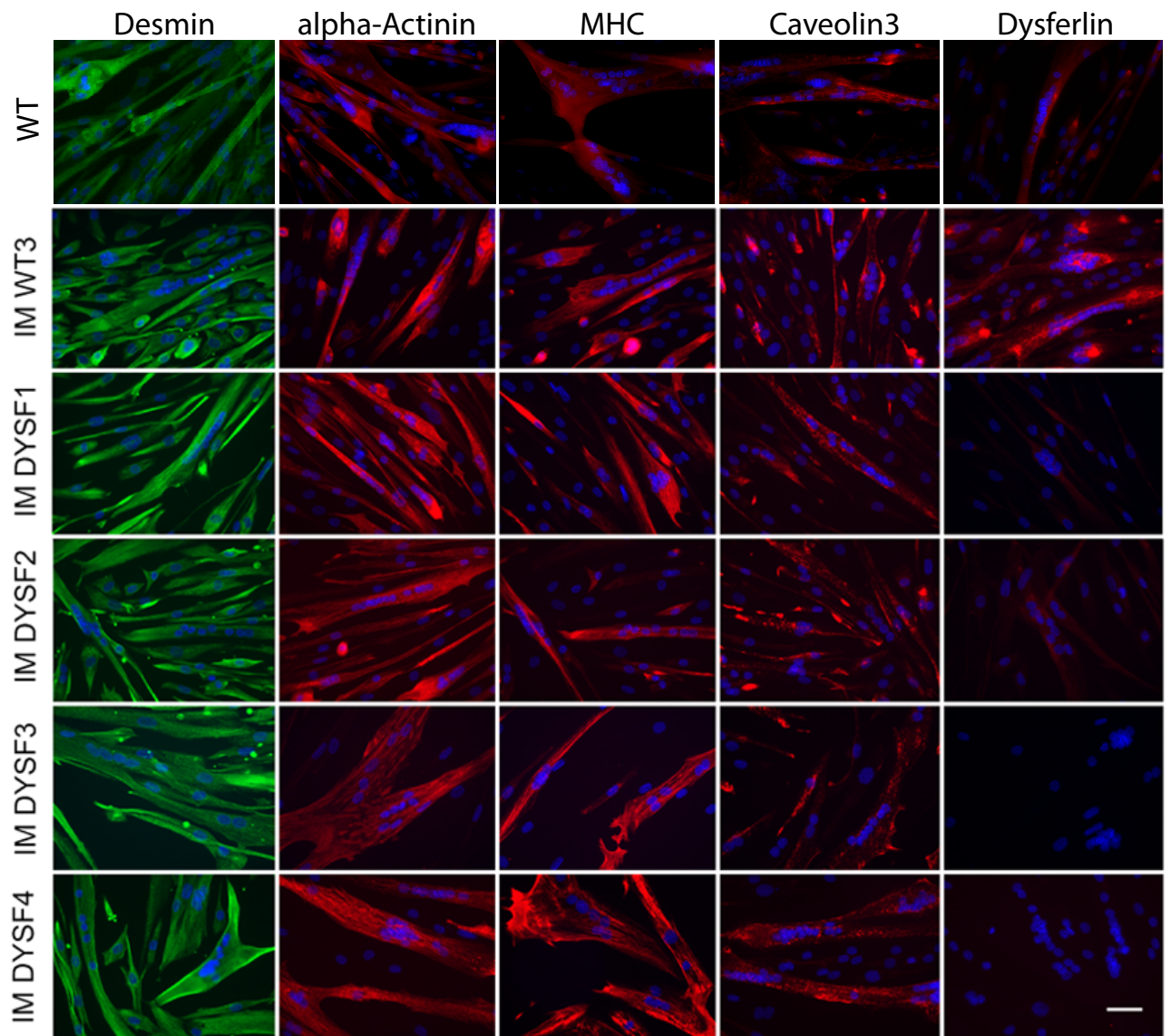
Figure 3.2: Immortalized myoblasts differentiate into myotubes. Myotubes at differentiation day 7 of WT, IM WT3, IM DYSF1, IM DYSF2, IM DYSF3 and IM DYSF4 were immunostained for desmin, alpha-actinin, myosin heavy chain, caveolin-3 and dysferlin. (Figure modified from Philippi et al. (2012))
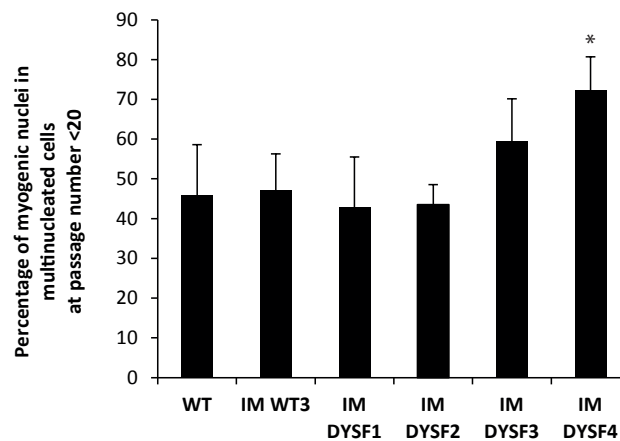
Figure 3.3: The fusion index does not differ significantly between primary (WT) and immortalized wild-type myoblasts (IM WT3)., and neither between IM WT3 and immortalized dysferlin-deficient myoblasts IM DYSF1, IM DYSF2 and IM DYSF3, whereas a significant difference was observed between IM WT3 and IM DYSF4. Data represent means of five different experiments ±SD. *$p < 0.05$ in unpaired Student's t-test.

membrane-associated caveolins, the caveolin-3, and dysferlin were analysed. Caveolin-3 detection in myotubes derived from IM WT3 and IM DYSF cell lines showed membranous localisation of the protein, regionally densed, indicating proper muscle membrane differentation including t-tubuli development and caveolae formation, as was detected in myotubes from primary human WT myoblasts (Fig. 3.2). Dysferlin was detected faintly intracellularly and localized to the membrane, partly in membranous agglomerations in myotubes derived from both wild-type myoblast lines, WT and IM WT3. As expected due to their missense *DYSF* mutations, the dysferlin protein was detected at faint intracellular abundance in IM DYSF1 and IM DYSF2 myotubes. Myotubes derived from IM DYSF3 that harbours a nonsense mutations combined with an mRNA decay inducing mutation (Wenzel et al., 2006) and IM DYSF4 that harbours a mutation most likely leadling to nonsense mediated decay (Supplementary Fig. 7.1) showed complete absence of dysferlin protein (Fig. 3.2). Dysferlin protein expression has been detected weakly for IM DYSF1 and 2 and not at all in IM DYSF3 and 4 derived myotubes by immunoblot experiments performed by Stephanie Meyer (Spuler laboratory, ECRC Berlin) (data not shown, Philippi et al., 2012).

As a further aspect of differentiation potential, the fusion index, i.e. the percentage of myogenic nuclei present in multi-nucleated myotubes was compared between primary and immortalized wild-type myoblasts WT and IM WT3, and does not differ significantly. Fusion indeces of the IM DYSF lines were compared with the index of IM WT3, wherein no significant differences were calculated, except for IM DYSF4 exhibiting a significantly higher fusion index then IM WT3 (Fig. 3.3).

3.1.2 Investigation of membrane integrity by laser-mediated membrane wounding on myotubes

To investigate the capability to reseal induced membrane injury in myotubes derived from the immortalized myoblast cell lines, laser-mediated membrane wounding assays were performed. The

resaeling capability following membrane injury in myotubes derived from all IM DYSF lines was compared to IM WT3 myotubes. Myotubes were incubated in Tyrode solution supplemented with fluorescent membrane dye FM1-43 and were wounded at their membrane frontier. Observation during the following 280 seconds after the wounding event showed that IM WT3 derived myotubes were capable of membrane repair as no FM1-43 dye influx was detected (Fig. 3.4). As expected for myotubes expressing mutated dysferlin, IM DYSF1 and IM DYSF2 depicted disruption of the membrane repair process by staining of intracellular compartments due to influx of the fluorescent FM1-43 dye during the 280 seconds following the wounding. Myotubes generated from IM DYSF3 myoblasts only partly showed a disrupted response to membrane injury and otherwise showed formation of blebs at the wounding site, possibly inhibiting strong FM1-43 influx. IM DYSF4 myotubes showed membrane repair capability mostly indifferent from IM WT3. The increase in fluorescence intensity versus time was quantified for all experiments. The increase in fluorescence intensity after wounding for IM DYSF1, IM DYSF2 and IM DYSF3, but not IM DYSF4 differed signifcantly from IM WT3 (*$p < 0.001$).

3.2 *Trans*-splicing as an approach to dysferlin gene repair

3.2.1 Definition of a test set of dysferlin pre-mRNA *trans*-splicing target introns

In order to identify criteria for a functional *trans*-splicing approach, the aim was the identification of a suitable target intron (TI) for the 3'mRNA replacement in human dysferlin *(DYSF)* pre-mRNA. In consideration of the mutation profile of the *DYSF* gene TIs were chosen that located in the central region of the pre-mRNA to replace the 3'moiety of the *DYSF* open reading frame. To assess the impact of intron internal 3'SS strength, four TIs were chosen which were ranked with unequal scores using the MaxEntScan::score3ss bioinformatic tool (Yeo and Burge, 2004, chapter 4.1). Among the *DYSF* TIs 30, 31, 35 and 36 the 3'SS of TI31 was ranked with the lowest MaxEnt score as already indicated by the purine at intron internal position -3 deviating from the strongly conserved pyrimidine in metazoan 3'SS sequences (Burge et al., 1999). TI31 was followed by TI35, TI 30 and TI36 with increasing MaxEnt scores (Fig. 3.5A). As an experimental approach to evaluate 3'SSs of the chosen TIs a splice-switching experiment was performed on each TI. An exon with a weak 3'SS was assumed to be more easily excluded from the mature transcript than an exon with a strong 3'SS. 2'-O-methyl phosphorotioate antisense-oligonucleotides (AONs) were designed to interfere with the splicing process of the *DYSF* pre-mRNA by masking the 5'SS downstream of each respective TI by covering the region from exon internal position -3 to intron internal position +17. For simplification the exon upstream of the TI is called Ex, the exon downstream of the TI Ey and the next downstream exon Ez (Fig. 3.5B). In case the 3'SS of the TI was a weak 3'SS, the disruption of the exon Ey definition would lead to exclusion of the exon Ey in the splicing process. In case the TI encoded a strong 3'SS, at AON application exon Ex would be linked to the downstream exon Ey leading to no splice-switching. The application of AONs targeting TIs 30, 31, 35 and 36 was performed in human IM WT3 myoblasts to exclude any impact of mutations on the splicing process. Only the TI 31 of the human *DYSF* pre-mRNA exhibited a weak 3'SS as AON
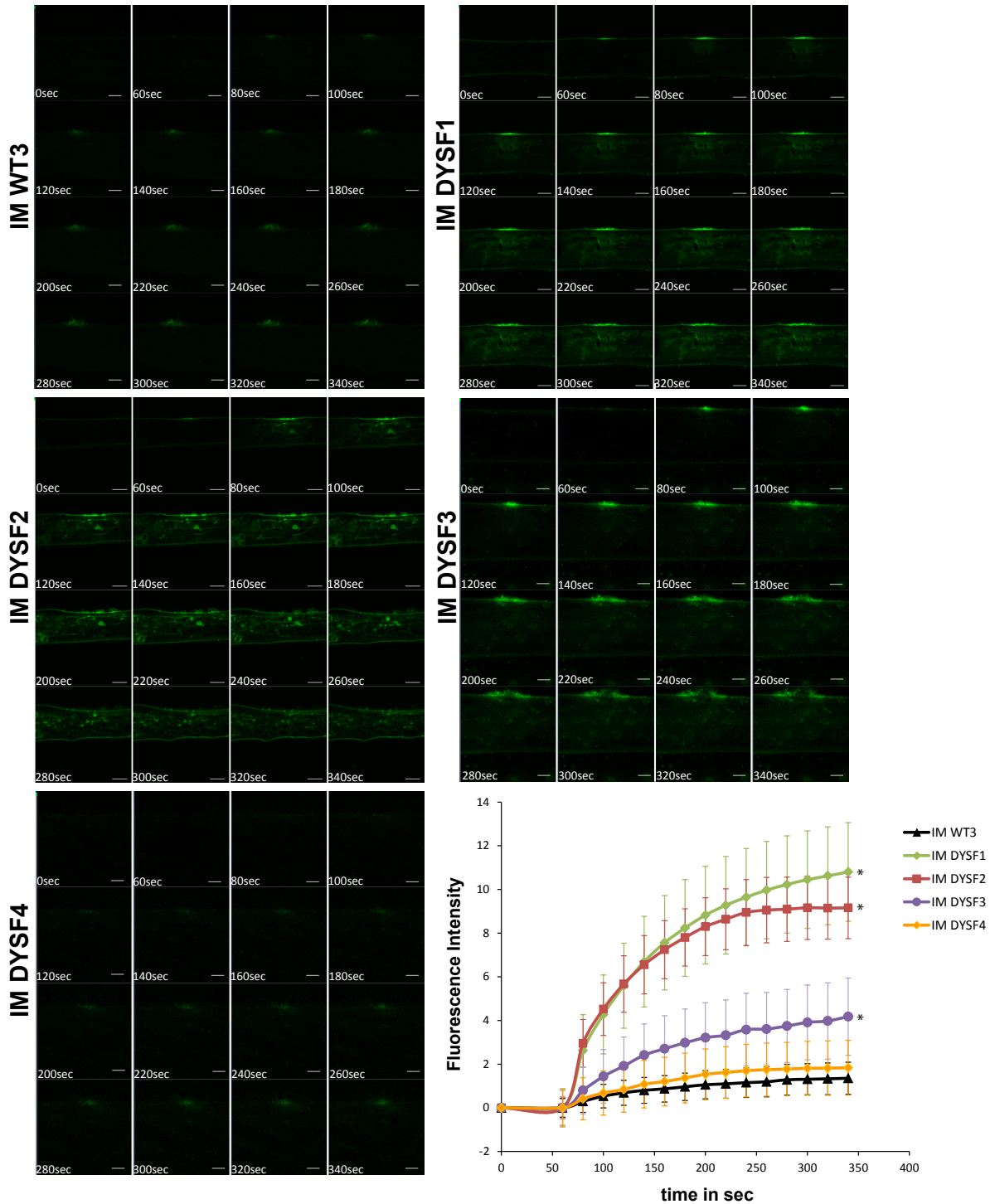
Figure 3.4: Laser-mediated membrane wounding of myotube membranes in IM DYSF1, IM DYSF2 and IM DYSF3 lead to a significant increase of fluorescence intensity in myotubes compared to IM WT3, whereas wounding of IM DYSF4 does not. Data represent mean values of n experiments ± SE (IM WT3 n=7; IM DYSF1 n=8; IM DYSF2 n=11; IM DYSF3 n=7; IM DYSF4 n=5). *p≤0.001 by unpaired student's t-test. (Figure modified from Philippi et al. (2012))

A

TI #	Size	3'Splice Site	MaxEnt	3'Splice Site in PTM	MaxEnt
30	15221bp	AACCAGCUUCGUGUCUCCAGggc	6.45	UUUUUUUUUUUAAUUAACAGggc	10.03
31	543bp	UGUUUUUUCCCUUGGUGAAGaug	4.44	UUUUUUUUUUUAAUUAACAGaug	10.06
35	1247bp	AUCCCAUGGCUGUGGGCCAGgug	4.57	UUUUUUUUUUUAAUUAACAGgug	10.94
36	8427bp	CUACCUGCUGUCCACUGCAGucu	8.06	UUUUUUUUUUUAAUUAACAGucu	8.93

B
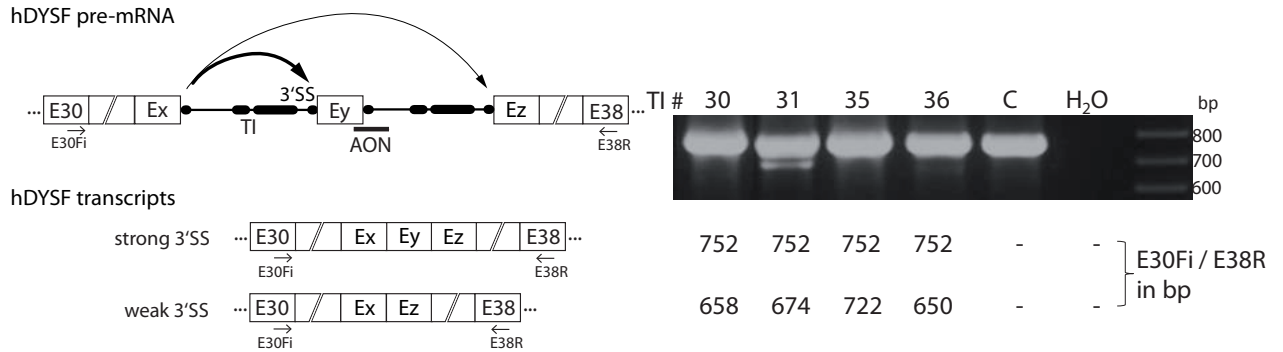
C
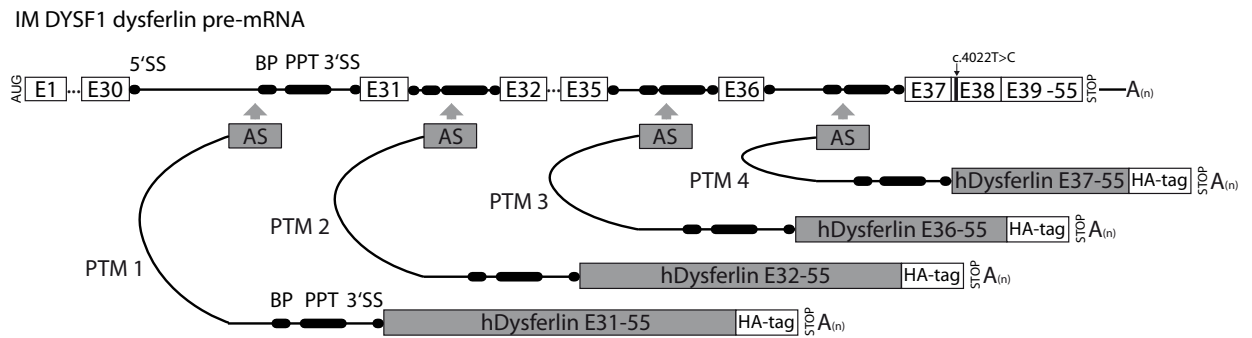
D
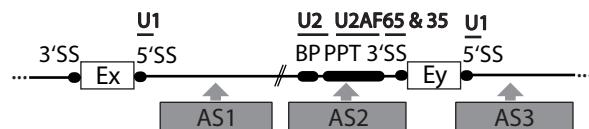
Figure 3.5: Screening of the *DYSF* pre-mRNA for target introns (TI) accessible for a 3'mRNA replacement by a pre-mRNA *trans*-splicing molecule (PTM). (**A**) The 3'splice sites (3'SS) of four human *DYSF* introns of different length as well as the hemi-intron of each respective PTM were ranked using MaxEntScan::score3SS. The highest value ever given to a 3'SS has been ~14 (Yeo and Burge, 2004). Intron internal sequence is capitalized and exon internal sequence lowercased. (**B**) Validation of the MaxEnt ranking by masking the 5'SS downstream of the ranked 3'SS using an antisense-oligonucleotide (AON) in the splicing process of unmutated *DYSF* in human IM WT3 myoblasts. In consequence of the AON application, the exon Ex, preceding the TI, attacks the exon Ey at the 3'SS of the TI or the exon Ez at the 3'SS of the downstream intron. The 3'SSs of all four TIs were tested and analyzed by nested RT-PCR using E30Fi and E38R as internal primers. Detected amplicons are shown with the expected amplicon sizes below according to a strong or weak 3'SS in the TI. (**C**) PTMs 1-4 targeting human *DYSF* introns 30, 31, 35 and 36 respectively in immortalized human patient myoblasts IM DYSF1 carrying a homozygous missense mutation in exon 38 (c.4022T>C). PTMs consist of an antisense sequence (AS), a hemi-intron encoding a conserved branchpoint sequence (BP), a poly-pyrimidine tract (PPT) and a 3'SS, the respective human *DYSF* cDNA sequence to be replaced in *DYSF* pre-mRNA, the influenza hemaglutinin tag (HA-tag) upstream of the STOP codon and a hemoglobin2 poly(A)-signal. (**D**) Each PTM was created with two different ASs, AS1 and AS2. PTM2 was additionally created with the AS3 masking the 5'splice site of the intron downstream of the actual TI. Binding regions of the U1 and U2 snRNPs and auxiliary factors U2AF65 and U2AF35 of the spliceosome are indicated.

application led to skipping of the downstream exon Ey, the *DYSF* exon 32, shown by the additional amplicon of 674bp (Fig. 3.5B). These findings predicted a high accessibility of the TI 31 as its recognition by the spliceosome based on the degree of the conserved splicing sequence motifs at its 3'SS were indicated to be weaker compared to all other TIs. In order to screen this hypothesis, PTMs targeting human *DYSF* TIs 30, 31, 35 and 36 were tested in human IM DYSF1 myoblasts.

3.2.2 Design of pre-mRNA *trans*-splicing molecules for dysferlin target introns

PTMs were constructed comprising (i) an antisense sequence (AS) functioning as their binding domain complementary to the TIs 30 (PTM1), 31 (PTM2), 35 (PTM3) and 36 (PTM4), (ii) a hemi-intron containing a 30 nucleotide (nt) long spacer sequence, a strongly conserved yeast branch point sequence (BP), a 20 nt long poly-pyrimidine tract (PPT) and a metazoan consensus CAG 3'splice site (3'SS), (iii) the respective unmutated human *DYSF* cDNA sequence to be replaced in the *DYSF* pre-mRNA by the PTM and (iv) an influenza hemaglutinin tag (HA-tag) to facilitate subsequent differentiation between *cis*- and *trans*-spliced versions of the *DYSF* mRNA (Fig. 3.5C).

The ASs were designed at a length of ~150 nt including minimal variations that arouse from constraints by considering prediction of disadvantageous secondary structures made by RNAfold software (http://rna.tbi.univie.ac.at/cgi-bin/RNAfold.cgi) (data not shown). The 3'SS emerging from the combination of the PTM hemi-intron with the initial exon of each respective coding sequence were all ranked by a MaxEnt values of ~10 which was higher than their endogenous 3'SS counterpart (3.1). For TI 36 the PTM 3'SS was ranked with a MaxEnt value of 8.93 only slightly higher than its endogenous 3'SS (Fig.3.5A). For each PTM two different ASs were designed. The binding position of AS1 was chosen approximately 200 nucleotides (nt) downstream of the TI's 5'SS placing the PTM in close proximity to the U1 snRNP (Fig. 3.5D). The AS2 was designed to mask the endogenous bp, ppt and 3'SS of the TI intended to thereby direct the spliceosome to recognize the splicing domain of the PTM instead. PTMs with AS1 were called PTM1.1, 2.1, 3.1 and 4.1, with AS2, PTM1.2, 2.2 and 3.2 (Fig. 3.5D). No PTM 4.2 was constructed as the AS2 designed complementary to the TI 36 3'SS region could not be amplified from human genomic DNA. For TI 31, the most promising PTM target according to the TI analysis, an additional AS3 was designed (PTM2.3) which masked the intron internal 5'SS downstream of the TI intended to combine localisation of the PTM and suppression of exon 32 recognition (Fig. 3.5D).

3.2.3 Target intron 3'splice sites ranked with low MaxEnt scores were accessible for dysferlin 3'mRNA replacement by a pre-mRNA *trans*-splicing molecule

Lentiviral vectors (LV) integrating the PTM constructs PTM1.1 and 1.2, 2.1, 2.2 and 2.3, 3.1 and 3.2, as well as 4.1 (Fig. 3.6 and 3.7) were produced and human immortalized dysferlin myoblasts IM DYSF1 were transduced at the multiplicity of infection (MOI) 3 that was determined the optimal MOI for *trans*-splicing detection (Supplementary Fig. 7.2). IM DYSF1 was considered a suitable screening cell line as it carries a homozygous point mutation downstream of all four TIs allowing the differentiation between *cis*- and *trans*-spliced transcript. Further, this mutation was not localized in the immediate downstream exon of any of the target introns which prevented any influence
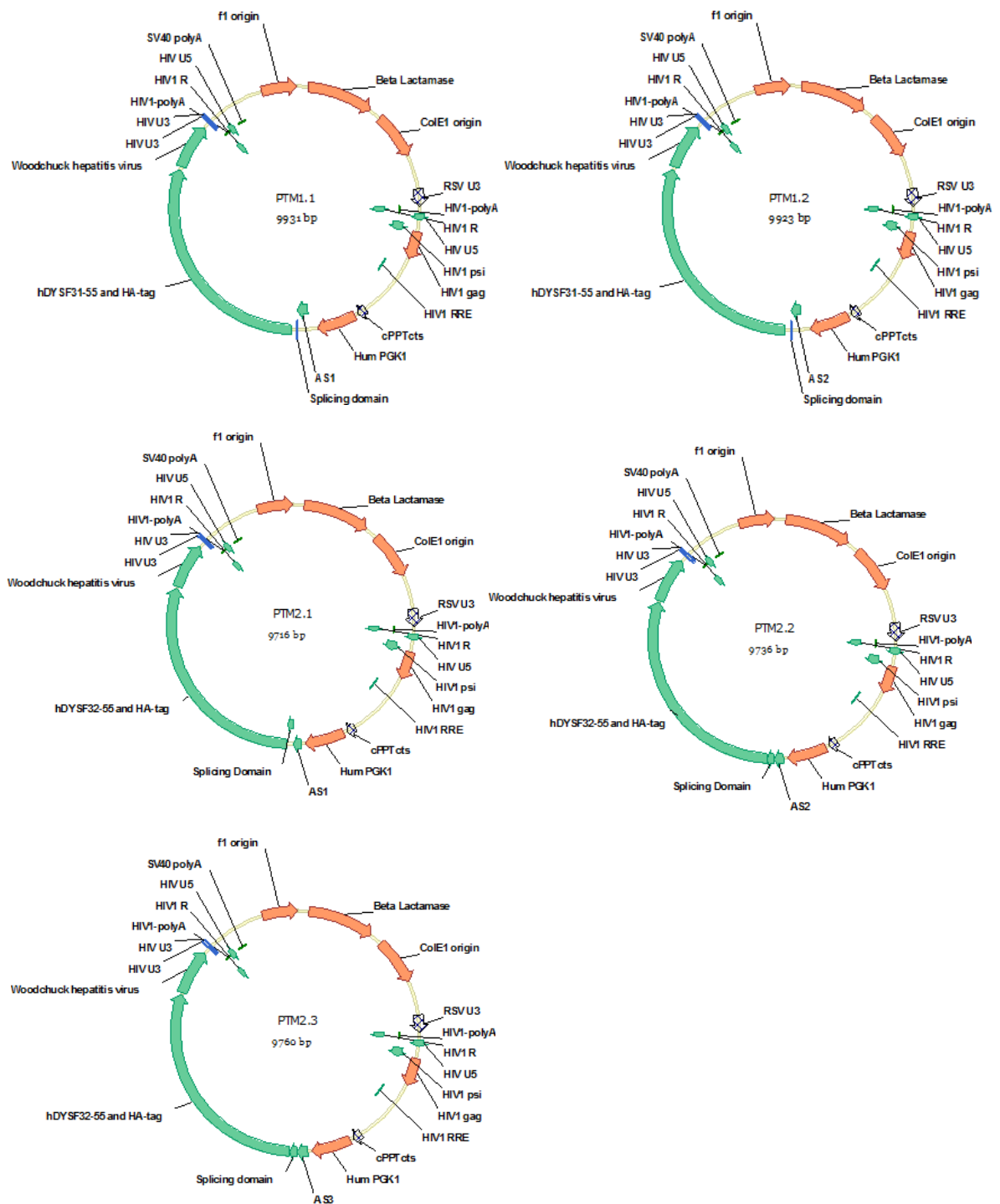
Figure 3.6: Lentivirus vector constructs for the introduction of PTM1.1, PTM1.2, PTM2.1, PTM2.2 and PTM2.3 into human IM DYSF1 myoblasts. Transgenes were expressed under the control of human PGK-1 promoter
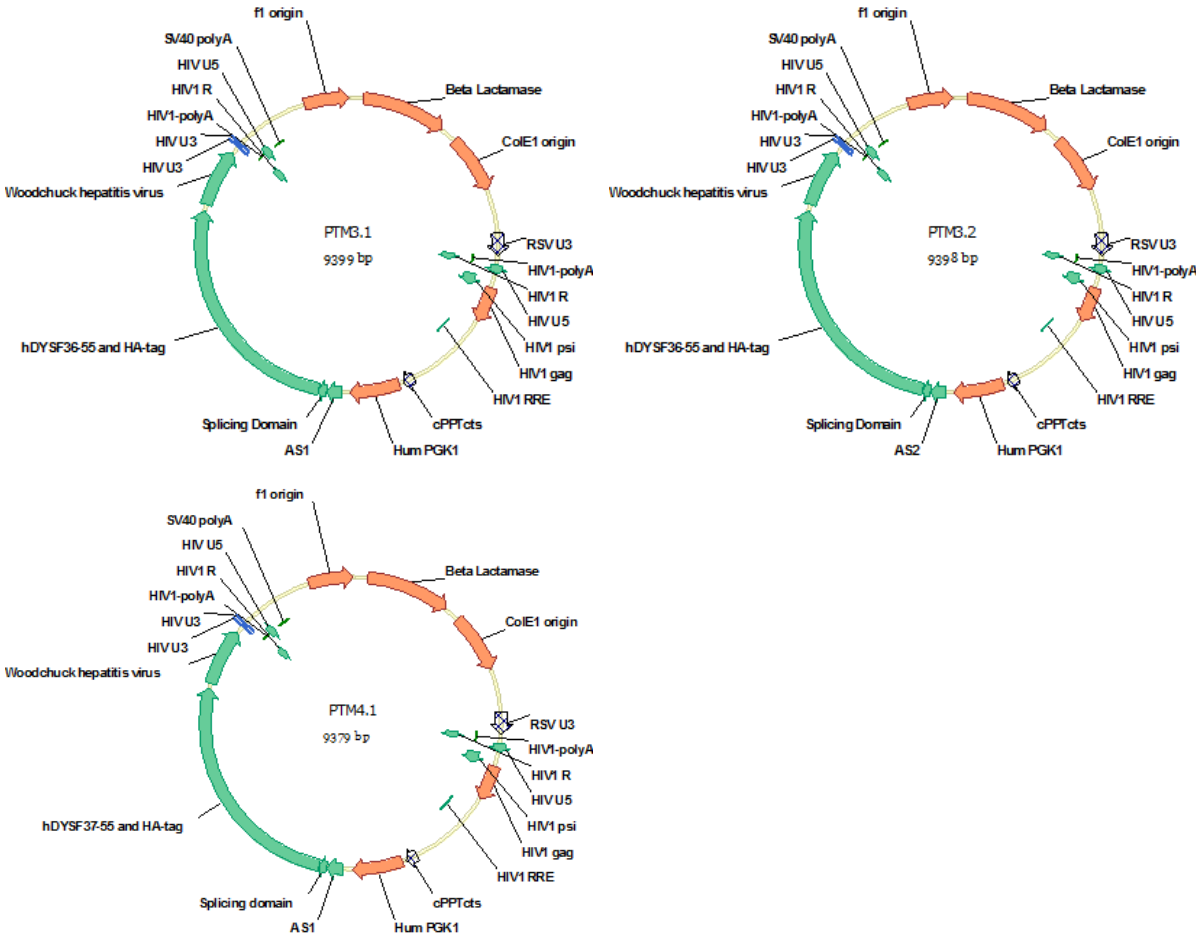
Figure 3.7: Lentivirus vector constructs for the introduction of PTM3.1, PTM3.2 and PTM4.1 into human IM DYSF1 myoblasts. Transgenes were expressed under the control of human PGK-1 promoter

of the mutation on the *trans*-splicing outcome. A LV carrying a GFP open reading frame was transduced in parallel demonstrating the high transduction efficiency and differentiation capability of transduced myoblasts (Supplementary Fig. 7.3). Myotubes were harvested at differentiation day 14 and analysed for *trans*-splicing of the human *DYSF* pre-mRNA. In order to detect the *trans*-spliced *DYSF* transcript after transduction by PTM1.1, 1.2 and 2.1, 2.2 and 2.3, reverse transcription-polymerase chain reaction (RT-PCR) was performed on total RNA using the human *DYSF* exon 30 specific forward (hE30F) and HA-tag reverse (HA-tagR) primers which exclusively amplified *trans*-spliced transcripts including the boundary between exon 30 and 31, and exon 31 and 32, of the endogenous and *trans*-spliced dysferlin transcript (Fig. 3.8A).

Trans-splicing by PTMs 3.1, 3.2 and 4.1 was analysed by RT-PCR on total RNA using hE35F and HA-tagR primers spanning the boundary of the *trans*-spliced transcript between exons 35 and 36 or exons 36 and 37, respectively. The efficient expression of each PTM following LV-transduction was analysed using the primer set hE48F/HA-tagR to amplify all transcripts coming from the PTMs. The overall presence of human *DYSF* transcript, including the *cis*- and *tran*s-spliced version, was detected by the hE30F/hE40R primer set. A *trans*-spliced *DYSF* transcript was detected following transduction by PTM2.1 and PTM2.3 both targeting TI 31, which had depicted the weakest 3'SS. As well targeting of TI 35 by PTM3.1 led to *trans*-splicing as expected by the low MaxEnt ranking of its 3'SS (Fig. 3.5A). All PTMs were approximately equally expressed and the overall expression of human *DYSF* transcript was detected at comparable levels for all transductions (Fig. 3.8B) indicating that all PTMs were studied under comparable conditions. Direct sequencing of the amplicons from the detected *trans*-spliced transcripts exhibited a continuous sequence including the intact boundary between *DYSF* exon 31 and 32, for *trans*-spliced transcripts by PTM 2.1 and 2.3, the intact boundary between exon 35 and 36, for transcripts *trans*-spliced by PTM3.1, and the unmutated sequence of exon 38 in all four transcripts (Fig. 3.8C). To detect the protein product translated from the *trans*-spliced *DYSF* transcript, fluorescence immunostaining on transduced myotubes was performed to co-detect the HA-tag at the extracellular C-terminus of the *trans*-spliced protein product and the dysferlin intracellular N-terminus. In myotubes transduced with PTM2.1 membrane-located HA-tag detection partly overlapped with the detected intracellular dysferlin signal (Fig. 3.9). However, this overlap was detected only as a sporadic event.

3.2.4   Targeting corresponding murine dysferlin target introns allowed 3'mRNA replacement *in vivo*

As a prerequisite to the transfer of the *trans*-splicing strategy to *in vivo* models, murine TIs (mTIs), mTI 30, 31, 35 and 36, were ranked using MaxEntScan::score3ss (Fig. 3.10A). As detetcted for human *DYSF* target introns, mTIs 31 and 35 were ranked by lower MaxEnt scores then mTI 30 and mTI 36. The mTI 31 as well encoded a pyrimidine at intron internal position -3 deviating from the conserved purine and was ranked by an extremely low MaxEnt score of 0.29. According to the analogy among the analysis of human and murine 3'SSs and the successful *trans*-splicing of TI 31 and TI 35, PTMs with two different ASs, AS1 and AS2 complementary to mTI 31 and mTI 35 (mPTMs) were designed (Fig. 3.11). Murine AS1 ans AS2 bind mTIs at intron internal positions
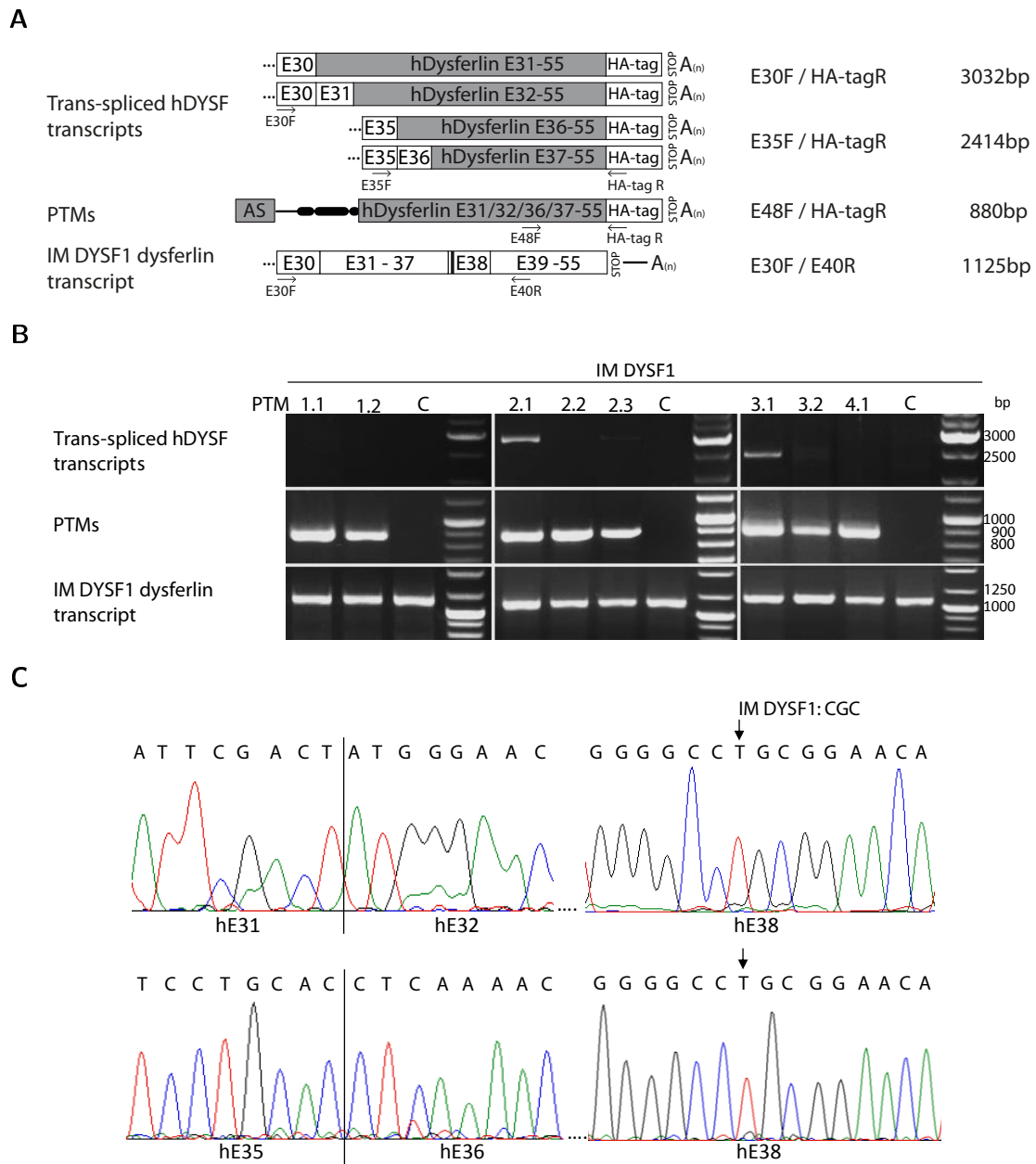
Figure 3.8: Detection of *trans*-spliced unmutated *DYSF* transcript after transduction with PTM2.1, 2.3 and 3.1. (**A**) *Trans*-splicing of the *DYSF* transcript by PTM1.1, 1.2 and PTM2.1,2.2 and 2.3 as well as PTM3.1, PTM3.2 and PTM4.1 was analysed by RT-PCR using the primers E30F/HA-tagR and E35F/HA-tagR respectively to amplify only the *trans*-spliced human *DYSF* (hDYSF) transcript on cDNA. The presence of the PTM was detected by PCR on cDNA using the primer set E48F/HA-tagR. The human *cis*-spliced hDYSF transcript was detected, and eventually the *trans*-spliced version as well, by the primers E30F/E40R. (**B**) Detection of *trans*-spliced *DYSF* transcript, PTM expression and endogenous human *DYSF* expression by RT-PCRs described above. All PCRs were performed at 30 cycles. **C** = untransduced cells. Results are representative of three independent experiments. (**C**) Sequencing of the amplicons obtained by PCR with primer sets E30F/HA-tagR and E35F/HA-tagR on cDNA from PTM2.1, 2.3 and 3.1 transduced cells. Arrows indicate repaired nucleotides.
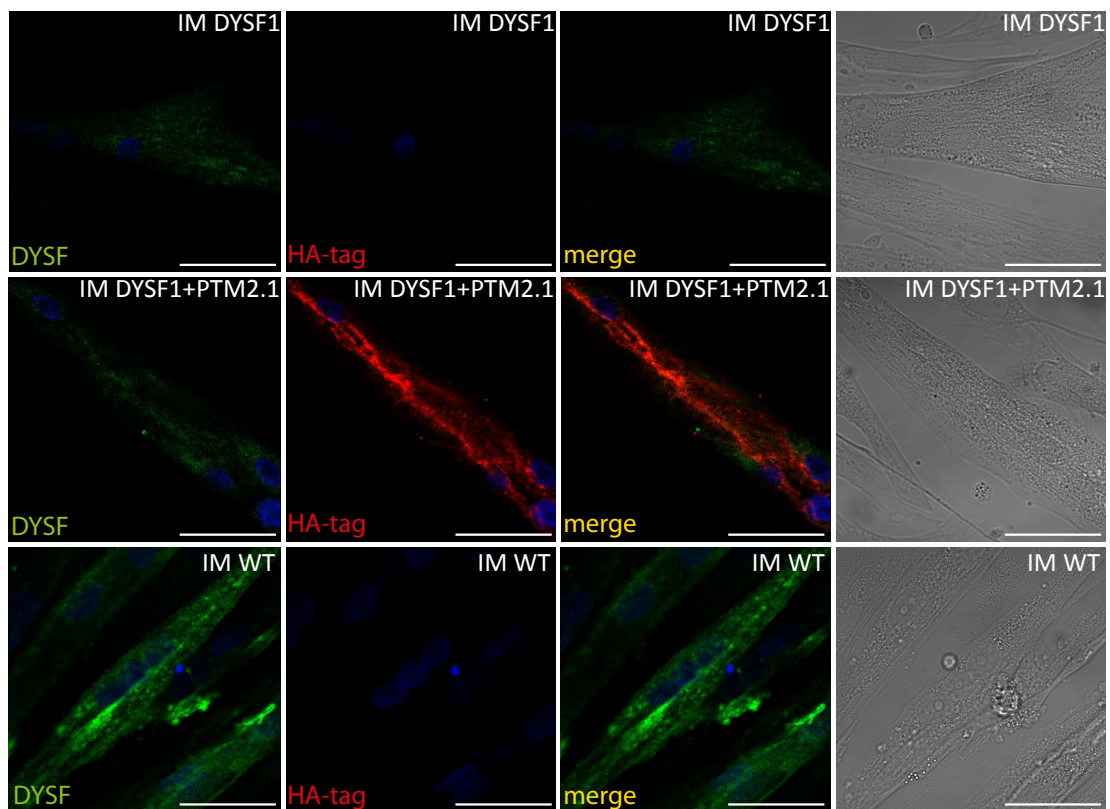
Figure 3.9: *Trans*-splicing of hDYSF pre-mRNA by PTM2.1 leads to membrane-bound HA-tagged *trans*-spliced dysferlin protein in IM DYSF1 myotubes. Myotubes are co-stained for dysferlin (DYSF), using Romeo antibody detecting dysferlin intracellular N-terminus, and HA-tag (HA-tag) to detect the *trans*-spliced dysferlin HA-tagged at its C-terminus. Scale bar depicts 50µm.

A

mTI #	Size	3'Splice Site	MaxEnt	3'Splice Site in mPTM	MaxEnt
30	13249bp	GAUAAGCUUUGUGUCUCCAGggc	6.41	UUUUUUUUUUUUAAUUAACAGggc	10.03
31	551bp	CUGUUUCCUCCUGAGUGAAGaug	0.29	UUUUUUUUUUUUAAUUAACAGaug	10.06
35	1236bp	CUGGAUGUGGCCCAUCACAGaug	4.24	UUUUUUUUUUUUAAUUAACAGgug	10.06
36	7722bp	ACUUUUGCUGUCUCCUGCAGacg	11.89	UUUUUUUUUUUUAAUUAACAGacg	8.91

B

C

D
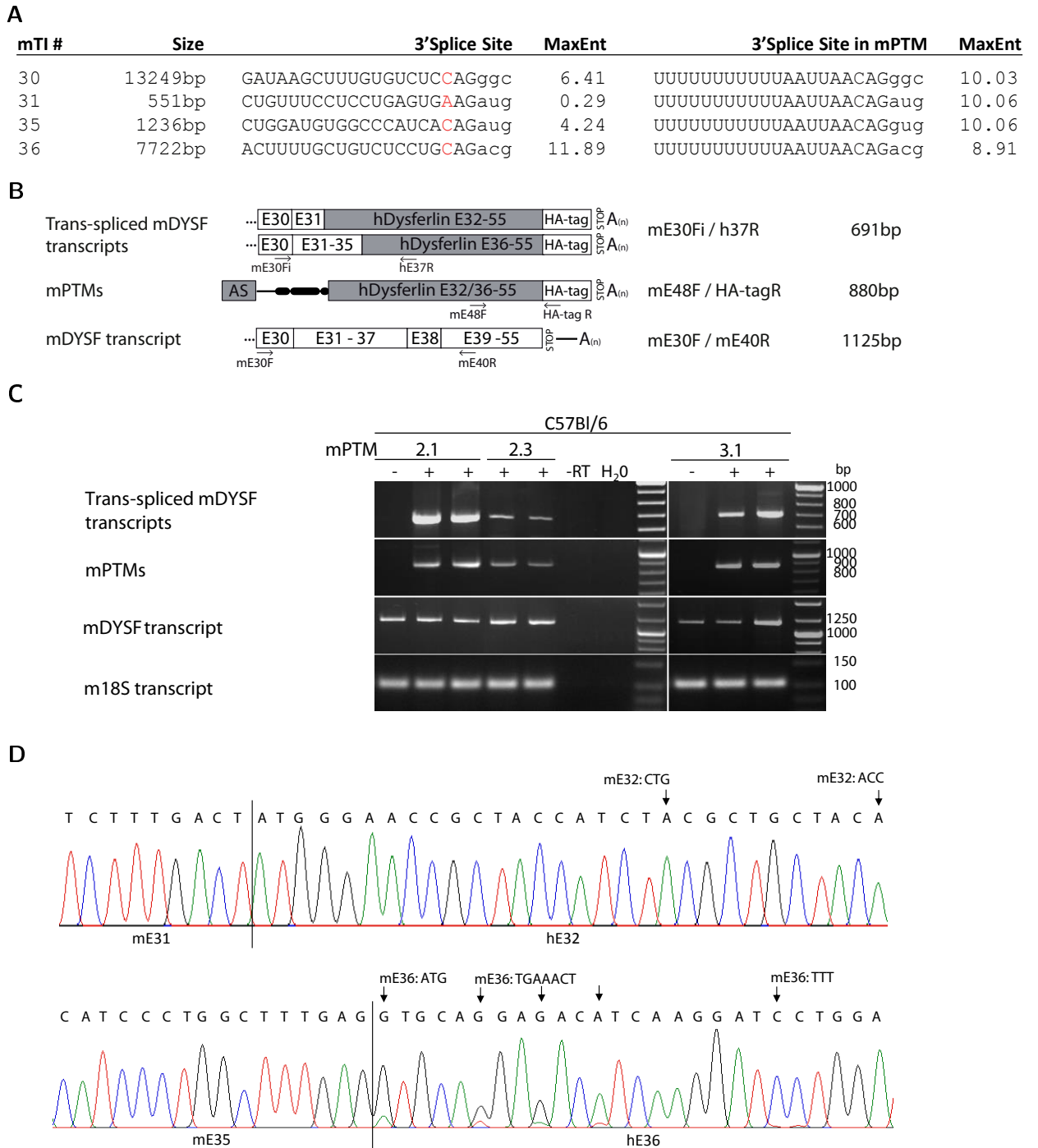
Figure 3.10: *Trans*-splicing of the unmutated murine dysferlin (mDYSF) pre-mRNA by mPTM 2.1 , 2.3 and 3.1 following intramuscular injection of rAAV-mPTM2.1, rAAV-mPTM2.3 and rAAV-mPTM3.1 into *tibiales anteriores* of C57Bl/6 mice. (**A**) The 3'SSs of the mDYSF target introns (mTIs) and their mPTM counterparts were ranked using MaxEntScan::score3SS. (**B**) To detect the *trans*-spliced transcript, that is a chimera of mDYSF and hDYSF sequence, nested PCR on cDNA using mE30Fi and hE37R as internal primers was performed. The mPTMs were detected by PCR on cDNA using E48F/HA-tagR. The *cis*-spliced mDYSF transcript was detected by mE30F/mE40R amplification on cDNA. (**C**) All PCRs were performed on equal amounts of cDNA and at 35 cycles, including both runs of nested PCR. Reverse transcription omitting the reverse transcriptase (-RT) lead to no amplification proving the absence of DNA in the reaction. One data set of two representative sets is shown. (**D**) Sequencing of the PCR fragments received by PCR using m30Fi/h37R primers. Arrows indicate nucleotides identifying the human sequence in starting from exon 32 and 36 on due in *trans*-spliced transcripts.

39
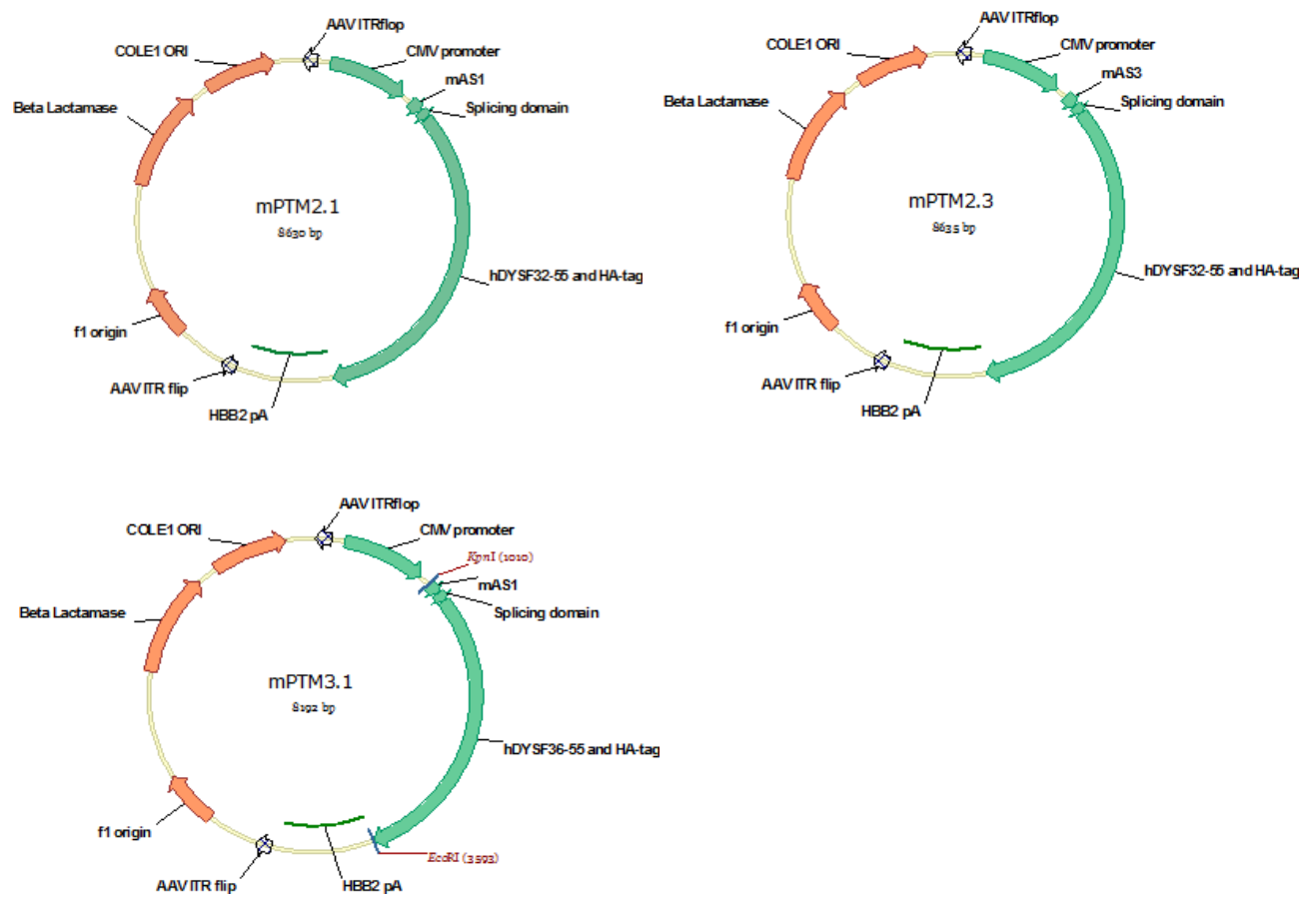
Figure 3.11: rAAV2/1 vectors rAAV2/1-mPTM2.1, rAAV2/1-mPTM2.3 and rAAV2/1-mPTM3.1 for the introduction of mPTM2.1, mPTM2.3 and mPTM3.1 in C57Bl/6 mice.

that were described for the human TIs (Fig. 3.8D). The splicing sequences as well as the human *DYSF* coding sequence of the PTMs were let identical, meaning that a trans-spliced transcript would be a chimera of human and murine *DYSF* sequence. Recombinant adeno-associated viruses 2 pseudotyped by serotype 1 capsids (rAAV2/1) were produced expressing mPTM2.1, mPTM2.3 and mPTM3.1. *Tibiales anteriores* (TA) of C57Bl/6 mice at the age of two months were injected with rAAV2/1-mPTM2.1, rAAV2/1-mPTM2.3 and rAAV2/1-mPTM3.1 and analysed four weeks after the injection. To detect *trans*-splicing of the murine *DYSF* pre-mRNA nested RT-PCR was performed on total extracted RNA employing a murine *DYSF* specific internal forward primer (mE30Fi) and a human *DYSF* specific internal reverse primer (hE37R) amplifying a region of the transcript which included the intact boundary between murine exon 31 (mE31) and human exon 32 (hE32) after *trans*-splicing by mPTM2.1 and mPTM2.3. The intact boundary of murine exon 35 (mE35) and human exon 36 (hE36) resulting from *trans*-splicing by mPTM3.1 was detected using the same internal primer set in nested RT-PCR as well (Fig. 3.10B). The expression of all mPTMs was detected by RT-PCR on total RNA using the m48F/HA-tagR primer set. The endogenous murine *DYSF* transcript was detected using the murine *DYSF* specific primers mE30F and mE40R and the murine 18S transcript by primers m18SF and m18SR showing that all analyses were performed at comparable initial RNA concentrations. *Trans*-spliced transcripts were detected in all TAs in jected with mPTM2.1, mPTM2.3 and mPTM3.1 (Fig. 3.10C), and the *trans*-splicing events were confirmed by sequencing showing the intact chimeras of murine and human *DYSF* sequence (Fig. 3.10D). As observed in the experiments in human myoblasts, RT-PCR suggested that mPTM2.1 led to more efficient *trans*-splicing than mPTM2.3 while mPTM3.1 was only slightly less efficient than mPTM2.1 (Fig. 3.10C) This suggested that splicing of mTI 31 can be more efficiently manipulated than of mTI 35.

Consequently, the translation of the *trans*-spliced transcript was analysed by immunoblot. The protein product of the *trans*-spliced wild-type *DYSF* messenger could not be detected by immunoblot against the HA-tag introduced by the coding sequence of the PTM. As has previously been reported in other *trans*-splicing strategies for PTMs, translation of one of the provided mPTMs, the mPTM3.1, by the usage of an artificial start-codon in the PTM sequence could be detected using anti-HA-tag antibody at ~85kDa. No translation of mPTM2.1 could be detected. As a further control, samples were as well investigated by immunoblot against anti-dysferlin Hamlet antibody. The translated mPTM3.1 was as well detected by the Hamlet antibody. A faint signal could be detected at the size of a possible translated mPTM2.1 (~100kDa). However, this signal was considered unspecific as it was as well detected in the negative control and samples expressing the shorter mPTM3.1.

3.2.5   Dysferlin rescue *in vivo*

To investigate whether mPTM2.1 and mPTM3.1 could facilitate the dysferlin protein restoration in murine skeletal muscle and therefore underpin the therapeutical implication of the designed *DYSF trans*-splicing strategy, the rAAV2/1-mPTM2.1noHA and rAAV2/1-mPTM3.1noHA were injected into tibiales anteriores of *DYSF-/-* mice. *DYSF-/-* mice carry a deletion of *DYSF* exon 53
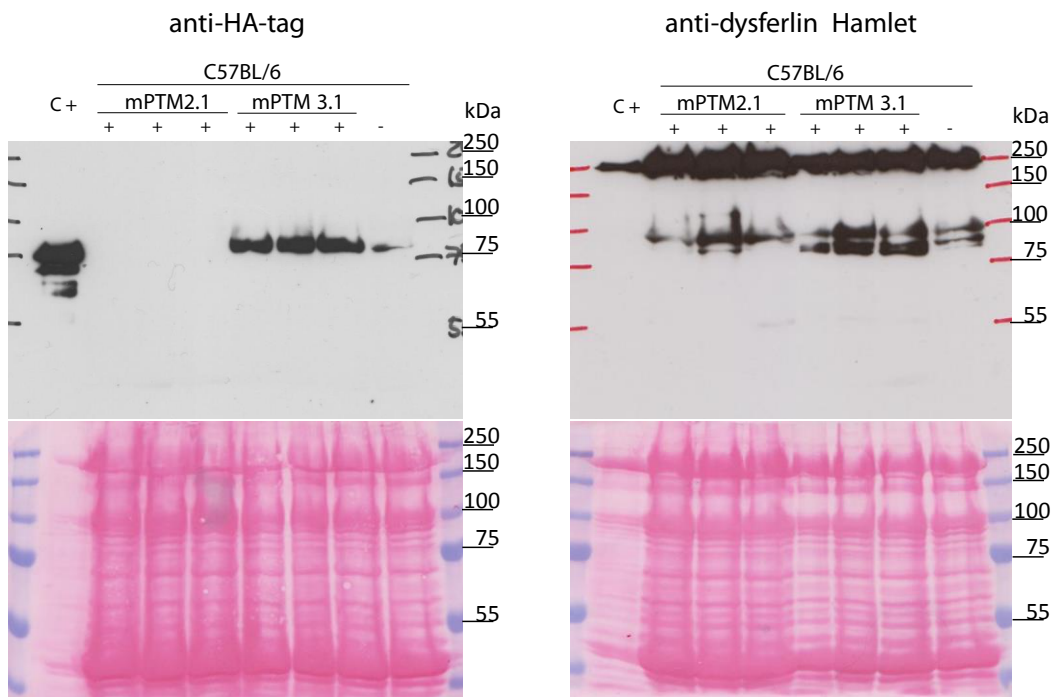
Figure 3.12: Translation of the t*rans*-spliced dysferlin transcript in C57Bl/6 mice could not be detected by immunoblot against HA-tag. The translation of mPTM2.1 itsslef (~100kDa) was not detectable by anti-HA-tag antibody, whereas translated mPTM3.1 (~85kDa) was detectable (left). Immunoblot against dysferlin using Hamlet antibody does not depict any further translation products beside mPTM3.1. Ponceau Red stainings depict high protein abundance at the size of 100kDa for all samples except positive controls. Seperation of 80μg lysate is shown for each sample, positive control lysates were 2μg (HA-tag Ctrl.) and 10μg (Dysferlin-Ctrl.).
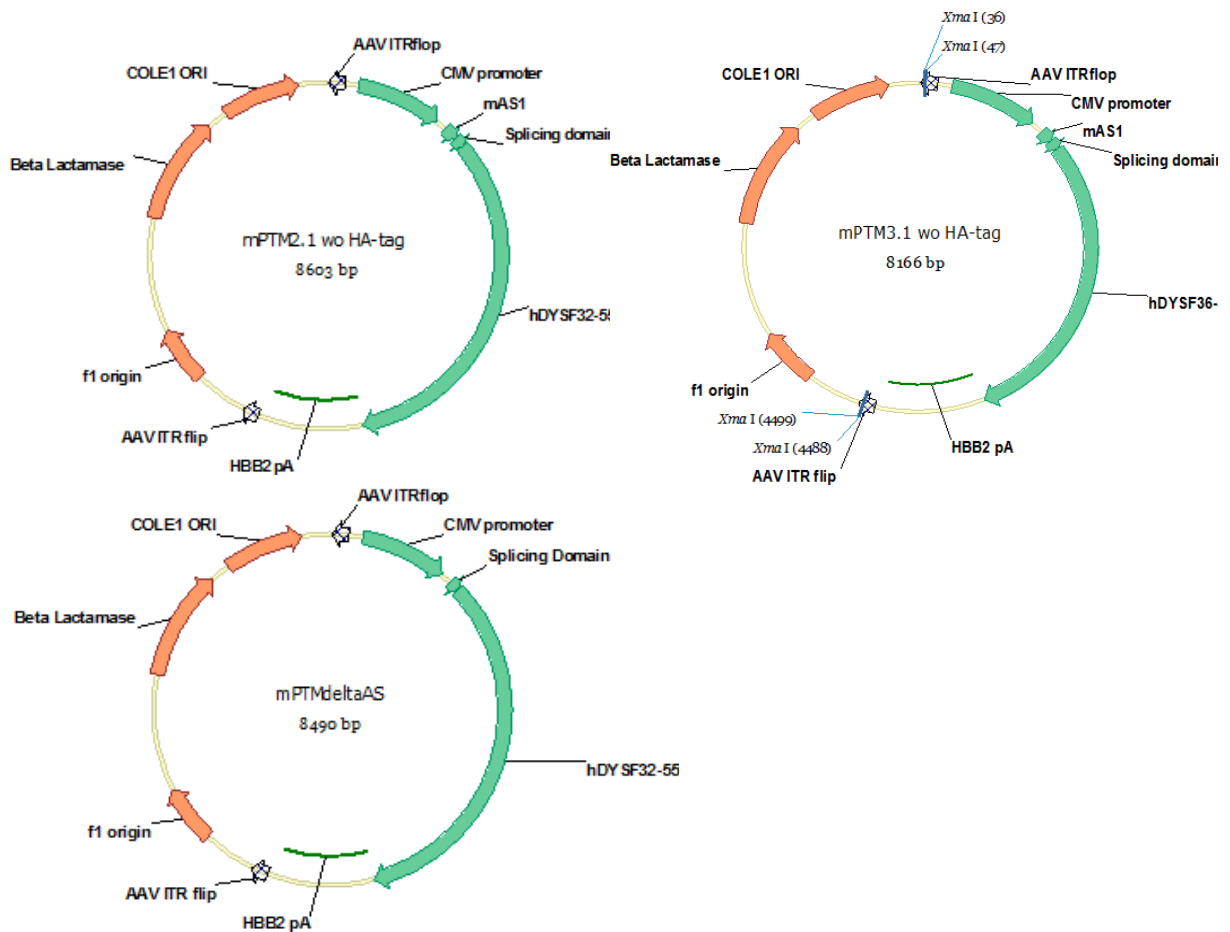
Figure 3.13: rAAV2/1 vectors rAAV2/1-mPTM2.1, rAAV2/1-mPTM3.1 nd rAAV2/1-PTMΔAS for the introduction of mPTM2.1, mPTM3.1 and mPTMΔAS in DYSF-/- mice.

and 54 leading to a complete knock-out of the dysferlin protein and progressive muscular dystrophy pronounced in proximal skeletal muscle (chapter 4.6 Fig. 4.2). rAAV2/1-mPTM2.1noHA and rAAV2/1-mPTM3.1noHA expressed mPTM2.1 and 3.1 without the C-terminal HA-tag sequence. The HA-tag was excluded from the PTM coding domain to avoid any functional alteration of the restored protein. This seemed particularly crucial since the dysferlin C-terminal end is located only 14 amino acids downstream of the dysferlin transmembrane domain and the HA-tag might interfere with its proper localisation. Additionally, an rAAV2/1 expressing a defective PTM lacking the AS (mPTMΔAS) was injected to demonstrate the necessity of targeting the suitable TI for the proper location of the PTM to induce *trans*-splicing and to exclude the show specifity of the *trans*-splicing detection primers (Fig. 3.13). Injections were performed in mice at four months of age and muscle was analysed for *trans*-splicing of *DYSF* after four weeks. A *trans*-spliced murine *DYSF* transcript following injection of mPTM2.1noHA and mPTM3.1noHA was detected performing single RT-PCR on total extracted RNA using a murine *DYSF*-specific forward primer (mE30F) and a human *DYSF*-specific reverse primer (hE40R) (Fig.3.14A and B). The injection of PTMΔAS led to no *trans*-splicing at a PTM expression (HemiF / hE37R) comparable to that of the functional mPTMs (Fig.3.14A and B). Endogenous murine *DYSF* mRNA transcript could

A
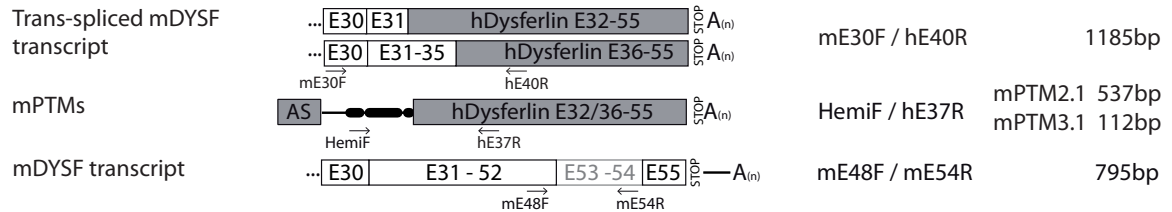
B
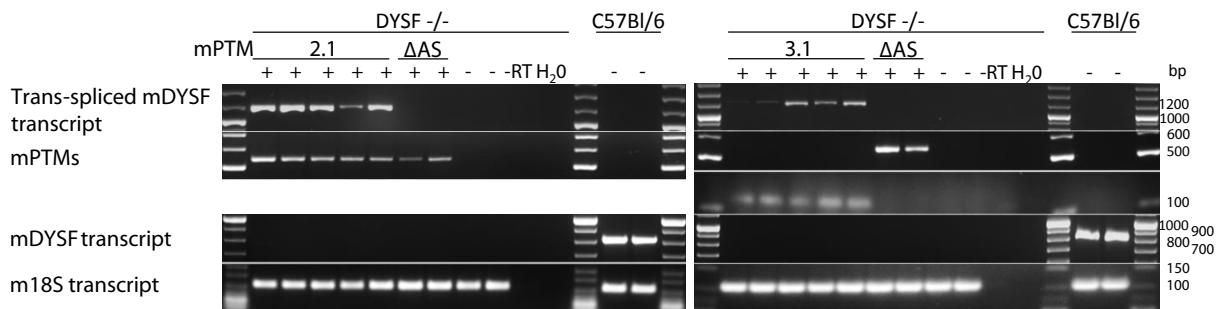
C
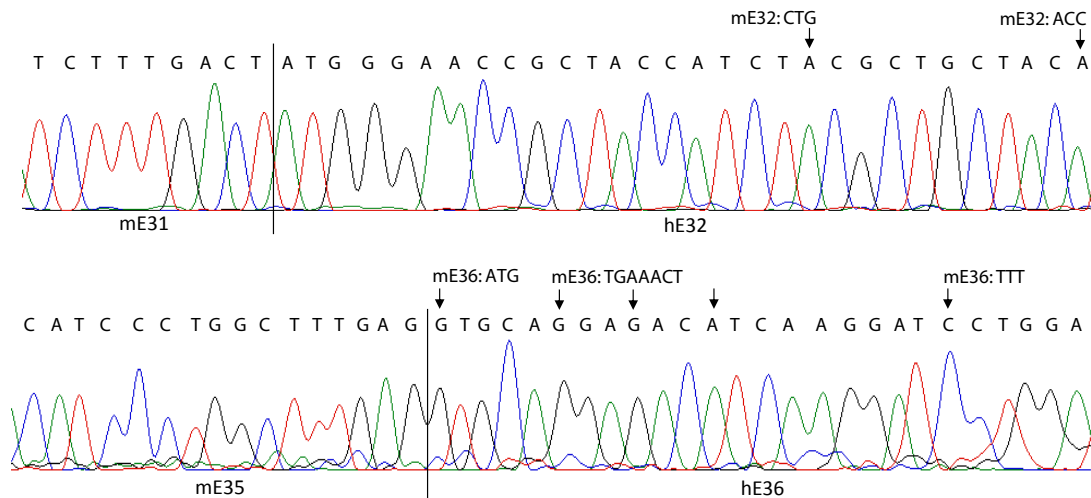
Figure 3.14: *Trans*-splicing of the murine *DYSF* pre-mRNA by mPTM2.1noHA and mPTM3.1noHA following intramuscular injection of rAAV2/1-mPTM2.1noHA and rAAV2/1-PTM3.1noHA into *tibiales anteriores* of *DYSF-/-* mice. (**A**) The *trans*-spliced chimera of mDYSF and hDYSF was detected by PCR on cDNA using mE30F and hE40R primers. The PTM2.1, PTM3.1 and the control PTMΔAS, lacking an AS, were detected by PCR on cDNA using the HemiF/h37R primer set. The murine *DYSF* transcript was amplified using the primer set mE48F/mE54R, where mE54R is situated in the KO region. As a quantitative control m18S was amplified on the cDNA samples. (**B**) All PCRs were performed at 35 cycles. Reverse transcription omitting the reverse transcriptase (-RT) lead to no amplification proving the absence of DNA in the reactions. (**C**) Sequencing of the amplicons received by PCR using the m30F/h40R primer set on cDNA. Arrows indicate nucleotides identifying the human *DYSF* sequence replacing the mDYSF 3'mRNA portion.

not be detected by RT-PCR on total RNA extract from all injected *DYSF-/-* mice using the same primer set as for the detection of endogenous *DYSF* in wild-type mice before (data not shown). Instead RT-PCR using a reverse primer situated in the deleted gene region (mE54R) was performed to confirm the homozygous knock-out on mRNA level (Fig.3.14A and B). Detected amplicons of *trans*-spliced mDYSF were sequenced exhibiting the respective chimeras of the murine and human *DYSF* sequence comprising the respective intact boundaries after *trans*-splicing by mPTM2.1noHA and mPTM3.1noHA (Fig.3.14C). By fluorescence immunostaining on transversal sections using the dysferlin Hamlet antibody that recognizes the dysferlin C-terminus, it was shown that 3'mRNA replacement of the *DYSF* messenger by mPTM2.1noHA and mPTM3.1noHA in *DYSF-/-* mice facilitated the rescue of dysferlin protein (Fig.3.15). However, the rescued protein was detected exclusively in groups of fibres on transversal sections and the overall abundance of rescued protein was not high enough to be detected by immunoblot (Fig.3.16). As observed before after mPTM2.1 injection in *C57Bl/6 tibialis anteriores,* no translation of the mPTM2.1 could be detected.

3.3 RNA-based dysferlin repair by excision of dysferlin exon 32 using tricyclo-DNA splice-switching oligonucleotides

3.3.1 Feasibility of dysferlin exon 32 excision for dysferlin protein rescue by tricyclo-DNA antisense oligonucleotides *in vitro*

To design splice switching antisense-oligonucleotides (AON), the human *DYSF* exon 32 was analysed using the bioinformatical tool ESE finder 3.0 ((Cartegni et al., 2003), chapter 4.1) to identify putative exon splicing enhancer (ESE) sequences. Identified ESEs are putative binding sites of the Sr-proteins SF2/ASF, SC35, SRp40 and SRp55, which are crucial for exon recognition by the spliceosome during the pre-mRNA splicing process. The intention was to disrupt binding of SR-proteins to ESEs by masking them and to therefore provoke the omission of the exon 32 by the spliceosome resulting in its excision together with the up- and dowonstream lying introns. Integrating the intended therapeutic application, the aim was to identify the most effective AON when applied singly and not in combination with other AONs. The five different AONs hAON1, hAON2, hAON3, hAON4 and hAON5 complementary to the human *DYSF* exon 32 sequence were designed, each masking one or several putative ESEs (Fig. 3.18A). AON sequences were analysed using the blastn algorithm on the refseq_rna database of the BLAST online software (http://blast.ncbi.nlm.nih.gov/Blast.cgi?CMD=Web&PAGE_TYPE=BlastHome) to exclude sequences that exhibited high complementarity to off-target binding sites. AONs were also analysed for secondary structure formation using the vector NTI® oliconucelotide analysis for thermodynamic properties to exclude sequences that led to the formation of AON dimers or hairpins. The percentage of guanosine and cytosine nucleotides inherent to each hAON design (GC-contents) was determined and the predicted melting temperature was calculated using OligoTM software (chapter 4.1) (Fig.3.18B). tcDNA-hAONs of the designed sequences were synthesised by the collaborating laboratory of Christian Leumann at the University of Bern, CH. Testing for exon skipping feasibility was performed by transfection of myoblasts of the human myoblast lines IM WT3 and human
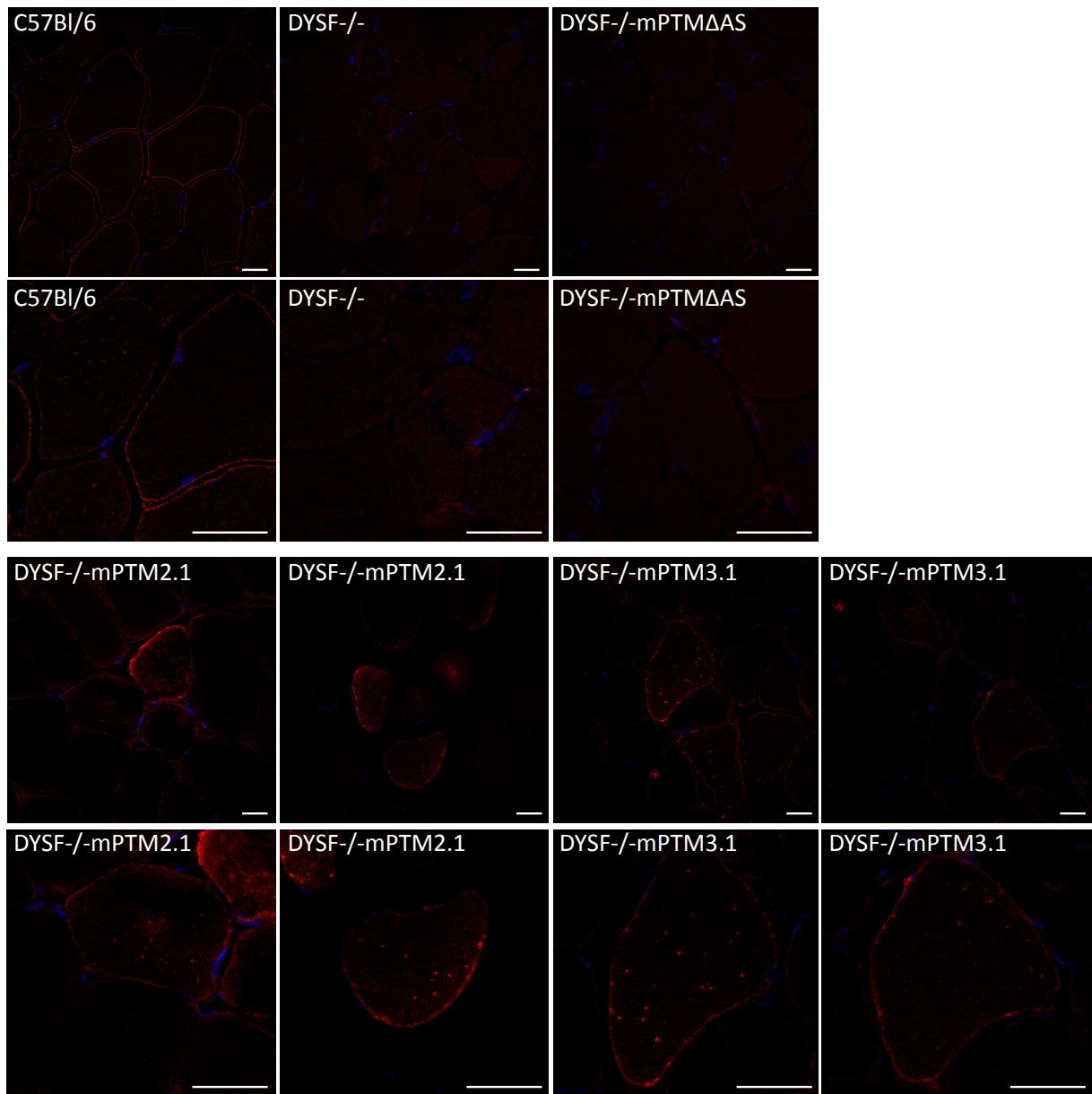
Figure 3.15: Dysferlin rescue by *trans*-splicing of the *mDYSF* pre-mRNA after intramuscular injection of rAAV2/1-mPTM2.1noHA (here mPTM2.1) and rAAV2/1-mPTM3.1noHA (here mPTM3.1). *Tibiales anteriores* transversal sections were immunostained for dysferlin protein using Hamlet antibody recognizing the dysferlin C-terminus. Scale bar for lower magnification depicts 20μm and for high magnification 50μm.
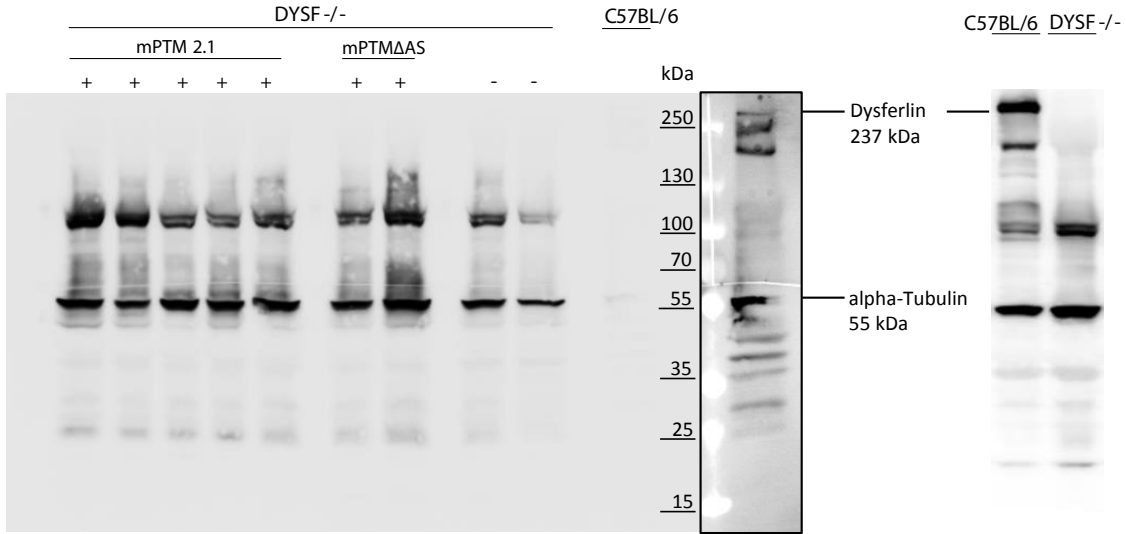
Figure 3.16: Detection of dyserlin protein rescue by *trans*-splicing in *DYSF-/-* was not possible by immunoblot. Lysates from injected (rAAV2/1-mPTM2.1noHA and -mPTMΔAS) and uninjected *DYSF-/-* TAs (80µg) and a *C57Bl/6* TA (10µg) were seperated by SDS-page electrophoresis and dysferlin protein was detected by anti-dysferlin Hamlet antibody at 237kDa. alpha-Tubulin protein detection served as a loading control. The control *C57Bl/6* lysate is additionally shown (framed) after a longer exposure. The seperation of 80µg *C57Bl/6* and *DYSF-/-* lysate from another immunoblot is shown on the right to indicate the proper migration of murine dysferlin protein and the detection profile of Hamlet antibody on *DYSF-/-* skeletal muscle lysate.
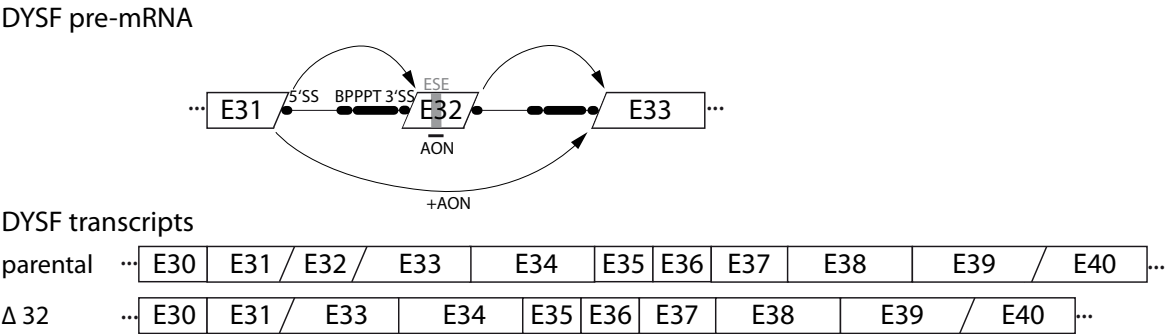
Figure 3.17: Schematic of *DYSF* exon 32-skipping induced by antisense olignucleotides (AONs) masking exon splicing enhancer sequences (ESEs). The application of an effective AON leads to the disruption of exon definiton in the splicing process of *DYSF* pre-mRNA resulting in the excision of the exon together with the up-and downstream lying introns. A portion of total present *DYSF* transcripts is modified into Δ32-transcripts. Out-of-frame encoding exons are indicated by diagonal separation.
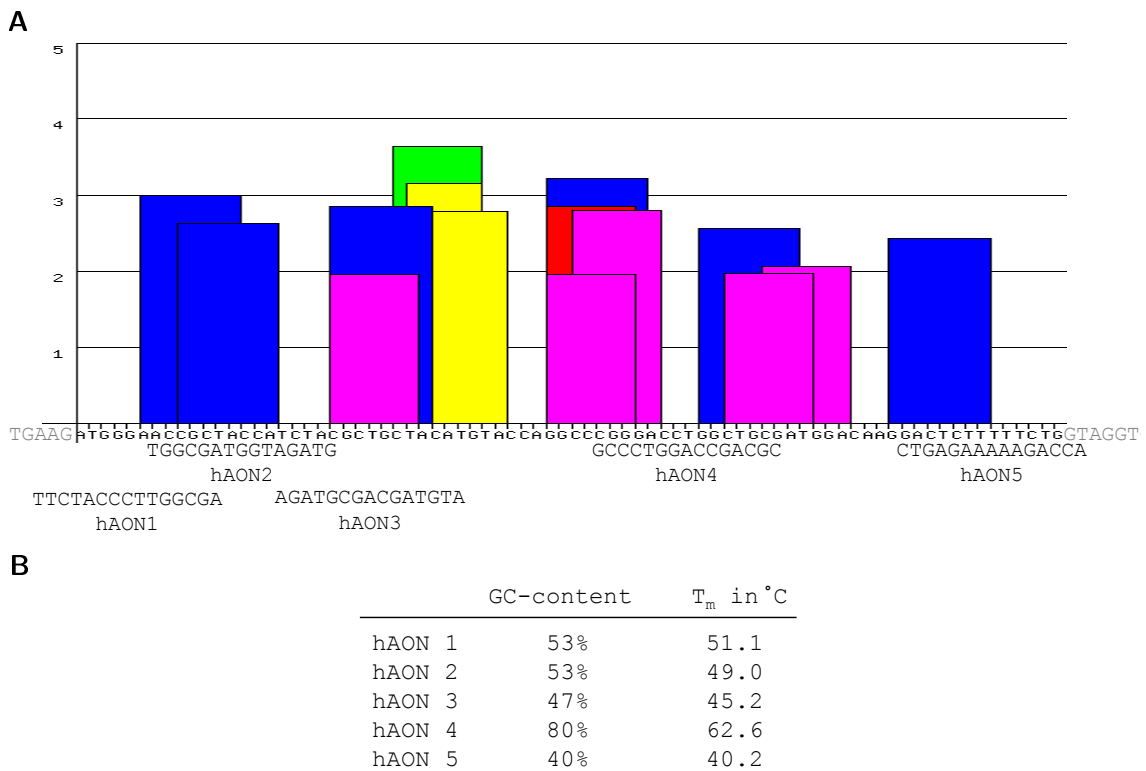
Figure 3.18: 15-mer antisense-oligonucleotides (AONs) complementary to human dysferlin exon 32 were designed in order to mask ESE sequences. (**A**) Graphical presentation of high-scores for putative ESEs identified in human dysferlin exon 32 from ESE finder 3.0 software. Designed hAON1, hAON2, hAON3, hAON4 and hAON5 sequences complementary to the human exon 32 sequence. (**B**) Percentage of guanine and cytosine harbouring tri-cyclo-desoxynucleosides in sequence composition (GC-content) and melting temperature (Tm) of hAONs 1 to 5.

immortalized dysferlinopathy patient myoblasts IM DYSF5 (shared by the Cell line platform of the Institute Myologie in Paris, France). Testing of hAONs in the IM WT3 myoblasts was pursued to analyse exon skipping feasibility under no impact of any mutation in the *DYSF* gene. The IM DYSF5 cell line harboured a heterozygous compound mutation of the *DYSF* gene affecting the 5'SS of intron 4 (c.342+1G>A) and exon 32 (delTT c.3516_3517) and the mutation in exon 32 does not depict any influence on the ESE prediction for exon 32 (Supplementary Fig.7.4). Detected excision of exon 32 was therefore considered independ of the mutations in IM DYSF5. Both mutations evoke a STOP codon (Supplementary Fig.7.5), which was confirmed by the fact that no dysferlin protein could be detected at the size of full-length dysferlin (237kDa) in IM DYSF5 myotube protein extracts (data not shown). This rendered the cell line suitable for the investigation of protein rescue by exon 32 excision.

Myoblasts of IM WT3 and IM DYSF5 cell lines were treated by a single transfection of 10µg of the five different tcDNA-hAONs. Exon skipping feasibility for each hAON was analysed three days following the transfection by nested RT-PCR on total extracted RNA using the human *DYSF* specific internal primer set hE30Fi/hE38R (Fig.3.19A). The Δ32-transcript was detected at highest abundance after application of hAON2 and hAON3 in IM DYSF5 and IM WT3. In both cases, the parental *DYSF* transcript was less abundant in IM DYSF5, as only one allele was targeted in IM DYSF5 due to the compound heterozygous allelic state. Interestingly, treatment by hAON4 masking a sequence including six putative binding sites for SR-proteins led to almost exclusive detection of the Δ32-trasncript and no detection of the full-length parental *DYSF* transcript. Nested PCR using a second set of primers amplifying a larger region of the *DYSF* transcript was performed, but no parental *DYSF* transcript could be detected neither. Notably, the Δ32-transcript was detected not strong enough to possibly depict complete exon skipping efficieny as equal amounts of RNA input were analysed for all five AONs.

Treatment by hAON1 masking the intron internal 3'SS besides a predicted ESE was only weakly effective in IM WT3 myoblasts as only a very faint band at the size of 673bp was detected. hAON1 was therefore not tested in IM DYSF5. hAON5 masking the intron internal 5'SS of the downstream intron induced exon skipping weakly in both cell lines comparing abundance of wild-type- and Δ32-transcript. This was especially prominent in IM DYSF5 myoblasts where only after hAON5 treatment a strong amplification of the parental transcript was detected.

The exact excision of exon 32 after all hAON applications was confirmed by sequencing of excised amplicons (Fig.3.19B). Treatment by hAON3, besides efficient exon skipping, also led to a recurrent side product at the amplicon size of 521bp (Fig.3.19A). Sequencing of the additional amplicon revealed a precise skipping of exon 34 besides the skipping of exon 32 (Fig.3.19C). Alignment on the human genomic *DYSF* sequence depicted an eight nucleotide long match of hAON3 (TCTACGCT) to intron 33 internal sequence (position -9 to -17).

For dysferlin protein rescue by exon 32 excision in IM DYSF5, optimization of the transfection protocol to three consecutive transfections of 10µg tcDNA-hAON was necessary. Differentiation was induced in transfected myoblasts and two further transfections were performed on myotubes. Protein extraction was performed on differentiation day 12 and whole-cell lysate was analysed by immunoblot against dysferlin using anti-dysferlin Romeo antibody which recognized the N-

A

hDYSF transcripts
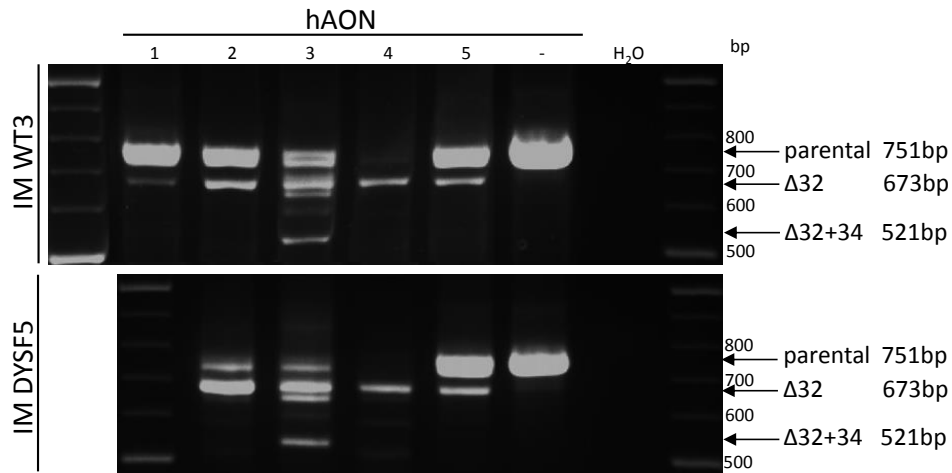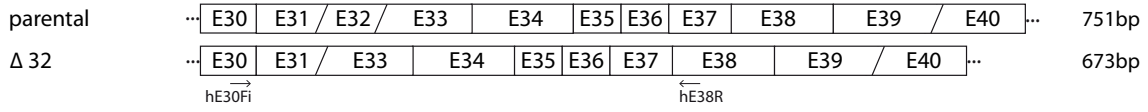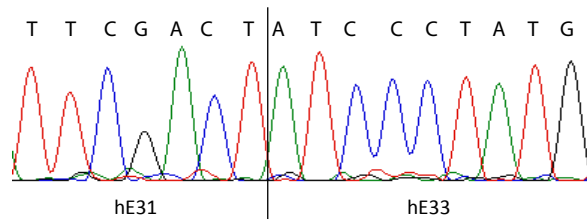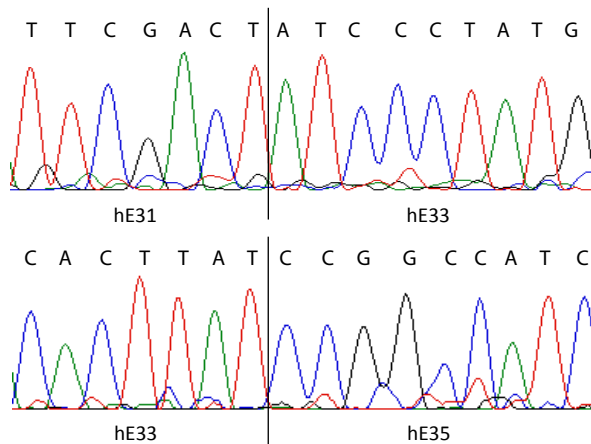
Figure 3.19: Application of tcDNA-hAONs in human myoblast lines IM WT3 and IM DYSF5 leads to skipping of dysferlin exon 32. (**A**) Detection of exon 32 skipping by nested PCR using internal primers hE30Fi/hE38R on cDNA from IM WT3 and IM DYSF5 myoblasts three days after transfection. Exon-phasing is indicated by vertical or diagonal separation, the first depicting exons encoding complete triplets. Data shown are representative for three independently performed experiments. (**B**) Sequence showing the precise exclusion of *DYSF* exon 32 representative for experiments in IM WT3 and IM DYSF5. (**C**) Sequence of a solid recurrent side product of exon 32 skipping induced by hAON4 showing the additional skipping of *DYSF* exon 34.
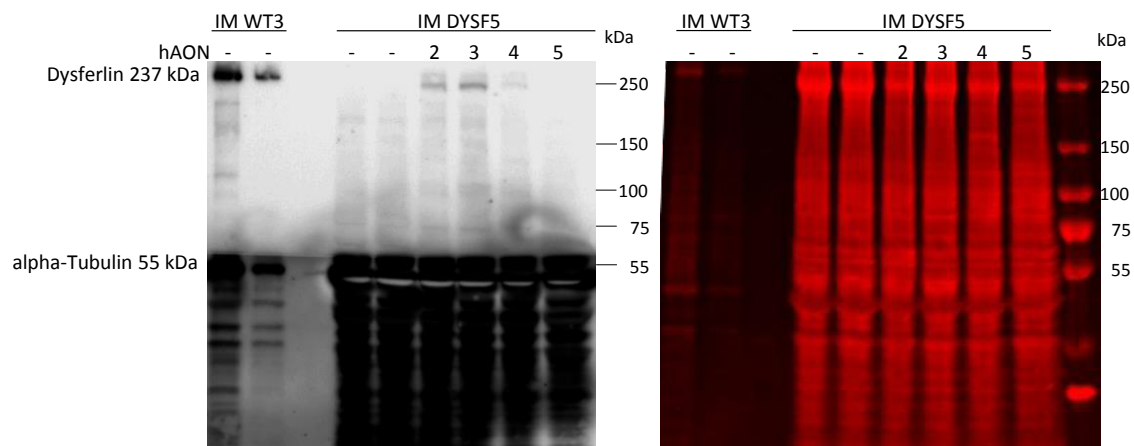
Figure 3.20: Three consecutive transfections of tcDNA-hAONs hAON1, hAON3 and hAON4 led to dysferlin protein rescue in IM DYSF5 by exon 32 excision. Immunoblot against dysferlin using Romeo anti-dysferlin antibody and alpha-Tubulin as a loading control (left). Fluorescent scan of SDS-PAGE (right). Data are representative of two independently conducted experiments.

terminus of the dysferlin protein. Transfections with hAON2, hAON3 and hAON4 led to dysferlin protein rescue (Fig.3.20). hAON 2 and hAON3 induced protein rescue most effectively which was in accordance with the detected high skipping efficiency on RNA level. In contrast, hAON4 revealed to induce protein rescue at a low rate, further suggesting that the result detected on RNA level did not display complete exon 32-skipping. Notably, hAON2 was feasable to induce dysferlin protein rescue in contrast to its comparably low exon skipping efficiency on RNA level. No dysferlin protein rescue was induced after transfection by hAON5 which was slightly contradictive as exon skipping efficiency on RNA level was comparable to hAON4. A high mortality of myotubes was observed following consecutive transfections of hAON4 on myotubes (data not shown), suggesting that hAON4 induced side effetcs which led to a low survival rate of transfected cells. Myotubes were observed to be in a vital condition following all three transfections by the other hAONs (data not shown).

3.3.2 tcDNA-AONs are suitable to induce dysferlin exon 32 skipping *in vivo*

To investigate efficiency of the AON designs tested in human myoblasts and to validate tcDNA a feasible chemistry for *DYSF* exon 32 skipping *in vivo* four 15mer AON sequences were designed complementary to the murine *DYSF* sequence. mAONs were numbered according to their hAON positional counterpart on the human exon 32 sequence (Fig.3.21A). Due to the ESE motif predictions (ESE finder 3.0) for murine *DYSF* exon 32 and analysis of secondary structure formation of AON sequences (vector NTI® oligonucleotide analysis for thermodynamic properties) the counterpart of the hAON3, the murine AON3 (mAON) was not considered. Sequences of the designed mAON1, mAON2, mAON4 and mAON5 were analysed by blastn as described before. GC-content and melting temperatures were determined as for hAONs (Fig.3.21B). Skipping efficiency of the syntheziseed tcDNA-mAONs complementary to the murine exon 32 (synthesis by Christian Leuman laboratory, University of Bern, CH) was first tested *in vitro* in murine C2C12 myoblasts. Cells were

A

B

	GC-content	T_m in °C
mAON 1	54%	51.6
mAON 2	60%	50.3
mAON 4	74%	60.5
mAON 5	54%	40.3
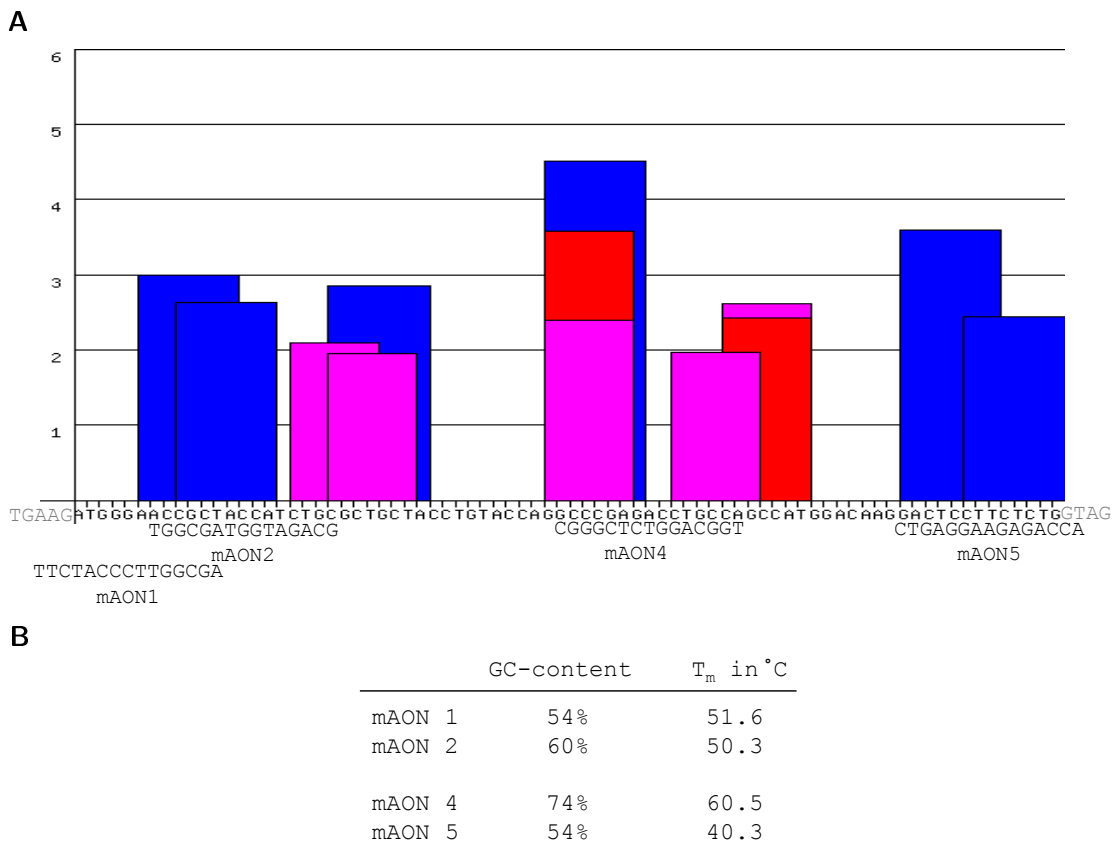
Figure 3.21: Four mAONs were designed masking ESEs of murine exon 32 in order to induce exon 32 exclusion. (A) Graphical presentation of high scores for putative ESEs identified in murine exon 32 from ESE finder 3.0 software. (B) GC-content and melting temperature Tm of mAONs.

A

mDYSF transcripts
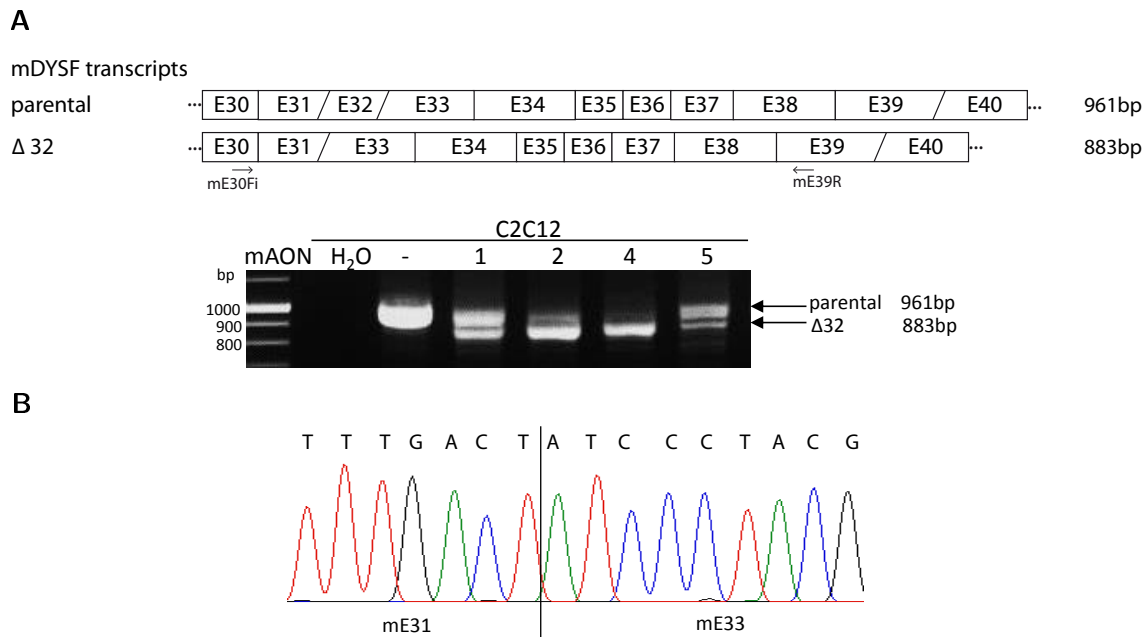
Figure 3.22: Application of tcDNA-mAONs mAON1, mAON2 , mAON4 and mAON5 led to skipping of murine exon 32 in C2C12 cells. (A) Detection of exon 32 skipping by nested RT-PCR using internal primers mE30Fi / mE39R on total RNA from C2C12 cells three days after transfection detecting the parental *DYSF* transcript at 961bp and the Δ32-transcript at 883bp. Data shown are representative for three independent experiments. (B) Sequencing of the Δ32-transcript depicted the exact exclusion of murine exon 32.

transfected with tcDNA-mAONs and *DYSF* exon 32 skipping was analysed after 72 hours by nested RT-PCR on total RNA using the internal primer set mE30Fi/mE39R specific to the murine *DYSF* sequence (Fig.3.22A). Exon 32-skipping at near complete efficiency was induced by mAON4, masking six putative ESE motifs. Interestingly, near complete absence of the parental *DYSF* transcript was as well observed for hAON4 before, likewise masking six putative binding sites for Sr-proteins. Abundance of the murine Δ32-transcript induced by mAON4 was as well surprisingly weak assumimg that exon 32-skipping had taken place at complete efficiency. mAON2 induced very efficient exon 32 excision, as was likewise observed for hAON2. mAON1 and mAON5, masking intron internal 3' and 5'SS framing the exon, respectively, induced skipping at lower levels than exon internally masking mAON2 and mAON4 (Fig.3.22A). This was observed before for hAON1 and hAON5 equally masking intron internal splice sites. The precise excision of murine exon 32 was confirmed by sequencing of all amplicons detected at 883bp size (Fig. 3.22B).

Consequently, all four mAONs were injected into *tibiales anteriores* of 8 week old *C57Bl/6* wild-type mice. Application of tcDNA-mAONs was conducted in wild-type mice to analyse the *in vivo* efficiency of exon 32-skipping under no influence of mutations in the *DYSF* sequence. Injections were performed as a one-time dose of 100μg tcDNA-mAON per muscle. Exon skipping was analysed after four weeks by nested RT-PCR on total extracted RNA using the internal primer set mE30Fi/mE39R. Results obtained from RT-PCR showed all mAONs to induce *DYSF* exon 32-skipping. Analysing the RT-PCR results, mAON4 induced exon skipping most efficiently, followed by mAON2 (Fig.3.23A). Both mAONs were very effective, but did not induce near

A

B

C
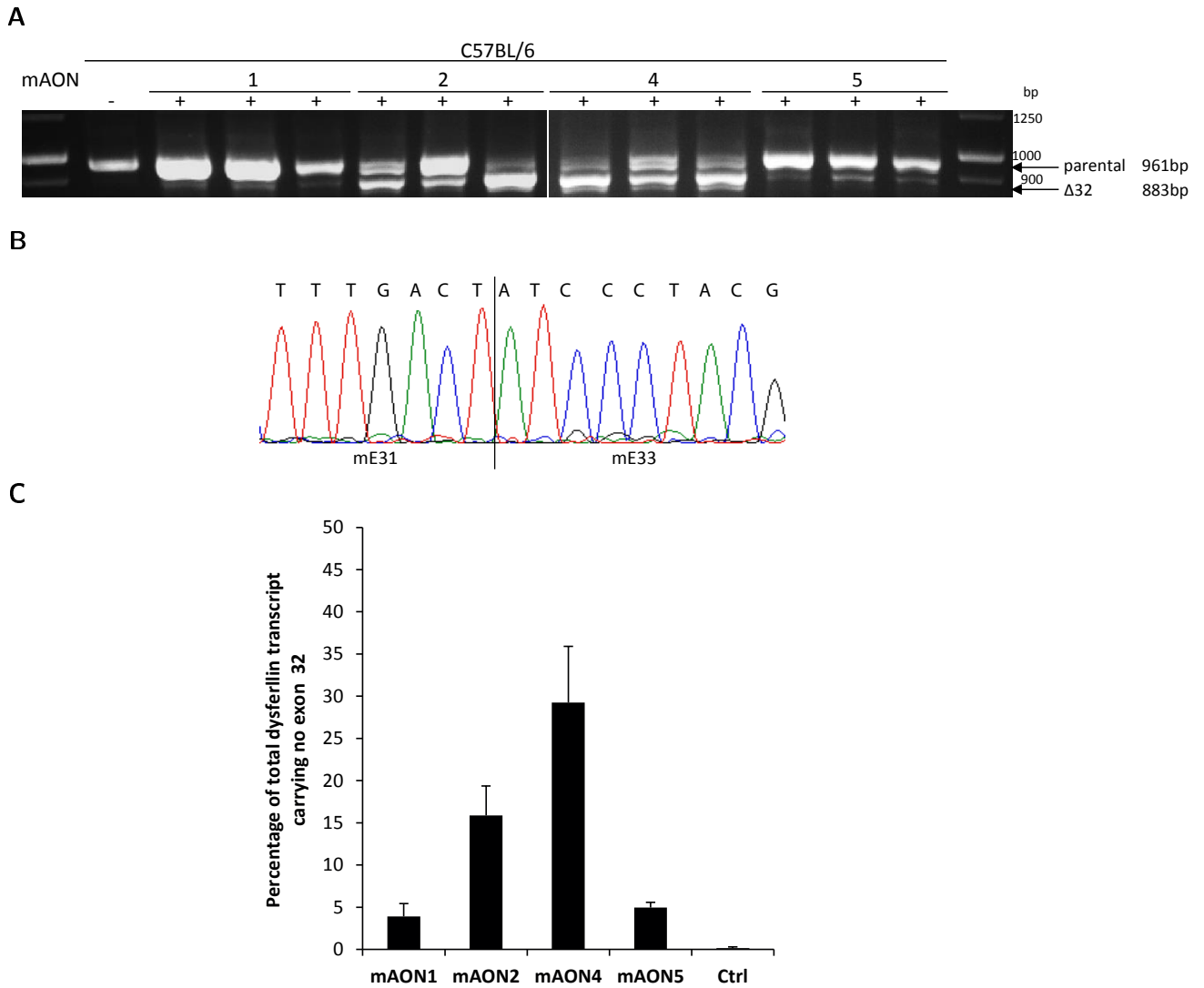
Figure 3.23: Injection of a one-time dose of 100μg of tcDNA-mAONs mAON1, mAON2 , mAON4 and mAON5 in *tibiales anteriores* of C57Bl/6 mice induced skipping of murine exon 32 . (**A**) Detection of exon 32 skipping by nested RT-PCR using internal primers mE30Fi/mE39R on total RNA four weeks after injection detecting the parental dysferlin transcript at 961bp and the Δ32-dysferlin transcript at 883bp. Data shown are representative for two experimental sets of n=3. (**B**) Sequencing of the Δ32-dysferlin transcript exhibited the exclusion of murine exon 32. (**C**) Quantification of present Δ32-dysferlin transcript by qRT-PCR on one of two experimental sets. Percentage of total dysferlin transcript comprising no exon 32 (±STDEV) is presented.

complete absence of the parental dysferlin transcript as was observed in the *in vitro* testing. RT-PCR results further suggested that mAON1 and mAON5, masking intron internal sequence, led to exon 32 excision in a very low number of dysferlin transcripts (Fig. 6A).

Precise excision of murine *DYSF* exon 32 *in vivo* was confirmed by sequencing of the detected Δ32-transcripts (Fig.3.23B). To determine the accurate skipping efficiency of the four mAONs, quantitative RT-PCR (qRT-PCR) using SYBR green assay was performed on one sample set. As indicated by the RT-PCR results, mAON4 induced exon 32 excision most efficiently followed by mAON2 (Fig.3.23C).

4 Material and Methods

4.1 Bioinformatic analysis of RNA and DNA sequences

The evaluation of 3'SS strength was performed using MaxEntScan::score3ss (http://genes.mit.edu/burgelab/maxent/Xmaxentscan_scoreseq_acc.html) (Yeo and Burge, 2004). By this algorithm intron internal 3'SS sequences (position -20 to +3) were given a score exploiting a modelled consensus sequence motif based on the maximum entropy principle. Established models were tested on a data set of ~12000 metazoan introns by Yeo et al. Identified motifs in a sequence are ranked with a value reflecting their conservation, hence their signaling strength in the splicing process. The highest value ever given to a 3'SS was ~14.

For the identification of exonic splicing enhancers (ESEs) ESE finder 3.0 was employed (http://rulai.cshl.edu/cgi-bin/tools/ESE3/esefinder.cgi?process=home) (Cartegni et al., 2003; Smith et al., 2006). ESE finder 3.0 was developed employing positional weight matrices corresponding to binding motifs of Sr-proteins SF2/ASF, SC35, SRp40 and SRp55 for the identification of putative ESEs. ESE finder 3.0 displays scores of motifs identified in 1 nucleotide increments by high-score values that exceed a preset default threshold. Default thresholds were calculated as the median values of the highest high-scores of detected motifs in a set of thirty 20nucleotide-long mammalian sequences by Cartegni et al. For all presented ESE predictions the default threshold settings were used.

The secondary structure of antisense sequences and their targets was analysed on RNAfold WebServer (http://rna.tbi.univie.ac.at/cgi-bin/RNAfold.cgi) (Hofacker, 2003) using settings to display minimum free energy structure and base-pairing probability matrix. Antisense sequences showing a low likeliness to form closed inaccessible secondary structures were chosen (data not shown).

Melting temperatures of primers and antisense oligonucleotides were calculated using the OligoTM software (http://www.dsi.univ-paris5.fr/bio2/OligoTM.html) that calculates melting temperatures according to the nearest neighbour method (Breslauer et al., 1986; Freier et al., 1986).

4.2 Pre-mRNA *trans*-splicing molecule constructs

DYSF cDNA sequences were amplified from a human *DYSF* cDNA plasmid (NM_003494.2) (gift from Dr. Steven Laval, Newcastle Upon Tyne, UK) by polymerase chain reaction (PCR) integrating the described splicing sequences and the influenza hemaglutinin-tag (HA-tag) (constructions

primers are listed in 8.1.1.1). Amplicons were purified and subcloned into pSMD2 (Snyder et al., 1997) after Kpn1 and EcoR1 digestion. Antisense sequences (AS) were amplified on human and murine genomic DNA according to the human intron internal dysferlin sequences (NG_008694.1) integrating the spacer sequence (Rodriguez-Martin et al., 2005). For trans-splicing of intron 30 AS1 was complementary to nucleotide position +604 to +761, AS2 from -150 to -1 of intron 30; for intron 31 AS1 from position +211 to -188, AS2 from -96 tov-1 of intron 31 and for AS3 from +3 of exon 32 to +137 of intron 32; for intron 35 AS1 from position +383 to +533, for AS2 from -150 to -1 of intron 35 and for intron 36 AS1 from +549 to +709 and AS2 from -153 to -1 of intron 36. They were purified and subcloned into the respective cDNA-pSMD2 construct. For lentiviral vector production the entire PTM cassettes were subcloned into pRRLSIN.cPPT.hPGK-MCS.WPRE at the Xba1 site (Follenzi, 2000). For the construction of mPTMs containing the HA-tag, ASs in the original pSMD2 constructs were exchanged for the murine ASs. For mPTMs lacking the HA-tag cDNA sequences were reamplified on PTM-pSMD2 constructs excluding the HA-tag. They were subcloned into pSMD2 and murine ASs (NC_000072.5) were integrated. For trans-splicing of murine intron 31 mAS1 was complementary to nucleotide position +266 until -166, for AS3 from +3 of exon 32 to +109 of intron 32 and for murine intron 35 AS1 from position +249 to +368 and AS2 from -123 to -1. All cassettes integrated into pSMD2 were run under a CMV promotor and controlled by a poly-A signal. pRRL constructs were analysed by restriction analysis using Hind3 and pSMD2 constructs by Hind3 or BamH1 restriction enzymes (Fig.4.1A and B). All constructs were sequenced and quantified using a photospectrometer prior virus production.

4.3 Lentivirus production

VSV glycoprotein G-pseudotyped lentiviral vectors were produced by transient quadri-transfection of 293T cells with pBaRev, pMDG, pHDMH gpm2 and the transgene carrying pRRLSIN.cPPT.hPGK-MCS.WPRE (Follenzi et al., 2000). pHDMH gpm2 encoded the structural precursor protein gag and the pol protein encoding the viral reverse transcriptase, RNaseH, integrase and HIV1 protease. pBaRev encoded the HIV1 Rev protein essential for viral replication. pMDG encoded the VSV glycoprotein G pseudotyping the generated viruses. pRRLSIN.cPPT.hPGK-MCS.WPRE is a self-inactivating HIV1 based lentiviral backbone, carrying a 400nt deletion in the 3'LTR, thus abolishing the promotor activity of the LTR and hence the replication competence of the generated viral vectors (Zufferey et al., 1998). Transgenes expressed by pRRLSIN.cPPT.hPGK-MCS.WPRE were driven by a human phosphoglycerate kinase-1 (PGK-1) promoter. Following the quadri-transfection the culture medium was collected and pooled after 24, 36 and 72 hours. Collected medium was concentrated by ultra-centrifugation and subsequent discard of supernatant. Viral vectors were resuspended in 0.1%BSA in PBS and stored subsequently at -80°C. Quantification of viral vectors was conducted by quantitative real-time PCR performing SYBR green assay (ROX qPCR Master Mix, SABiosciences™) on genomic DNA from transient transductions of HCT116 cells with a serial dilution of produced viral vectors. Amplification on viral LTRs was normalized to amplification of the human albumin (hALB) gene. A standard curve was obtained from LTR and hALB amplification on known molecule concentrations of a serial dilution of pRRLSIN.cPPT.hPGK-

A

Hind3

| PTM | 1.1 | 1.2 | | 2.1 2.2 2.3 | | 3.1 | 3.2 | | 4.1 |

PTM1.1	PTM1.2	PTM2.1	PTM2.2	PTM2.3	PTM3.1	PTM3.2	PTM4.1
3338	3338	3368	3395	3412	3338	3338	3338
2953	2945	3338	3338	3338	2421	2420	2401
1080	1080	1059	1052	1059	1100	1100	1080
609	609	584	584	584	589	589	609
584	584	556	556	556	584	584	584
556	556	499	499	499	556	556	556
499	499	312	312	312	499	499	499
312	312				312	312	312

B

mPTM2.1	mPTM2.3	mPTM3.1
5822	5822	5849
2808	2813	1320
		1023

mPTM2.1noHA	mPTMΔAS	mPTM3.1noHA
5822	5822	5849
1461	1348	1320
1320	1320	1023

Figure 4.1: Restriction analysis of pRRL and pSMD2 constructs. (**A**) Hind3 restriction analysis of PTM constructs inserted into pRRLSIN.cPPT.PGK-MCS.WPRE (left). Hind3 restriction fragment sizes for PTMs in bp (right). (**B**) Hind3 and BamH1 restriction analysis and fragment sizes in bp of mPTM constructs including (left) and lacking HA-tag inserted into pSMD2 (right).

MCS.WPRE and pMOI-ALB and were used to quantify amounts of viral and albumin molecules present in experimental samples (Charrier et al., 2005).

4.4 Immortalized human myoblast culture, transduction and transfection

Human immortalized myoblasts (IM DYSF1, IM DYSF2, IM DYSF3, IM DYSF4, IM DYSF5 and IM WT3) were cultured (at 37˚C in humdifiied atmosphere and 5% CO_2) in proliferation medium consisting of a 1:4 ratio of Medium199 (+GlutaMAX™; +Earle's Salts) (Life Technologies) and DMEM (+4.5g/L D-Glucose; +L-Glutamine; +Pyruvate) (Life Technologies) supplemented with 20% fetal calf serum (Life Technologies) and 50μl/mL gentamycin (Life Technologies) (Mamchaoui et al., 2011).

Myoblasts were transduced with lentivirus vectors in 6-well plates in 800μl reduced proliferation medium (5% fetal calf serum) directly after their trypsination at a multiplicity of infection (MOI) of 3; 5 and 10 and were diluted 24hrs later by 1200μl proliferation medium. Cells were washed and incubated in fresh proliferation medium another 24hrs later. 3 to 5 days after transduction, differentiation was induced by incubation in serum-reduced Opti-MEM (Reduced Serum Medium) (Life Technologies) until differentiation day 14.

Myoblast transfection with tcDNA-AONs was performed emplyoing Oligofectamine™ Reagant (Life Technologies). The standard Oligofectamine™ Reagant transfection procedure for 6-well plates was followed as described. 12μl of a 1:2 ratio of Oligofectamine™ Reagant and DMEM (+4.5g/L D-Glucose; +L-Glutamine; +Pyruvate) (Life Technologies) were added to 90μl DMEM supplemented by 10μg tcDNA-AON for complex formation. The complexes were applied in a volume of 800μl DMEM per well. 1200μl of proliferation medium was added four hours post transfection. Transfected myoblasts were harvested 72 hours post transfection for exon-skipping analysis on RNA level. To yield dysferlin protein rescue, differentiation was induced 96 hours after the first transfection by replacing proliferation medium with serum-reduced Opti-MEM (Reduced Serum Medium) (Life Technologies). The second transfection was performed on differentiation day 2 and the third on differentiation day 7. Instead of DMEM transfections on myotubes were performed using serum-reduced Opti-MEM. Myotubes were harvested on differentiation day 12 and stored at -80˚C.

4.5 Murine myoblast culture and transfection

Murine C2C12 immortal myoblasts (Blau et al., 1985) were cultured in DMEM (+4.5g/L D-Glucose; +L-Glutamine; +Pyruvate) (Life Technologies) supplemented with 10% fetal calf serum (Life Technologies) and Penicillin (100units/mL)/Streptomycin (100μg/mL) (Gibco). Transfection with tcDNA-AONs was performed as described for human immortalized myoblasts using C2C12 myoblast proliferation medium. Myoblasts were harvested 72 hours post transfection and stored at -80˚C.

4.6 Recombinant adeno-associated virus production and animal experiments

Recombinant adeno-associated viral vectors of serotype 2 pseudotyped with an AAV serotype 1 capsid (rAAV2/1) were produced by a tri-transfection protocol using helper plasmids pXX6 and pLT RCO2 (Riviere et al., 2006) and the transgene carrying pSMD2 plasmid (Snyder et al., 1997). Transgenes cloned into pSMD2 were expressed under the control of a cytomegalovirus (CMV) promoter and a hemoglobin2 (HBB2) poly(A)-signal. pLT RCO2 encodes AAV1 capsid proteins and the AAV2 rep protein, whereas pXX6 is an adenovirus helper plasmid encoding a mini-adenovirus genome that is incapable of producing infectious adenovirus allowing rAAV production without adenovirus helper virus (Xiao et al., 1998). All rAAVs were produced by Guillaume Precigout (Garcia Lab, UFR UVSQ, France). Intramuscular injection of viral vectors at titres between 5E+11 and 2E+13 viral genomes per ml (vg/ml) in phosphate buffered saline was performed into tibiales anteriores of 4 months old C57Bl/6 and DYSF-/- mice at a volume of 45µl. Intramuscular injection of a one-time does of 100µg of tcDNA-mAONs was performed in a 20µl volume of 0.9 molar sodium chloride solution. Four weeks following the injection animals were sacrificed, *tibiales anteriores* were extracted and snap-frozen in liquid nitrogen-chilled isopentane and stored at -80˚C. Successful rAAV delivery was verified by PCR on cDNA reverse-transcribed from total RNA extraction of injected muscle, using primers sets E48F/HA-tagR and HemiF/hE37R, wherein HA-tagR and HemiF are specific for PTM amplification(primer sequences listed in 8.1.1.2). Successful tcDNA-mAON delivery was verified by the detection of the Δ32-dysferlin transcript in injected versus uninjected TAs (primer sequences listed in 8.1.2). C57Bl/6 mice were obtained from Charles River Laboratories and B6.129-Dysftm1Kcam/J (here referred to as DYSF-/-), first described as 129-Dysftm1Kcam/J (Bansal et al., 2003) from The Jackson Laboratory. As well as described for 129-Dysftm1Kcam/J, B6.129-Dysftm1Kcam/J showed complete knock-out of the dysferlin protein and progressive muscular dystrophy predominantly in proximal limb muscle (Fig.(4.2)). All animal experiments were performed under appropriate biological containment according to protocols approved by state institutions (Germany: LaGeSo Berlin Reg. 0183/13).

4.7 RNA isolation and reverse transcription-PCR analysis

4.7.1 Dysferlin *Trans*-splicing detection

Total RNA was isolated from human myotubes and frozen mouse muscle using RNeasy Mini Kit® and RNase-free DNase Set® (Qiagen). RNA concentration was quantified by NanoDrop® technology. Standardized 300ng of RNA were reverse-transcribed using SuperScript® III First-Strand Synthesis SuperMix (Life Technologies) including OligodT primers. Total human dysferlin transcripts from myotubes were amplified on cDNA using hE30F and hE40R PCR primers (all primer sequences are listed in 8.1.1.2). *Trans*-spliced dysferlin transcripts were amplified by the hE30F/HA-tagR primer set after trans-splicing by PTM 1.1,1.2, 2.1, 2.2 and 2.3 and by the primer set E35F/HAtagR after trans-splicing by PTM 3.1, 3.2 and 4.1. Successful PTM delivery

A
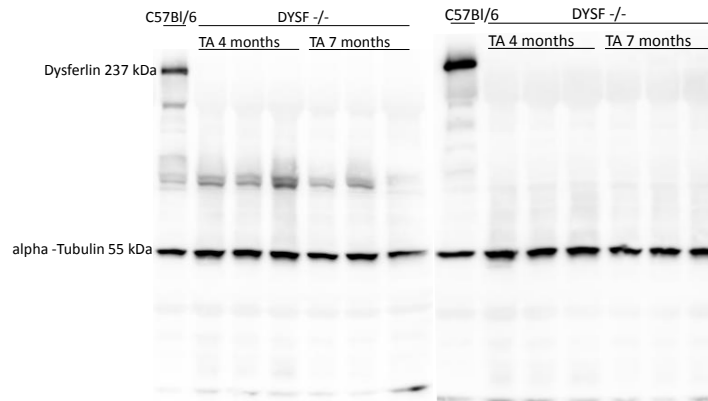
B
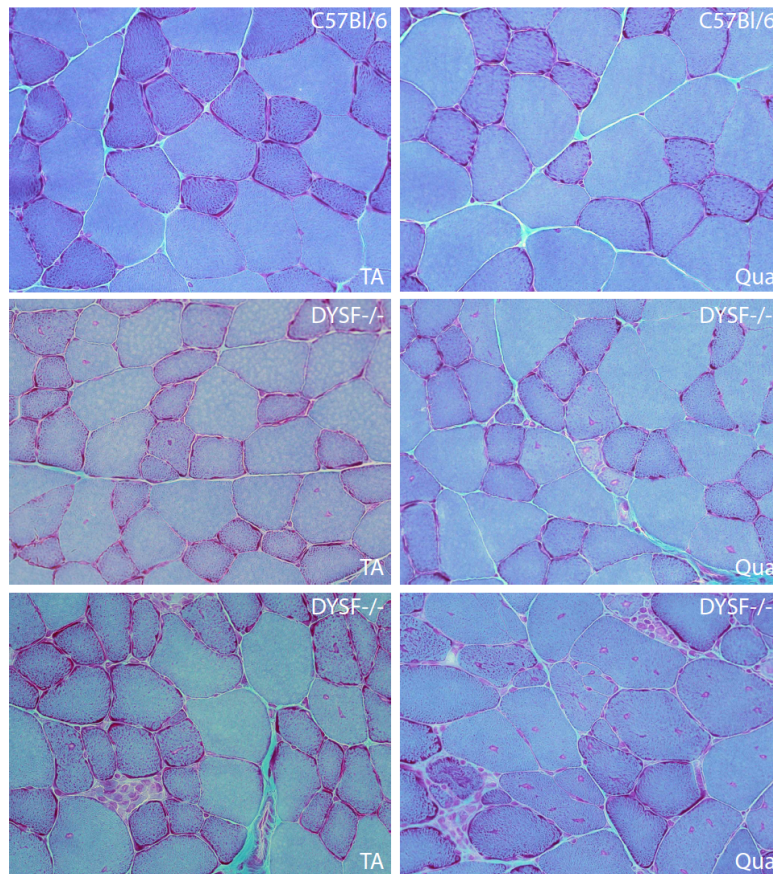
Figure 4.2: DYSF-/- mouse model (B6.129-Dysftm1Kcam/J) depicts complete absence of dysferlin protein and progressive muscular dystrophy with stronger symptomes in proximal muscle than in distal muscle, as described for the human pathology LGMD2-B. (**A**) No dysferlin protein can be detected using anti-dysferlin antbodies Hamlet (Novocastra) and Romeo (abcam). (**B**) Gomori's trichrome staining of TA and Quadriceps (Qua) transversal sections showing C57Bl/6 TA and Qua at 4 months of age, and DYSF-/- TA and Qua at 4 and 7 months of age. The number of centrally nucleated fibres increases with age and is higher in the proximal muscle, as well as abundance of necrotic and inflammatory tissue.

into myotubes was analysed by PCR using primers E48F and HA-tagR. Total murine dysferlin transcripts from C57Bl/6 mice were detected using the primer set mE30F/mE40R. *Trans*-spliced chimeras of murine and human dysferlin after injection of mPTM2.1, mPTM2.3 and mPTM3.1 were detected by nested PCR using the external primers mE30F and hE40R in a 25-cycle PCR and the internal primers mE30Fi and hE37R performing 35 cycles of PCR. The mPTM expression was analysed by PCR on cDNA using the E48F/HA-tagR primer set. *Trans*-spliced dysferlin transcripts from DYSF-/- mice were detected as described for C57Bl/6. Successful delivery of mPTM2.1noHA and mPTM3.1noHA was detected by PCR on cDNA using the HemiF and hE37R primers. The dysferlin knock-out was verified by PCR using the primer set E48F/E54R. The murine 18S rRNA transcript was detected by PCR on cDNA using m18SF/m18SR primers in all animal experiments. PCRs were performed using Phusion High-Fidelity PCR Master Mix with GC-buffer and Dynazyme II PCR Master Mix (Thermo Scientific). Standard protocols were followed apart from optimization of primer annealing temperatures, PCR cycle numbers and addition of Dimethyl Sulfoxide (DMSO).

4.7.2   Dysferlin exon 32-skipping detection

Dysferlin exon 32 excision from the dysferlin pre-mRNA in human myoblasts was detected by nested RT-PCR on extracted total RNA three days after the transfection of IM WT3 and IM DYSF5 human myoblasts using the external primer set hE30F/hE40R and the internal primer set hE30Fi/hE38R (all primer sequences are listed in 8.1.2). Dysferlin exon 32 excision from murine dysferlin pre-mRNA following tcDNA-mAON injection was detected by nested RT-PCR using mE30F/mE40R external primers and mE30Fi/mE39R internal primers. All RT-PCRs were performed using Access Quick™ RT-PCR System (Promega) including external primer pairs. Internal PCRs were performed on unpurified PCR products using PCR Master Mix (Promega) including respective internal primer pairs.

All RT-PCR products were separated by gel electrophoresis in 2-3% agarose gels and purified using NucleoSpin Gel and PCR Clean Up® (Macherey and Nagel) before Sanger sequencing (GATC Biotech and Source Bioscience Sequencing Berlin).

4.8   Quantitative reverse transcription-PCR analysis

Skipping efficiency was quantified by comparing the presence of Δ32-dysferlin transcript to the inherent full-length dysferlin transcript abundance in each sample employing ΔΔCt calculation (Schmittgen and Livak, 2008). The Δ32-dysferlin transcript was amplified using mE31F/mE31_33R primers, wherein mE31_33R anneals on murine dysferlin exon 31 by its first three nucleotides only (all primer sequences are listed in 8.1.2). The full-length dysferlin transcript was amplified using mE31F/mE31_32R primers. Amplification of both transcript versions was normalized to inherent murine 18S amplification in each sample prior calculation of skipping efficiency. Primer efficiency was determined on serial dilution of Δ32-dysferlin and full-length dysferlin RT-PCR product. All quantifications were performed by SYBR green assay using Sso Fast™ EvaGreen®

Supermix (Bio-Rad).

4.9   Fluorescent immunochemical stainings

4.9.1   Human myotubes

Staining of immortalized myoblasts was performed using mouse monoclonal antibodies anti-myosin heavy chain (slow) and anti-dysferlin Hamlet (both Novocastra) (both 1:20), anti-human desmin (Dako) (1:100), anti-caveolin3 (Santa Cruz Biotechnology) (1:30) and anti-alpha-actinin (sarcomeric) (both Sigma-Aldrich) (1:2000) in combination with secondary Alexa 488- or Alexa 568-conjugated anti-mouse IgG antibodies (Life Technologies) (1:500). Human myotubes treated with PTMs were immunostained using Alexa 488-conjugated anti-dysferlin Romeo antibody (Abcam, customized) (1:20) and mouse monoclonal anti-HA-tag (Covance) (1:1000) as primary antibodies combined with secondary Cy3-labelled donkey anti-mouse IgG antibody (Jackson ImmunoResearch) (1:500). In preparation of the immunostaining myoblasts and myotubes were washed in PBS (Life Technologies) and fixed for 15 minutes in 4% formaldehyde in PBS, followed by three washes in PBS 5 minutes each. Cells were permeabilized by incubation in a 0.2% TritonX100 (Sigma) dilution in PBS for 20 minutes. A blocking step using 5% BSA in PBS was performed at room temperature (RT) for 1 hour. Incubation with primary antibodies was performed in 1%BSA in PBS overnight at 4°C and high humidity. The following day myotubes were washed 3 times in PBS 5 minutes each and incubated with the secondary antibody in 1% BSA in PBS for 45 minutes at RT followed by three washes for 5 minutes each in PBS. Nuclei-staining using Hoechst 33258 (1:2000) (Life Technologies) was performed for 3 minutes followed by another three washes in PBS. Stained cells were kept at 4°C until micoscropic investigation was performed using a Zeiss LSM-510 Meta Miscroscope.

4.9.2   Murine cryo-sections

Transversal cryo-sections of 10μm were cut from mice *tibiales anteriores* and immunostained using mouse monoclonal anti-Dysferlin Hamlet antibody (Novocastra) (1:20). For secondary detection the M.O.M. Basic Kit (Vector Labs) in combinaton with Cy3-labeled Streptavidin (Jackson ImmunoResearch) (1:500) were used. In preparation of the staining cryo-sections were air-dried for approximately 30 minutes. Antigen-retrival was performed incubating sections in Vector® Antigen Unmasking Solution (Vector Labs) at 70°C for 60 minutes. Sections were fixed in 100% acetone at -20°C for 5 minutes. Sections were washed in PBS once for 2 minutes. The standard protocol of M.O.M. Basic Kit was followed with the exception of incubating sections with the primary antibody at 4°C overnight. Sections were stained with Hoechst 33258 (Life Technologies) (1:1000) nuclei-staining for 5 minutes, were washed 5 times in PBS for 5 minutes each, mounted in Vectashield® (Vector Labs) and kept at 4°C until microscopic analysis was performed. Mounted sections were analysed by a Zeiss LSM-510 META confocal miscroscope.

4.10   Histochemical Gomori's trichrome staining

Transversal cryo-sections were cut at 10μm from frozen murine *tibiales anteriores* and air-dried 30 minutes prior the staining procedure. Sections were stained in filtered Hematoxylin (Merck, modified according to Gill II) for five minutes and were rinsed by dipping in distilled water until clear. Subsequently sections were stained in freshly filtered Gomori's Trichchrome (Sigma, HT 10316 LG Solution at pH 3.4) for 10 minutes and differentiated in 0.2% acetic acid until clear. Before mounting sections were dehydrated by a short dip in 95% ethanol and five dips each in three consecutive baths of 100% ethanol. Finally sections were cleared in xylene and mounted using Vitro-Clud® embedding medium (R. Langenbrinck).

4.11   Immunoblot

Protein lysate of myotubes was produced by lysing cell material grown on approximately 10cm2 in 40μl protein extraction buffer (50mM Tris pH7.4, 150mM NaCl, 0.5% Triton X-100, 0.5% Na-deoxycholate, 1mM EDTA, 50mM NaF, 1mM Na-vanadate including protease inhibitors (Pierce)). Protein lysate of murine TAs was produced by lysing 20 sections cut at 12μm in 45μl protein extraction buffer on dry-ice. Lysates were kept on ice for 30 minutes, centrifuged at 1500rpm for 5 minutes at 4˚C and supernatants were transferred into fresh 1.5ml tubes. Protein quantification was performed using BCA Protein Assay Kit™ (Pierce) following the standard protocol. Required amount of protein was mixed with the appropriate amount of SDS sample-running buffer and heated at 45˚C for 15 minutes. Samples were separated in NOVEX® Tris-Glycine 8-16% Mini Protein gels in an XCell SureLock™ Mini Cell Electrophoresis System (Life Technologies) migrating at 140V. Protein extraction and separation were always performed on the same day. Proteins were transferred onto nitrocellulose membranes (Amersham Protran 0.45NC, GE Healthcare) by semidry transfer (Trans-Blot® SD Semi-Dry Electrophoretic Transfer Cell, Biorad) using methanol supplemented transfer buffer at 18V for 1.5 hours. Membranes were blocked in 10%milk in PBS for 1 hour at RT. Primary mouse monoclonal antibody Hamlet anti-Dysferlin (Novocastra) (1:100), mouse monoclonal antibody anti alpha-Tubulin (Sigma-Aldrich) and rabbit monoclonal antibody Romeo anti-Dysferlin (abcam) were applied to membranes in 4%milk in PBS and membranes were incubated at 4˚C overnight. HA-tagged PTMs were detected using mouse monoclonal anti-HA-tag antibody (HA.11 Clone 16B12; Covance) (1:1000) applied in 10% milk in PBS and membranes were incubated at 4˚C overnight. The following day membranes were washed in PBS containing 0.05% Tween-20 three times at RT for 10 minutes. Secondary antibody HRP-conjugated Goat anti-mouse IgG and HRP-conjugated Goat anti-rabbit IgG (Life Technologies) (1:5000) were applied in 4%milk in PBS for 1 hour at RT. HRP signal was detected using SuperSignal West Dura Chemiluminescent Substrate (Pierce).

4.12 Laser-mediated membrane wounding

Shortly before performing the membrane wounding myotubes were washed once in Tyrode solution (140 mM NaCl, 5 mM KCl, 2 mM $MgCl_2$, 2.5 mM $CaCl_2$ and 10 mM HEPES, pH 7.2). The wounding experiment was performed in Tyrode solution supplemented with the FM1-43 dye (2.5µM; Molecular Probes, Invitrogen, Paisley, UK). Myotubes were wounded by the irradiation of a 2.5 x 2.5µm surface area for 58 s at 50% of the laser power (30mW argon-laser) employing a Zeiss-LSM 510 META confocal microscope. Images were taken with a 63x oil immersion objective every 20s for 280s after wounding and were processed using the Zeiss LSM Image Browser software. Changes of fluorescence intensity were calculated using ImageJ software. Fluorescence intensities are indicated ±SEM. Significance was calculated using unpaired two-tailed student's t-test comparing values of each cell line with values of IM WT3 (*p<0.001). Values were tested for normal distribution by D'Agostino & Pearson omnibus normality test.

5 Discussion

5.1 Immortalized human myoblasts differentiate into multi-nucleated muscle cells

The immortalization of once purely myogenic primary myoblast cultures from dysferlinopathy patient biopsies by stable integration of human telomerase reverse transcriptase *(hTERT)* and cyclin-dependent kinase-4 *(cdk-4)* genes (Zhu et al., 2007) allowed uncomplicated cultivation and proliferation of the immortalized myoblasts. A crucial aspect was to investigate myogenicity and differentiation potential of immortalized myoblasts to secure their applicability for the study of new therapeutical approaches in place of primary human myoblasts.

The investigation of the differentiation potential by immunocytochemistry for skeletal muscle structural proteins depicted comparable myogenic differentiation between the immortalized and non-immortalized control myoblast lines IM WT3 and WT (Fig.3.2). Immortalized dysferlinopathy patient myoblast lines IM DYSF1, IM DYSF2 and IM DYSF3 differentiated into multi-nucleated muscle cells that depicted known patterns of cytoplasmatic and membranous structural proteins (Fig.3.2). Mytotubes coming from IM DYSF4 myoblasts depicted the same differentiation potential but formed remarkably large myotubes comprising excessively high numbers of nuclei. The significantly higher fusion index of IM DYSF4 myoblasts compared to WT and IM WT3 myoblasts was in congruence with this observation. Primary myoblasts that were immortalized by transduction with *hTERT* and *cdk-4* genes were depicted before to differentiate more fiercely into large myotubes harbouring a higher number of nuclei than their primary counterparts (Zhu et al., 2007).

Besides the immortalized myoblast lines established from dysferlinopathy patients analysed here, immortalized human myoblast lines have been established from patients with other muscle diseases including facioscapulohumeral muscular dystrophy (MD), Duchenne MD, congenital MD and oculo-pharyngeal MD by overexpression of *hTERT* and *cdk4* (Mamchaoui et al., 2011; Stadler et al., 2011). These other immortalized primary myoblasts were as well shown to proliferate and differentiate into intact myotubes. The fusion capability was observed to be drastically decreased after a population doubling PD above 100 in immortalized facioscapulohumeral MD patient myoblasts (Stadler et al., 2011) which was attributed to epigenetic drift and the constant selection for proliferation. The immortalized myoblast cell lines from biopsies presenting the remaining mentioned MDs were investigated between 27 and 57 PDs (Mamchaoui et al., 2011). Notably, fusion indeces presented here for IM DYSF1, IM DYSF2, IM DYSF3 and IM DYSF4 and IM WT3

cell lines were calculated for myoblasts at a PD below 30 at their entry into differentiation and it was not determined whether at higher PDs fusion capability dereased.

The common feature of the above described immortalized myoblast lines is the overexpression of *hTERT* and *cdk-4* genes. The overall impact the overexpression of the two genes might have, besides telomere elongation and circumvention of cell cycle arrest, might not be neglectable, especially because of the tendency for fast and vehement differentiation observed in low population doublings. It was shown in immortal human GM 847 fibroblasts that hTERT overexpression has yet undefined additional functions besides telomere elongation (Stewart et al., 2002), that were hypothesized to lie in the upregulation of growth factors (Smith et al., 2003) and for *mTERT* the ability to upregulate expression of Wnt-regulated genes (Park et al., 2009). These are both possibilities of misregulation with great impact on myoblasts, as growth factors and Wnt-regulated gene expression regulate myoblast prolifertation and differentiation (Wolf et al., 1992; reviewed in von Maltzahn et al., 2012). The overexpression of *cdk-4* was argued to leave cells capable of undergoing cell-cycle regulation and to withdraw from it, as well at the accumulation of p16^{INK4a} induced by the *cdk-4* overexpression (Ramirez et al., 2003). Taken together the *hTERT* overexpression might bear a greater risk to uncontrollable effects by the immortalization process.

Further, it might be considerable that provoking artificial elongation of telomeres in MD patient myoblasts could have inversive effects on the specific disease-caused features of these cells, presenting the crucial point of their existence. Shortened telomeres in muscle stem cells are strongly hypothezised to be part of the etiology for cardiac muscle defects in DMD patients as was shown in the *mdx/mTR* mouse model (Mourkioti et al., 2013) which presents the human DMD disease-phenotype in skeletal muscle due to the knock-out of telomerase (Sacco et al., 2010). If the erosion of telomerase elicits features caused by a certain MD by hindering proliferation and thus regeneration as postulated by Mourkioti et al. (2013), then myotubes generated from hTERT-overexpressing immortalized myoblasts might not reflect the features present in primary diseased differentiated muscle cells and testing of therapeutical strategies would be misleading. Further, new therapeutic technologies tested positive on normally proliferating immortalized myoblasts lines, could fail in patients, as diseased human muscle cells might lack this degree of proliferative potential which could hinder the therapeutic effect to emerge.

A disparate factor among the analysed cell lines, and other cell lines immortalized equally, is the insertion event following the transduction of *hTERT*- and *cdk-4*-retrovirus-vectors. Retroviruses are known to integrate their genome at active sites of gene expression (Coffin, 1990) which implicates the possibility of insertional mutagenesis. Investigation of the virus insertion sites could be of interest, since cells were transduced by two different retrovirus constructs, since the phenotype of increased fusion potential specifically following immortalization was observed in independent experimental settings. However, such analysis was not performed here. It needs to be mentioned that the immortalized myoblast lines analysed here were derived as well from single clones of transduced primary myoblasts as the previously described myoblast lines (Zhu et al., 2007; Mamchaoui et al., 2011; Stadler et al., 2011) which on the contrary limits the probability of insertional mutagenesis compared to a transduced population.

The investigated immortalized dysferlinopathy patient myoblasts present a model closer to the

human primary myoblast than the model of converted fibroblasts (Chaouch et al., 2009), which are patient dermal fibroblasts immortalized by transduction of the telomerase gene and can be converted into myoblasts by inducible MyoD expression. Dysferlin-deficient converted fibroblasts were observed to be incapable of fusion into multi-nucleated myotubes (oral communication, data not shown). Immortalization of primary patient myoblasts was also performed successfully by the combination of *hTERT* overexpression with *Bmi-1* overexpression (Cudré-Mauroux et al., 2003). Nevertheless, control myoblasts overexpressing these genes were incapable to differentiate. Apart from that only murine dysferlin-deficient myoblast lines were available so far (Belanto et al., 2010; Humphrey et al., 2012), that unavoidably include the difference in species when used for the testing of gene or cell therapeutic approaches.

There are discrepancies in the literature about the role of dysferlin in myoblast fusion to multi-nucleated myotubes. In the present results immortalized dysferlin-deficient myoblasts have been shown to fully differentiate in respect of myoblast fusion and activation of myogenic pathways as compared to wild-type primary and immortalized myoblasts. These results and the finding of others that dysferlin is not expressed in the initial differentiation phase of myoblasts but only later around differentiation day 4 (Davis et al., 2002; Doherty et al., 2005; Klinge et al., 2007; Posey et al., 2011) support myoblast-myoblast fusion to be dysferlin-independent. Instead, myoferlin, another member of the ferlin protein family that is well expressed already in myoblasts, has been described to be essential for myoblast-myoblast and also myoblast-myotube fusion (Doherty et al., 2005, 2008). The accumulation of dysferlin at a myoblast-myotube alignment site was shown by Klinge et al. (2007), whereas they could not show this for myoblast-myoblast alignment sites, further supporting dysferlin to exclusively be involved in late differentiation. However, some groups have attributed a reduced (Demonbreun et al., 2011) or delayed differentiation potential to dysferlin-deficient myoblasts (De Luna et al., 2006; Belanto et al., 2010). These discrepancies might be caused by the use of different cellular models, species, culture conditions, *in vitro* cultivation time or donor organism age that finally result in a different myogenic potential and differentiation kinetics, as was partly discussed above (Stadler et al., 2011).

5.2 Myotubes from immortalized dysferlin-deficient myoblasts responded disparately to laser-mediated membrane wounding assay

To assess new therapeutical approaches *in vitro* is of great significance and ideally involves proving the proper function of the restored protein. This can be achieved partially by analysis of the correct intracellular localisation and the size of the protein using immunochemical approaches. In the case of dysferlin the assumption that dysferlin is indispensable in sarcolemma repair (Bansal et al., 2003; Lennon et al., 2003) opens the possibility for a direct functional assay by laser-mediated membrane wounding in cultured myotubes and myofibres. Membrane integrity of myotubes derived from IM WT3, IM DYSF1, IM DYSF2, IM DYSF3 and IM DYSF4 was investigated by laser mediated membrane-wounding of the plasma membrane in the present work. Myotubes derived

from IM WT3 myoblasts were capable to reseal injury of the plasma membrane frontier in the presence of calcium, as no fluorescent dye influx was observed following the wounding. The wounding of IM DYSF1, IM DYSF2 and IM DYSF3 myotubes led to increased fluorescence influx detectable in proximity of the injury site and of cytoplasmatic compartments. Wounding of IM DYSF4 myotubes did not lead to fluorescence influx, but resembled the membrane repair process observed in myotubes derived from IM WT3 myoblasts.

The present finding of wild-type behaviour in response to the membrane wounding assay in myotubes derived from IM DYSF4 myoblasts cannot be explained easily. Intact membrane resealing is attributed to myotubes and myofibres coming from healthy organisms in human and murine myotubes and murine myofibres in comparison to the incapability of plasma membrane repair in multi-nucleated muscle cells derived from organisms that lack dysferlin (Bansal et al., 2003; Lennon et al., 2003), mitsugumin53(Cai et al., 2009b), annexin-1 (McNeil et al., 2006) or different calpains (Mellgren et al., 2009). The IM DYSF4 cell line harbours a 5'SS mutation in intron 26 that can be assumed to lead to mRNA decay of the dysferlin transcript. The most likely case arising due to this type of mutation is the excision of the exon 26 (Nakai and Sakamoto, 1994; Berget, 1995), which would cause an open reading frame-shift leading to a STOP codon within exon 27. The possibility observed second most frequently was the recognition of the closest possible cryptic 5'SS splice site (Nakai and Sakamoto, 1994), which would lead to an elongated exon 26 and an intact reading frame (see appendix Fig.7.1). As no dysferlin protein can be detected in lysates of IM DYSF4 myotubes (Philippi et al., 2012) the first possibility is assumed to be present in IM DYSF4. If a truncated version of the dysferlin protein was present, the observed result might have been explainable. It was shown that not the full-length dysferlin protein is essential for membrane repair by the introduction of a *DYSF* minigene encoding only the c-terminus of the protein into murine myofibres (Krahn et al., 2010b). This was further supported by the finding that dysferlin can be detected at plasma membrane wounding sites only by the dysferlin Hamlet-1-antibody detecting the c-terminus of the protein, but not by dysferlin Romeo-antibody detecting the n-terminus of the protein (Lek et al., 2013). However, a shortened dysferlin version only encoding the protein c-terminus is not present in IM DYSF4 myotubes. A differential response to membrane-wounding by differently mutated versions of the dysferlin protein as observed for different specific mutations in overexpressed caveolin3 (Cai et al., 2009b) can be excluded here.

Wounding experiments were performed under standard conditions (tyrode solution supplemented by calcium) under which a wild-type-like reaction has never emerged before to membrane-wounding in myotubes derived from primary as well as other immortalized myoblasts harbouring either nonsense or missense mutations in the dysferlin gene (Schoewel et al., 2012; Marg et al., 2012; Philippi et al., 2012). A risky hypothesis would be to claim a rescue of the membrane repair process by another protein taking part in the process instead. Dysferlin was suggested to co-function with mitsugumin53 and caveolin3 in sarcolemma repair (Cai et al., 2009b,a). It was shown recently that caveolin3 very likely is not involved in the process (Marg et al., 2012; Lek et al., 2013) and a sudden rescue of the plasma membrane mechanism by any of the involved proteins, like mitsugumin53, annexin-1 or m- and μ-calpains (McNeil et al., 2006; Cai et al., 2009b; Mellgren et al., 2009; Lek et al., 2013) would be a result that was as well never described before

(Bansal et al., 2003; Lostal et al., 2010, 2012; Krahn et al., 2010b; Schoewel et al., 2012; Marg et al., 2012; Philippi et al., 2012).

Another possible explanation of the present result goes back to the possible adverse effects of the immortalization by *hTERT* and *cdk-4* overexpression discussed above. It was shown that membrane repair caused by dysferlin-deficiency could be rescued by the overexpression of myoferlin in dysferlin-deficient murine myofibres (Lostal et al., 2012). Myoferlin is involved in the differentiation of myoblasts as it drives myoblast-myoblast and myoblast-myotube fusion (Doherty et al., 2005, 2008). In the assumption that *hTERT* overexpression was actually misregulating the differentiation process in immortalized human myoblasts, by upregulating Wnt-regulated genes that promote myoblast differentiation, a gene like myoferlin could be differently expressed in immortalized myoblasts than in primary human myoblasts. A hint at upregulated differentiation due to the immortlaization is the increased dysferlin protein expression detected in IM DYSF2 myoblasts and myotubes compared to primary DYSF2 myoblasts and myotubes (Philippi et al., 2012). It would be of interest to compare abundance of myoferlin protein expression in primary and immortalized human myoblasts. Further, an inversive effect of *hTERT* overexpression on the specific disease-associated features of the immortalized myoblasts discussed before (Mourkioti et al., 2013) could explain a wild-type reaction of myotubes coming from immortalized myoblasts. Myotubes of this differentiation degree might not have been arisen rom primary human diseased myoblasts.

Taken together the presented results determine the immortalization of human primary myoblasts a feasible possibility to maintain primary human myoblasts for a prolonged number of population doublings. Further, myoblasts immortalized by this procedure are capable to differentiate into intact myotubes, as was shown by others as well (Mamchaoui et al., 2011; Stadler et al., 2011). To investigate the feasibility of a pre-mRNA *trans*-splicing molecule or effectiveness of antisense-oligonucelotides to induce exon excision, they present a cellular model which can be handled without complication and which harbours, a crucial point for RNA-therapies, the respective human target sequence. However, the results found by the laser-mediated membrane-wounding assay suggest that features of the human immortalized dysferlinopathy myoblasts might not be fully congruent with features of primary human dysferlinopathy myoblasts.

5.3 Short target introns harbouring weak 3'splice sites allow access to the splicing process by a pre-mRNA *trans*-splicing molecule

The criteria for efficient 3'mRNA replacement by SMaRT for the repair of monogenic mutations are a yet undefined matter. In strategies for gene transcripts featuring diverse coding sequences in respect of open reading frame size, disease-causing code alterations and strength of splicing signals in the respective addressed pre-mRNA, the focus has mainly been laid on the design of the pre-mRNA *trans*-splicing molecule (PTM) itself other than the structure of the pre-mRNA whose splicing was to be manipulated (Puttaraju et al., 1999; Liu et al., 2002, 2005; Chao et al., 2003; Coady et al., 2007, 2008; Lorain et al., 2010, 2013). Here I focussed on the analysis of the

pre-mRNA target intron (TI) and its immediate sequence surrounding to determine their impact on the susceptibility of the splicing process of the target intron to be manipulated by a PTM.

To analyse the involvement of pre-mRNA target intron qualities in *trans*-splicing, the target introns 30, 31, 35 and 36 of the human *DYSF* pre-mRNA were chosen to be targeted by a PTM as they differed distinctively in length and degree of conservation of their 3'splice site (3'SS). The performed bioinformatic analysis using the MaxEntScan::score3ss software (Yeo and Burge, 2004) ranked 3'SSs of TIs 31 and 35 with the lowest values (human TIs MaxEnt 4.44 and 4.57 and murine TIs MaxEnt 0.29 and 4.24, respectively). This was in accordance with the fact that the TI 31 3'SS sequence AAG deviates from the metazoan 3'SS consensus YAG, wherein Y was defined to be a pyrimidine (Burge et al., 1999). Splice switching experiments reinforced the low ranking of the TI 31 3'SS, as the exon 32 was excised from dysferlin pre-mRNA by masking the 5'SS of intron 32. Masking one of the splice sites flanking an exon in most cases leads to skipping of the exon (Nakai and Sakamoto, 1994) as the exon definition is disrupted (Berget, 1995). The compensation of an unfunctional intron internal 5'SS was shown to be possible by a strong 3'SS signal in the upstream intron (Tsukahara et al., 1994) supporting the finding that exon 31 and 37, both preceded by strong 3'SSs, were not skipped in the splice switching experiments. It is contradictive that exon 36 was not skipped as well, since the TI 35 3'SS was ranked equally low as the TI 31 3'SS. Exon 36 is a particularly short exon (30nt). It possibly might not be recognized by exon definition due to the great sterical proximity between the 3'SS and 5'SS defining it (reviewed in Berget, 1995). The 7 nucleotide long mini-exon of the troponin 1 gene was uncovered to be recognized only in combination with the exon preceding it in an exon-intron-exon unit (Sterner and Berget, 1993). This might be a recognition mode for *DYSF* exon 36 as the 3'SS of exon 35 (within the possible exon-intron-exon unit) is strong (MaxEnt 9.00) and might not facilitate the exon 35-intron-exon 36 unit to be skipped by masking the exon 36 5'SS. The low MaxEnt value for the weak TI 35 3'SS was yet considered an indicator for effective *trans*-splicing by targeting this TI.

The subsequent finding that the TI 31 and TI 35 effectively were most accessible for a PTM *in vitro* and *in vivo* implicated TI 3'SS strength to depict a true criterion for *trans*-splicing feasibility. This finding is further reinforced by the analysis of TIs successfully addressed in previous *trans*-splicing approaches. Analysis of the targeted pre-mRNA sequences further implied the involvement of the exon downstream of the TI to play a role for the susceptibility to splicing manipulation by a PTM (Table5.1). Like the *DYSF* TIs successfully targeted here, the β-subunit human chorionic gonadotrophin gene 6 (*β-hCG6*) intron 1 targeted by Puttaraju et al. (1999) encodes a weak 3'SS ranked with a low MaxEnt score (3.30). Experiments showing the successful *trans*-splicing of the gene were carried out in human lung cancer H1299 cells expressing the unmutated *β-hCG6* pre-mRNA. As well in the *trans*-splicing approach for the *DMD* gene (Lorain et al., 2010, 2013) an intron which encoded an extremely weak 3'SS (*DMD* intron 22, MaxEnt 1.94) was targeted. It was shown to be accessible for *trans*-splicing equally efficient in wild-type and *mdx4Cv* mice, next to *mdx* mice. Like wild-type mice, the *mdx4Cv* mouse model harbours an unmutated exon 23 directly downstream of the TI exhibiting no alteration in its exon defining signals. The *DYSF* TI 48 of the human *DYSF* pre-mRNA, targeted by Monjaret et al. (2014) is as well ranked by a relatively low MaxEnt value of 5.67. In all three examples targeted TIs are relatively short, as well

	Gene	TI	Size	MaxEnt	exon downstream of TI	antisense binding position
	hDYSF	31	551 bp	4.44	unmutated	5'SS proximity
	hDYSF	35	1247 bp	4.57	unmutated	5'SS proximity
	mDYSF	31	551 bp	0.29	unmutated	5'SS proximity
	mDYSF	35	1236 bp	4.24	unmutated	5'SS proximity
Puttaraju M, 1999	hGC6	1	352 bp	3.30	unmutated	3'SS proximity; masking bp
Lorain S, 2010 and 2013*	mDMD	22	913 bp	1.94	unmutated in *mdx4Cv* and wt, nonsense in *mdx* mice	5'SS proximity
Monjaret F, 2014	hDYSF	48	269 bp	5.67	unmutated	3' and 5'SS proximity masking ppt and bp
Liu X, 2002&2005	hCFTR	9	10640 bp	6.56	ΔF508 c.1521_1523delCTT	3'SS proximity
Rodriguez T, 2005 and 2009;Avale ME, 2013*	htau	9	13645 bp	5.70	excessively ΔE10-causing in *htau* mice	3'SS proximity; masking bp
Chao H, 2003*	mF8	15	2706 bp	10.76	neomycin insertion(E16+17) in *F8E16* mice	3'SS proximity; masking 3'SS
Coady T, 2007*, 2008* and 2010*	hSMN2	6	5769 bp	10.92	ΔE7-causing *mSMN-/-;hSMN2* mice	3'SS proximity; masking bp and ppt

Figure 5.1: Qualities of target introns (TIs) succesfully *trans*-spliced on endogenous pre-mRNA in this work and in previous studies. 3'SSs were analysed by MaxEntScan::score3ss software (Yeo G and Burge C, 2004). In publications marked with * the protein translated from the *trans*-spliced transcript was shown. For the table depicting 3'SS sequences see appendix 7.7.

as the TIs addressed here (Fig.5.1). Taken together, in these cases *trans*-splicing was feasible at a relatively short TI harbouring a weak 3'SS followed by an unmutated downstream exon depicting constitutive splicing signals.

The 3'SS of intron 9 of the cystic fibrosis transmembrane conductance regulator (*CFTR*) gene targeted by Mansfield et al. (2000) and Liu et al. (2002) is ranked by a MaxEnt score ranging slightly higher at 6.56, yet in the lower half of the possible MaxEnt value range (ranging from 0.29-~14(Yeo and Burge, 2004)). In the tissue and cell line empoyed in these experiments, the downstream exon of the targeted intron depicted the *CFTR* Δ-*F508* mutation (Zielenski and Tsui, 1995). Comparison of the ESE analysis (ESE finder 3.0) of the mutated versus the unmutated human *CFTR* exon 10, showed the deletion of a putative ESE by the Δ-*F508* mutation indicating a possible weakening of the exon 10 definition (Supplementary Fig.7.6). As recognition of splice sites is highly dependent on exon definition directed by ESEs in large introns (Berget, 1995; Yeo and Burge, 2004) a weaker defined exon downstream of a long TI like *CFTR* intron 9 (10640bp), is likely to support *trans*-splicing feasibility. Further, PTMs are generally constructed harbouring strong splicing signals in their splicing domain and a coding sequence that encodes an unmutated exon that is constitutively included (Fig.2.11). *Trans*-splicing of the endogenous human *tau* intron 9 (13654bp) was addressed in the *htau* mouse model that shows a higher expression of the 3R isoform of the Tau protein from a transcript lacking exon 10 (Andorfer et al., 2003) implicating that *tau* exon 10 exclusion is promoted in the *htau* mouse model. The exon definition of *tau* exon 10

primarily inducing its exclusion is as well likely to be supportive for *trans*-splicing to take place, next to the relatively weak 3'SS of *tau* intron 9 (MaxEnt 5.70) (Rodriguez-Martin et al., 2005).

Definition of the exon downstream of the TI is also very likely to play a rol in the *trans*-splicing strategy for the human survival motor neuron 2 (*SMN2*) gene (Coady et al., 2007). The 3'SS of *SMN2* TI 6 is evaluated as a strong 3'SS with a MaxEnt value of 10.92. The mutation known to predominantly lead to the *SMN2*-mRNA transcript has been assumed to be caused by the creation of an exonic splice silencer in exon 7 which binds hnRNP A1 (Kashima and Manley, 2003). hnRNP A1 is an inhibitor of U2AF and U2 snRNP (Tange et al., 2001) and might directly inhibit their recognition of the endogenous 3'SS of the *SMN2* TI 6. This condition would strongly support binding of U2 snRNP and U2AF to the PTM splicing signals instead of the pre-mRNA splicing signals and assumably weaken the influence of the strong TI 6 3'SS drastically. As well murine coagulation factor 8 (*mF8*) *trans*-splicing was performed on a pre-mRNA target harbouring an exon downstream of the TI 15 whose sequence deviates strongly from a wild-type *mF8* exon 16 sequence (Chao et al., 2003). The F8E16 mouse model employed in this approach carries a neomycin insertion in exons 16 and 17 (Bi et al., 1995) which completely disrupts exon internal and partly intron internal sequence downstream of the TI 15. Apart from the otherwise strongly defined TI (MaxEnt 3'SS 10.76), the completely aberrant downstream exon and intron internal sequence implicate that the recognition of the exon 16 on the *mF8* pre-mRNA could not occur and a favoured recognition of the splicing signals of the PTM has taken place.

For diseases prevalently caused by manifest mutations as in the *CFTR* (Zielenski and Tsui, 1995) or the *SMN* gene (Lefebvre et al., 1995), the consideration of the mutated pre-mRNA sequence in the development of a therapeutic 3' mRNA replacement approach is reasonable (Mansfield et al., 2000; Liu et al., 2002; Rodriguez-Martin et al., 2005; Coady et al., 2007). Notably, this condition does not account for dysferlinopathies, wherein disease-causing mutations are spread over the entire dysferlin open reading frame (chapter 2.2.4, Liu et al., 1998; Krahn et al., 2009) and a 3'mRNA replacement approach was to be feasible regardless of a pre-condition like a weak definition of the exon downstream of the TI. In regard of this, the findings made in human IM DYSF1 myoblasts were validated in wild-type mice (*C57BL/6*) and subsequently in the dysferlin knock-out (*DYSF-/-*) dysferlinopathy mouse model (Bansal et al., 2003). The *DYSF-/-* mouse carries a deletion of exon 53 and 54 at the 3' end of the *DYSF* mRNA, that most likely had no impact on the successful *trans*-splicing event at murine TIs 31 and 35 and thereby created a screening condition comparable to the wild-type mouse model. The feasibility of the presented strategy can therefore be attributed strongly to the weak 3'SS in both *trans*-spliced TIs.

Apart from the observation of aberrant pre-mRNA splicing in the presence of certain mutations and the possibility to evaluate flanking 5'SS and 3'SS, it still remains impossible to precisely assess the strength of the definition of an exon. Using ESE finder 3.0 allows to calculate the median of high-score values of ESEs detected in an exon, nevertheless the creators of the software themselves explicitly state that values of high-scores were not interpretive of the activity of a detected ESE and could therefore not be indicative of its actual strength (Cartegni et al., 2003). Another exon evaluation software does not provide further information on this (Fairbrother et al., 2004). The precise degree of exon definition of mutated and unmutated downstream exons, could therefore not

be estimated.

Eventually, it can be reasoned that manipulation of the splicing process of an intron is feasible at TIs encoding weak 3'SSs, as shown by the present findings of successful *trans*-splicing of this type of TI (TI 31 and 35), in contrast to no *trans*-splicing feasibility of TIs harbouring strong 3'SSs that are followed by strongly defined downstream exons (TI 30 and 36). Weak and strong 3'SSs were never compared for *trans*-splicing accessibility before, but the previous findings of *trans*-splicing of the *β-hCG6* and *DMD* TIs (Puttaraju et al., 1999; Lorain et al., 2013), as well encoding weak 3'SSs, corroborate the present findings. Previous *trans*-splicing results indicate that target introns harbouring relatively stronger 3'SSs , according to their MaxEnt value, might be accessible for a PTM, when the downstream exon definition is disrupted.

It has been observed that strong intron internal splicing signals were found more frequently in smaller introns than in larger introns, which led to the assumption that they were more essential for precise splicing of small introns (Yeo and Burge, 2004). This is consistent with the concept of exon definition to be especially crucial in large introns (reviewed inBerget, 1995). It further suggests that a weak 3'SS might have greater negative impact on exon-intron border definition, and thus recognition by the spliceosome, in small introns. The successfully *trans*-spliced TIs carrying weak 3'SSs (*DYSF*, *β-hCG6* and *DMD*) were all short TIs (Fig.5.1). Congruently, large TIs successfully *trans*-spliced before that were followed by strongly defined downstream exons directing their exon definition, as well encoded relatively low ranked 3'SSs (*hCFTR*, and *htau* gene, Fig.5.1).

5.4 Antisense sequences binding in proximity of the target intron 5'SS facilitate *trans*-splicing of dysferlin target introns 31 and 35

An important aspect of focussing on the pre-mRNA TI was to identify criteria for the optimal binding position of the antisense sequence of the PTM binding domain. In previous investigations, antisense sequences were shown to be functional when binding to TI internal regions close to the TI 5'SS (Lorain et al., 2010, 2013; Monjaret et al., 2014) or in proximity of the TI 3'SS (Mansfield et al., 2000; Liu et al., 2002, 2005; Rodriguez-Martin et al., 2005), wherein some of them masked the endogenous branch point sequence (Puttaraju et al., 1999; Coady et al., 2007) or in addition to that the actual 3'SS di-nucleotide (Chao et al., 2003). In view of the feasibility of such diversely designed antisense sequences, three different intron internal binding positions for the antisense sequence of PTMs were initially assessed in the PTM screening targeting endogenous dysferlin pre-mRNA in IM DYSF1 human myoblasts.

The antisense sequence 1 (AS1) was designed to bind to the TI approximately 200 nucleotides downstream of the TI 5'SS. This binding position in close proximity of the U1 snRNP binding site in the TI (Mount et al., 1983) promised a feasible integration of the PTM into the splicing process as the U2 snRNP and the U2AFs bound to the PTM splicing signals consequently were in closer proximity than spliceosome subunits bound to the pre-mRNA 3'SS. They were therefore likely to interact easier with the U1 snRNP in the spliceosomal complex than the U snRNPs bound to the

endogenous splicing signals on the pre-mRNA (Kent and MacMillan, 2002; Dönmez et al., 2007). PTMs comprising the AS1 induced *trans*-splicing of the IM DYSF1 dysferlin pre-mRNA at TI 31 and 35 in the *in vitro* screening (Fig.3.8). Further, the translated *trans*-spliced *DYSF* transcript could be detected in myotubes after PTM2.1 transduction, though only as a sporadic event (Fig.3.9). As well in both *in vivo* models the PTMs directed by the mAS1 induced efficient *trans*-splicing of the murine *DYSF* pre-mRNA (Fig.3.10 and 3.14) and led to dysferlin protein rescue in *DYSF-/-* mice (Fig.3.15). These findings indicate that intron internal 5'SS proximity is a favourable binding position for a PTM, which is underpinned by the previous finding of Lorain et al. (2010 and 2013) who successfully targeted the *DMD* intron 22 by a PTM comprising an antisense sequence in 5'SS proximity.

In contrast, targeting introns by AS2, which bound to the intron internal region directly flanking the downstream exon, to mask the endogenous branch point, poly-pyrimidine tract and 3'SS sequence did not lead to *trans*-splicing. AS2 was designed in the assumption that masking of the endogenous sequences would induce the redirection of the spliceosome U snRNPs to the splicing sequences of the PTM. During the initial localisation of the PTM, an antisense sequence masking the endogenous branch point, poly-pyrimidine tract and 3'SS competes with the SF1/mBBP splicing factors (Arning et al., 1996; Berglund et al., 1997), the U2AF and the U2 snRNP for their pre-mRNA binding motifs (Zhuang et al., 1989; Zamore et al., 1992; Wu et al., 1999). Therefore the direct exon flanking 3'SS region might not be as accessible for the PTM antisense sequences as other intron internal regions. In former feasible *trans*-splicing approaches, antisense sequences designed to bind the TI in 3'SS proximity were not designed to mask poly-pyrimidine tract and 3'SS (Mansfield et al., 2000; Liu et al., 2002, 2005; Rodriguez-Martin et al., 2005), but bound further upstream of these sequences to intron internal sequence or masked the 3'SS leaving the poly-pyrimidine tract unmasked by an uncomplementary loop (Chao et al., 2003). The localisation of these PTMs might have been under less intense competition when binding to the TI. An exception builds the antisense sequence for the *trans*-splicing strategy of the *SMN2* gene, which was as well designed complementary to the intron internal region in 3'SS proximity masking both branch point and poly-pyrimidine tract. In targeting the *SMN2* pre-mRNA transcript (Coady et al., 2007, 2008; Coady and Lorson, 2010) this direct competition between the antisense sequence and spliceosome might not have been arisen, as binding of U2AF has most likely been inhibited by the hnRNP A1 (Kashima and Manley, 2003; Kashima et al., 2007).

Another reason for the unsuccesful *trans*-splicing by PTMs comprising AS2 might have been the small length of the spacer sequence of the here applied PTMs. As the PTM was fixed to the 3'SS of the TI by its antisense sequence, the interaction of the branch point of the PTM with the 5'SS of the TI would have required a very tight folding of the intron internal sequence of the TI, in general organized through the assembly of the complete spliceosome on intron internal splicing signals (reviewed in Wahl et al., 2009) as the spacer sequence provided in the here applied PTMs was only 30 nucleotides long. Since on the endogenous 3'SS no spliceosome assembled in case the PTM AS2 bound to this region the folding of the TI might not have been induced porperly. This would further corroborate why PTMs placed in 5'SS proximity by the AS1 were funtional.

A third antisense sequence was designed for the *DYSF* TI 31, as it was the most promising

trans-splicing target in the investigated TI set due to its very weak 3'SS (human TI 31 MaxEnt 4.44; murine TI 31 MaxEnt 0.29) (Fig.3.5). The design of AS3 was based on the idea to block *cis*-splicing of the exon downstream of the TI to inhibit the free exon in the splicing reaction to interact with the downstream exon to promote *trans*-splicing with the PTM instead. This strategy was pursued previously by Coady et al. (2008) to increase *trans*-splicing efficiency at *SMN2* intron 7. Since exon 7 is excluded by default in the *SMN2* pre-mRNA transcript (Kashima and Manley, 2003) they prevented *cis*-splicing of exon 8 by masking its intron-exon boundary with intron 7 and thereby promoted increased *trans*-splicing compared to their previous *trans*-splicing approach where they did not block the intron7-exon8 boundary (Coady et al., 2007). In *DYSF* pre-mRNA the exon 32 downstream of the TI 31 is not excluded as a default condition. Therefore suppression of this exon, instead of the next downstream following one, was assumed to promote *trans*-splicing over *cis*-splicing. AS3 was designed complementary to exon 32 and the 5'SS of intron 32 (position +3 until -137) thus integrating the attempt of exon 32 suppression and PTM localization in one molecule. However, the PTM containing the AS3 promoted *trans*-splicing, but much less efficient than PTMs comprising AS1, both in human IM DYSF1 myoblasts as well as in the *C57Bl/6* mice (Fig. 3.8; 3.10). The induced exclusion of exon 32 might have primarily promoted *cis*-splicing with the following 3'SS instead of promoting trans-splicing with the PTM. Furthermore, assuming that the AS3 bound its proper target, but failed to induce exon 32 suppression, the PTM splicing signals were now located further downstream than the endogenous splicing signals of the TI 31 3'SS region. Effectively bound U2AF and U2 snRNP on TI 31 was thus in an advantageous position to be included in the subsequent spliceosome complex finally bringing both exons together (Kent and MacMillan, 2002; Dönmez et al., 2007). The limited length of the PTM spacer sequence might have further inhibited the interaction of spliceosome subuntis bound to the PTM, as discussed before for AS2. A combination of PTMs directed by AS1 with blockage of the TI 31 3'SS might induce more efficient *trans*-splicing, as the interaction of the free exon 31 with endogenous exon 32 would be inhibited.

Eventually, the absence of *trans*-splicing after application of the PTMΔAS support that the localisation and steric placement of the PTM by an antisense sequence is essential for the efficient integration into the *cis*-splicing process as was also shown in other studies by the extreme reduction or absence of *trans*-splicing after the application of a PTM lacking the antisense sequence (Puttaraju et al., 1999; Kikumori et al., 2001; Rodriguez-Martin et al., 2005). The detection of none or vastly reduced *trans*-splicing after application of PTMs lacking an antisense sequence further confirms that detected *trans*-spliced transcripts are no artefacts of PCR detection. PCR templates that would produce such artefacts, which in the present work would include the PTMs encoding an AS and the PTMΔAS together with the pre-mRNA target, were present in the control and the detecting PCR reactions at comparable concentrations and detection of an artefact transcript should have taken place at equal strength for both kinds of reactions. This was not the case (Fig. 3.5, 3.10 and 3.14), confirming that PCR detection of *trans*-spliced transcripts wsa specific.

5.5   Spliceosome-mediated *trans*-splicing as RNA-based therapeutic approach for the dysferlin gene

As mutations in the *DYSF* gene do not coincide in a mutational hot spot (Krahn et al., 2009) gene repair strategies by which large portions of the gene can be recovered are desirable therapeutic approaches. The large open-reading frame of the *DYSF* gene (~6.5kb) (Liu et al., 1998; Bashir et al., 1998) exceeds the packaging limit of rAAV vectors known to efficiently transduce muscle tissue (Chao et al., 2000; Grieger and Samulski, 2005; Riviere et al., 2006) therefore classical gene therapy is no option for the *DYSF* gene. The strategy of therapeutical SMaRT (Puttaraju et al., 1999) integrated the opportunity to replace the entire 3'moiety of the *DYSF* mRNA and to thereby recover a large portion of disease-causing mutations of the gene. The fact that therapeutical *trans*-splicing does not manipulate transcription regulation of the target gene, by addressing the transcribed pre-mRNA, was especially crucial for the repair of *DYSF* mutations, since overexpression of dysferlin protein was shown to cause a progressive myopathy (Glover et al., 2010). The present results show a well detectable feasibility for *trans*-splicing of the endogenous *DYSF* pre-mRNA *in vitro* and *in vivo* (Fig.3.8; 3.10; 3.14). Nevertheless, the translation of the *trans*-spliced *mDYSF* transcript could only be detected by immunhistochemistry at a very moderate level in *DYSF-/-* mice (Fig.3.15). This level of rescued dysferlin protein was not sufficient to be detected by immunoblot (Fig.3.16). A possibility to provide further evidence of the presence of full-length rescued protein is concentration of the *trans*-spliced protein by immuno-precipitation assay, which is currently optimized.

Efficiency of *trans*-splicing strategies performed on endogenous pre-mRNA targets is still low on RNA level and results in low efficiency on protein level. Weak rates of rescued protein were as well detected after *in vivo trans*-splicing of the mutated *mF8* pre-mRNA (Chao et al., 2003) in the F8E16 mouse model (Bi et al., 1995) and also due to *in vivo trans*-splicing of the *htau* gene (Avale et al., 2013) in the *htau* mouse model (Andorfer et al., 2003). A low level of dystrophin protein rescue was detectable exclusively by immunohistochemistry in *mdx* and *mdx4Cv* mouse models (Lorain et al., 2013). This generally observed moderate *in vivo trans*-splicing efficiency on protein level is followed by an estimated rate of 0.2% of CFTR protein detected after *trans*-splicing on endogenous *CFTR* pre-mRNA *in vitro* (Liu et al., 2002). In the remaining strategies targeting endogenous pre-mRNA protein rescue could not be shown at all or was illustrated exclusively by functional assays reflecting the protein rescue (Puttaraju et al., 1999; Liu et al., 2005).

In contrast, *in vivo trans*-splicing of human *SMN2* pre-mRNA in the severe SMA mouse model *(mSMN1-/-;hSMN2+/+,* Monani et al., 2000) led to a protein level comparable to SMN protein expressed in heterozygous *SMN-/+* mice (Coady and Lorson, 2010). The coding domain of the PTM introduced in the *SMN2 trans*-splicing approach, encodes the SMN exon 7 directly followed by a poly(A)-signal. This allows completely intact exon definition of the PTM-encoded exon via the provided splicing signals upstream of the exon 7 in the PTM splicing domain and the downstream poly(A)-signal, which is essential for proper transcription termination (Dye and Proudfoot, 1999; Proudfoot, 2011). This degree of endogenous exon recognition by the spliceosome is not possible in PTMs that encode multi-exon mRNA coding domains lacking introns between the exons. The

SMN2-PTM splicing actually resembles the terminus of endogenous pre-mRNA. The influence of proper exon definition in the PTM coding domain was already investigated by Lorain et al. (2013). The inclusion of a mini-intron downstream of the first exon in the PTM coding sequence induced an increase of *trans*-splicing efficiency by ~10% compared to targeting the same minigene by a PTM lacking the mini-intron. This result is a promising hint, nevertheless it was obtained addressing a minigene construct *in vitro*. Further, the introduction of intron sequence in the coding domain of a PTM would stress the limited by rAAV packaging size.

As well noteworthy is that the PTM applied in *SMN2* intron 7 targeting approaches is short (Coady et al., 2007, 2008; Coady and Lorson, 2010) compared to PTMs applied in most other strategies. A PTM comprising a short coding domain was detected to induce *trans*-splicing more efficiently in a direct comparison to a multi-exon encoding PTM by Puttaraju et al. (1999). A smaller molecule might cause a higher bioavailability at the site of splicing due to less steric blockage in the nucleoplasm. Though Puttaraju et al. (1999) showed this exclusively *in vitro* targeting a co-transfected minigene, where bioavailability of the two molecules cannot be compared to the situation in targeting the endogenous pre-mRNA.

Criteria defined on minigene targets can in general only be considered under constraint. It was uncovered in several studies that *trans*-splicing efficiency obtained by investogations on minigenes deviated stronlgy from results obtained with endogenous pre-mRNA targets (Puttaraju et al., 1999; Mansfield et al., 2000; Coady et al., 2007; Lorain et al., 2013; Monjaret et al., 2014). A reason why the presented *DYSF trans*-splicing strategy was carried out exclusively on endogenous pre-mRNA, even in the initial *in vitro* screening.

In the here presented *in vivo* experiments, PTMs were administered to murine skeletal muscle via a rAAV2/1 vectors. AAV1 capsids are known to infect murine skeletal muscle efficiently (Chao et al., 2000; Riviere et al., 2006), which was shown before particularly for the delivery of the *DYSF* transcript in comparison to rAAV2/9 vectors (Lostal et al., 2010). In regard of a clinical trial it would be important to note that in humans the AAV1 neutralizing antibody (NAB) titre has been detected to be lower than the AAV2 NAB titre (Xiao et al., 1999b). The AAV1-capsid allowed two administrations of the PTMs in murine skeletal muscle within 24 hours, since humoral immune response to this serotype has been shown to neutralize viral particles only 72 hours after the first administration in murine skeletal muscle and no innate immune response occurs against the AAV1 capsid (Lorain et al., 2008).

Trans-splicing of *DYSF* pre-mRNA was analysed 28 days after administration of the PTM. This emerged as the optimal time point as *trans*-splicing was less efficient when analysing treated muscle after 14 days (data not shown) and was equally efficient when analysed after 42 days (oral communication by S. Lorain). As the delivery of the PTMs was performed by a vector system that proved to provide efficient and persistent expression of transgenes in muscle tissue in several other studies before (Goyenvalle et al., 2004; reviewed in Blankinship et al., 2006; Penaud-Budloo et al., 2008, Lostal et al., 2010), the cause of the low pre-mRNA *trans*-splicing efficiency assumably lies elsewhere. The effectiveness of the therapeutic molecule delivered by the rAAV can directly influence the persistence of its expression, as has been shown in *mdx* mice (Le Hir et al., 2013). The worsening of muscular dystrophy treated by rAAVs expressing no therapeutic molecule led to

increased loss of the rAAV episomes, as compared to muscle treated with an rAAV expressing an effective therapeutic molecule. This has not yet been investigated in dysferlinopathy mouse models.

5.6 The side effect of PTM-translation

In the *trans*-splicing approach for the *DMD* gene, it was already described that the applied PTM itsself was translated, assumably by an artifical start-codon although lacking a preceding complete Kozak-sequence (Lorain et al., 2013). Translation of the dystrophin PTM was not reported to cause impairment in the treated tissue and rescue of dystrophin protein could be shown, though at very moderate levels. No harmful effect by the translation of a dysrophin PTM could be assumed due to the fact that translation of portions of the *DMD* open-reading frame in mini-dystrophins or multiple-exon skipping approaches does not lead to adverse effects (Bostick et al., 2009; Aoki et al., 2012). However, it was suggested that in frame translated dysferlin protein c-termini initiated by cryptic start-codons in the PTMs could act cytotoxic in the treated murine muscle and have a titrating effect on the availability of the PTMs for *DYSF trans*-splicing (Monjaret et al., 2014). In this study it was not shown, if the elimination of the detected protein products identified to come from cryptically initiated PTM-translation, led to amelioration of the identified harmed muscle histology or to increase of the low *trans*-splicing efficiency. It needs to be mentioned, that the *in vivo* applied PTM was directed by a human-specific antisense sequence, which had only partly homology to the murine TI sequence, which might have led to unspecific *trans*-splicing events, causing the abundance of the many detected unspecific protein products. PTMs applied in the present work revealed differential susceptibility to translation-inititaion by an artifical start-codon. mPTM2.1 was not translated autonomously, whereas a single translation product of mPTM3.1 was detected. Both mPTMs induced *trans*-splicing detectable on RNA- and protein-level. Though the level of protein product from the *trans*-spliced transcripts was moderate, it did not appear particularly decreased in muscle treated by mPTM3.1 (Fig. 3.15) which could have indicated a possible toxic effect of the translated PTM. Further, muscle histology in the immunohistochemical stainings of treated *DYSF-/-* mice did not appear worsened compared to untreated muscle.

The translated c-terminus of the dysferlin protein was shown to rescue membrane repair incapability in dysferlin-deficient mice (Krahn et al., 2010b). Even though myopathic histology was not rescued by the partial dysferlin protein, a deterioration of the muscle phenotype due to expression of the dysferlin protein c-terminus was excluded. This finding was corrected lateron (Lostal et al., 2012) concluding that especially the expression of a partial dysferlin protein caused myopathic symptoms. However, the autonomous translation of a PTM must be differentially initiated, as in the presented study only one of the PTM sequences was translated. A precise investigation of the mPTM2.1 sequence is of great interest to possibly facilitate directed suppression of autonomous PTM-translation in further studies.

A possible hindrance of efficient translation of the well detectable *trans*-spliced *DYSF* transcripts (Fig. 3.10; 3.14) could lie in the omission of the 3' untranslated region (3'UTR) in the PTM coding sequence. The 3'UTR encoded signaling is crucial for nucleoplasmatic export and translation regulation of the mRNA transcript (reviewed in Matoulkova et al., 2012). Since processed *DYSF*

mRNA is yet a large molecule (~6900bp) transport into the cytoplasm assumably is more dependent on post-transcriptional signaling than it might be for much smaller mRNAs like the *SMN1* mRNA (~1600bp). Integration of the 3'UTR into the coding region of the *DYSF* PTM could possibly influence stability and nucleocytoplasmatic transport of the *trans*-spliced *DYSF* transcript, though this would reduce the size limit of the coding sequence in regard of rAAV packaging limit.

5.7 Effective dysferlin exon 32-skipping by masking exon internal splicing enhancer motifs

By the analysis of binding positions and features of 114 different AONs targeting the *DMD* pre-mRNA, Aartsma-Rus et al. (2005) found that AONs most effectively induced exon excision from *DMD* pre-mRNA that were masking ESE motifs predicted by high high-score values using the ESE finder 3.0 (Cartegni et al., 2003). Further, they found that AONs positioned in proximity of the 3'SS of the preceding intron were more effective. Motivated by this previous finding, hAONs applied here were designed to mask putative ESE sequences and particularly those that were predicted by high high-score values. The most effective hAONs 2 and 3 both mask sequence motifs that predict at least one ESE with the value of 3.0, a threshold that is exceeded only by three of the fifteen predicted ESEs in the human *DYSF* exon 32 sequence (Fig. 7.4). Of all three hAONs that masked exon internal sequence of *DYSF* exon 32 (hAON2, hAON3, hAON4) hAON2 and 3 were positioned closer to the 3'SS than the less effective hAON4. These results perfectly reflect the criteria identified by Aartsma-Rus et al. (2005). As mentioned by Aartsma-Rus et al. (2005), the majority of exons that were analysed reflected these criteria, whereas for some remaining exons they were not valid. This is further supported by the acknowledgment of Cartegni et al. (2003) that the actual value of high-score values predicted for ESEs do not necessarily define the activity of a putative ESE.

hAON1 targeting the intron internal 3'SS preceding exon 32 induced less efficient exon skipping than hAON5, targeting the intron internal 5'SS of intron 32. The slight difference in skipping efficiency induced by hAON 1 and 5 can possibly be explained by the qualities of the upstream intron internal 3'SS and the downstream intron internal 5'SS involved in the definition of the human *DYSF* exon 32, next to the exon internal ESEs (reviewed in Berget, 1995). According to the analysis by MaxEntScan::scoresplice, the 3'SS encoded by human intron 31 is weaker (MaxEnt 4.44) than the 5'SS in intron 32 (MaxEnt 8.37). The 5'SS might be more crucial for the definition of exon 32, a possible explanation why masking of the 5'SS might have led to a slightly stronger induction of exon 32-skipping. However, exon internally positioned hAON2 and 3 induced a higher exon skipping efficiency as had previously been reported for AONs to induce exon 51 excision of the human *DMD* gene (Arechavala-Gomeza et al., 2007; Goyenvalle et al., 2009).

The intron internal 3'SS preceding the exon 51 (MaxEnt 3.73) is as well weaker as the downstream 5'SS (MaxEnt 9.11), but the difference is not extreme likewise as for human *DYSF* exon 32. Effective targeting of the intron internal splice sites might be feasible due to an extreme difference in 3'SS and 5'SS defining the exon. An extreme disparity among splice site strength

is present in the splice sites framing murine *DMD* exon 23. The 3'SS of intron 22 is extremely weak (MaxEnt 1.94), whereas the intron internal 5'SS of the downstream intron is strong (MaxEnt 9.88). Masking of the downstream 5'SS has been shown to be a very effective AON target to induce exon-23 exclusion (Mann et al., 2001; Goyenvalle et al., 2004). Recognition of this exon might be highly dependent on recognition of the 5'SS, as suggested by very efficient skipping of the exon by 5'SS masking. Further supportive of this assumption is that 3'SS and 5'SS of an exon differing largely in strength due to mutation in one of them were shown to possibly cope for the other's weakness by provoked secondary mutations strengthening the respective stronger splice site (Carothers et al., 1993; Tsukahara et al., 1994).

The detected exon-skipping effectiveness of the applied hAON 2, 3 and 4 on RNA level is reflected by the obtained protein rescue through these AONs (Fig. 3.20). Three consecutive transfections might have been necessary to yield the dysferlin protein rescue, as only the transcript coming from one *DYSF* allele could be repaired by hAONs in IM DYSF5 myoblasts due the compound heterozygous mutation state.

Results obtained by targeting the murine pre-mRNA using mAONs1, 2, 4 and 5 mainly reflect the findings made for the hAONs. The mAON2 and mAON4 masking exon internal ESE motifs induced exon-skipping of murine exon 32 more efficiently than mAONs masking the intron internal splice sites. The *in vitro* investigations suggest mAON2 to be more efficient, which would be supportive of the finding by Aartsma-Rus et al. (2005), that proximity to the upstream intron internal 3'SS plays a role in AON efficiency. However, this *in vitro* result is not confirmed by the quantification of *in vivo* exon-skipping efficiencies of the mAONs. Quantitative PCR analysis showed that mAON4 induced more efficient skipping than mAON2 in *C57Bl/6* mice. mAON4 masks ESE motifs predicted with the highest high-score values among the predicted ESEs for murine exon 32. As mentioned before, actual values of ESE high score values have been identified to be indicative of AON efficiency by Aartsma-Rus et al. (2005), however, the opposite is stated by Cartegni et al. (2003). Further investigations of large scale testing of this coherence would be of great interest.

Exon 32-skipping efficiency by mAON1 and mAON5 is comparable as shown by qPCR analysis. In the case of the murine *DYSF* exon 32, the strength of intron internal 3'SS (MaxEnt 0.29) and 5'SS (MaxEnt 8.37) differ extremely, as in the murine *DMD* exon 23. However, the result obtained for the mAON5 is not conclusive with the hypothesis that masking a strong counter splice site of a weak splice site would lead to efficient excision of the exon. The 3'SS of murine *DYSF* exon 32 is evaluated by an extremely low value (MaxEnt 0.29), which even renders the constitutive inclusion of the exon surprising. This renders the influence of the splice sites on the splicing of the exon less important and further corroborates the effective splicing by masking of exon internal splicing enhancers.

5.8 Possible side effects of dysferlin tricyclo-DNA antisense oligonucleotides

For the design of small interfering (siRNA) strategies, sequences are usually analysed using BLAST software in order to exclude exon internal off-target binding sites. The same was done here for the hAONs 2, 3 and 4 sequences as they were designed to target exclusively exon internal sequence. Blasting against the human refseq-rna database did not reveal high sequence similarity to other mRNA sequences. However, the hAON3 was feasible to repeatably induce a skip of *DYSF* exon 34 besides skipping of its specific target, *DYSF* exon 32. The off-target binding site was identified to lie within intron 33 and overlap with the specific target by only 8 nucleotides. According to the intron internal binding position (intron 33 internal sequence position -9 to -17) and sequence composition (TCTACGCT) of the overlap and its intron internal surrounding, the off-target could possibly be part of the intron 33 poly-pyrimidine tract. The side product was detected as a weakly abundant amplicon by RT-PCR. The skip of exon 34 would lead to an additional in-frame exon excision and therefore a protein product could possibly be translated from the Δ32+34 mRNA transcript. The protein would differ from full-length dysferlin protein by only 73 amino acids which could not be differentiated in the immunoblot analysis (Fig. 3.20). The consideration of off-target binding due to relatively short overlapping sequence might be more crucial for backbone chemistries that emerge very high RNA affinity, such as the tricyclo-DNA (Renneberg and Leumann, 2002b).

The finding, that parental *DYSF* transcript was nearly not detectable after hAON4 transfection combined with a relatively low abundant Δ32-transcript was unlikely to be the result of complete skipping efficiency induced by hAON4. In the case of complete skipping efficiency, a higher abundance of Δ32-transcript should have been detected. Performing a second PCR using an external primer set that spanned a larger region of the parental *DYSF* open reading frame did not lead to the detection of parental *DYSF* transcript as well excluding the possibility that this was due to additional excision of a primer template region.

In retrospective, this result could be uncovered to most likely be caused by the high guanine- and cytosine-tricyclo-deoxynucleoside content (GC-content) oh hAON4 that has caused a detection artefact. The hAON4 GC-content of 80% led to a calculated melting temperature of the oligonucleotide at 62.6°C (whereas the calculated Tm for the remaining hAONs did not exceed 50°C (Fig. 3.18B). In the design of the relatively short 15mer AONs the GC-content was neglected as the focus was laid purely on the masking of putative splicing signals. The impact of a high GC-content has been discussed for the AON design but was considered a possible additional outcome of the investigations. The nested RT-PCR system applied to analyse skipping efficiency on RNA level (Access QuickTM RT-PCR System, Promega) conducts reverse transcription at 45°C without any prior heating step. As tcDNA-AONs that have entered the cell are present in the cytoplasm and nucleus and the hAON4 target lies within the exonic sequence, the hAON could as well bind to the exon 32 of mature *DYSF* mRNA in the nucleus and the cytoplasm. This duplex assumably would be very stable, due to the high GC-content of hAON4. Further, tcDNA does not induce RNase H nuclease activity when bound to RNA (Renneberg et al., 2002).

The cytoplasmatic tcDNA-RNA duplex might have survived the RNA extraction procedure and thus inhibited reverse transcription of the parental mRNA. The possibility of artefact creation by this detection method as well accounts for the detected result of the *in vitro* application of the mAON4 (GC-content 74%, Tm at 60.5˚C), but does not account for the analysis of exon 32-skipping in the murine *C57Bl/6* model, where extracted total RNA was reverse transcribed for the analysis by PCR and quantitative PCR using the SuperScript ® III (Life Technologies) protocol, which includes a pre-heating step at 65˚C prior to reverse transcription. The binding of hAON4 to the cytoplasmatic *DYSF* mRNA transcript might reveal two possible side-effects of tcDNA-AONs. Firstly, the cytoplasmatic hAON4-*DYSF* mRNA duplex possibly titrated the presence of hAON4 available in the nucleus to induce exon 32-skipping. A titration of hAON4 to the cytoplasm could explain the unexpected low skipping efficiency induced by hAON4. Secondly, the emerging tcDNA-mRNA duplex possibly inhibited the translation of the parental mRNA transcript in the cytoplasm, which could not be shown here, as the parental transcript is already not translated due to the nature of the mutations present in IM DYSF5. This feature would be of advantage to restrict the translation of dominant negative parental transcripts that whose pre-mRNA was not successfully modified in the nucleus. The controlled direction of this effect by a certain design of the tcDNA-AON might be difficult though.

6   Summary

6.1   RNA-based therapies for dysferlinopathies

Precursor-mRNA (pre-mRNA) *cis*-splicing is an attractive target for the repair of genes whose transcription regulation is determinative for protein function, as it is the case for the dysferlin (*DYSF*) gene. Mutation of the *DYSF* gene leads to muscular dystrophies of different disease phenotypes the majority of which manifests as Limb girdle muscular dystrophy 2B (LGMD2B) and Miyoshi myopathy 1. Two strategies of pre-mRNA *cis*-splicing modification for DYSF gene repair were pursued in the presented thesis, (i) spliceosome-mediated pre-mRNA *trans*-splicing (SMaRT) by an engineered pre-mRNA *trans*-splicing molecule (PTM) and (ii) antisense oligonucleotide (AON)-induced excision of *DYSF* exon 32 from *DYSF* pre-mRNA.

SMaRT by a PTM allows substitution of large portions of a pre-mRNA and the preservation of the full-length mRNA transcript of a gene. The approach is particularly suitable for *DYSF* gene repair, as disease-causing mutations were identified in the entire *DYSF* open-reading frame and gene replacement therapy by the expression of curtailed mini-dysferlin protein does not rescue muscular dystrophy. For the design of an efficient *trans*-splicing strategy, introns of the human *DYSF* pre-mRNA which revealed disparately strong splicing signals and further strongly differed in length were targeted by PTMs in human dysferlin-deficient myoblasts. Introns were targeted by PTMs encoding different pre-mRNA binding domains to either localize the PTM in close proximity of the intron internal 5'splice site or to mask the intron internal 3'splice site. *Cis*-splicing of target introns encoding weak splicing signals was more susceptible to manipulation by a PTM then of strongly defined introns and PTM localisation in close proximity to the 5'splice site and thus to the active spliceosomal U1 snRNP during the splicing process emerged as most effective. *Trans*-splicing of two *DYSF* target introns led to dysferlin protein rescue in the *DYSF-/-* mouse model. The level of protein recovery, however, was moderate, remindful of low protein yields obtained in previous *trans*-splicing strategies for other genes. Nevertheless, concordant qualities among successfully targeted *DYSF* introns and previously targeted introns by other strategies could be identified that might facilitate a systematic choice of future *trans*-splicing target introns.

The strategy of AON-induced excision of *DYSF* exon 32 was based on the knowledge that a naturally occurring *DYSF* exon 32-excision led to mild LGMD2B in a patient that was ambulant until high age. AONs of the tricyclo-DNA backbone chemistry were applied, which due to the additional two carbon ring entities within the single nucleoside are more rigid and show higher binding affinity to RNA than DNA does. The *in vitro* and *in vivo* application of designed AON

sequences corroborated findings of previous studies in which for particular exons masking of exon internal splice enhancer sequences induced exon exclusion most efficiently. Two of the designed exon internally binding AONs induced dysferlin protein rescue in dysferlin-deficient immortalized human myoblasts.

6.2   Utilisation d'ARN pour le traitement des dysferlinopathies

L'épissage en *cis* des précurseurs d'ARN messager (pre-ARNm) est une stratégie intéressante afin de réparer des gènes dont la régulation transcriptionnelle est déterminante pour la fonction de la protéine en résultant, comme dans le cas du gène codant pour la dysferlin (*DYSF*). Les mutations touchant le gène *DYSF* sont liées au développement de dystrophies musculaires aux phénotypes variés mais dont la majorité engendrent la dystrophie musculaire des ceintures de type 2A et la myopathie distale de Miyoshi. Deux stratégies visant à modifier l'épissage en cis des pre-ARNm du gène *DYSF* furent tester dans le travail présenté dans ce manuscrit, (i) le procédé SmaRT (pour spliceosome-mediated mRNA *trans*-splicing), une technique de réparation de l'ARN messager au moyen d'un complexe de trans-épissage appelé PTM (pour pre-mRNA *trans*-splicing molecule), et (ii) la suppression de l'exon 32 du gène *DYSF* à l'aide d'un oligonucléotide antisens (AON).

Le procédé SmaRT utilisant le complexe PTM permet le remplacement d'importantes portions de pre-ARNm tout en préservant l'intégrité totale du transcrit. Cette technique convient parfaitement à la réparation du gène *DYSF*, puisque les mutations pathogènes ont uniquement été identifiées dans la phase ouverte de lecture du gène et que les thérapies basées sur le remplacement du gène *DYSF* par l'expression de protéines tronquées ne permettent pas de soigner la dystrophie musculaire. Dans un soucis d'obtenir un trans-epissage efficace, seuls les introns humains codant pour les pre-ARNm de *DYSF* présentant de forts signaux d'épissage répartis de façon disparate ainsi que des tailles très différentes furent ciblées par les PTMs dans des myoblasts humains ne possédant pas de dysferlin. Ces introns furent ciblés par des PTMs codant pour différents domaines de fixation au pre-ARNm afin que le PTM soit à proximité du site interne d'épissage en 5' de l'intron ou bien que le PTM masque le site d'épissage interne en 3'. L'épissage en cis d'introns codant pour des signaux d'épissage faibles fut plus sensible à la manipulation par un PTM que les introns fortement définis. De plus, les PTM localisés à proximité du site d'épissage en 5' étant aussi à proximité du complexe d'épissage U1 snRNP se révélèrent les plus efficaces. Le trans-épissage de deux introns ciblés du gène *DYSF* engendra une formation correcte de la protéine dysferlin dans des mutants *DYSF-/-* de souris. Les niveaux de protéine fonctionnelle furent toutefois modérés, mais similaires aux taux de récupération obtenus par des stratégies précédentes de trans-épissage ciblant d'autres gènes. Néanmoins, parmi les introns ciblés avec succès dans cette étude et dans des essais précédents, des critères concordants ont pu être identifiés afin de faciliter le choix des introns à cibler pour de futures stratégies de *trans*-épissage.

La stratégie consistant à exciser l'exon 32 du gène *DYSF* fut basée sur la connaissance d'un cas naturel d'excision de cet exon, engendrant des symptômes de dysferlinopathie faibles chez un sujet qui resta ambulant jusqu'à un âge avancé. Les AONs furent synthétisés à partir de tricyclo-ADN, une conception chimique qui grâce à l'ajout de deux atomes de carbone se retrouve plus rigide et démontre une plus grande affinité de fixation à l'ARN que l'ADN classique. L'utilisation in vitro et in vivo de séquences d'AON confirmèrent les observations précédentes, en particulier que la dissimulation de sites internes accentuant l'épissage entrainent une exclusion plus efficace de l'exon en question. Deux AONs se fixant sur l'exon 32 entrainèrent une restauration de la protéine dysferlin dans des myoblasts humains immortalisés et ne possédant pas la dysferlin.

6.3 RNA-basierte Therapieansätze für Dysferlinopathien

Das *cis*-Spleißen von präkursor-mRNA (prä-mRNA) ist ein besonders geeigneter Angriffspunkt für die Korrektur von Genen, deren Transkriptionsregulation, wie im Fall des Dysferlin (*DYSF*) Gens, ausschlaggebend für die Funktionalität des enkodierten Proteins ist. Mutationen des *DYSF* Gens führen zu unterschiedlichen Arten der Muskeldegeneration, die in den meisten Fällen als Gliedergürtel dystrophie des Typs 2B (engl. Limb girdle muscular dystrophy 2B, LGMD2B) oder Muskeldystrophie Miyoshi 1 (engl. Miyoshi Myopathy 1, MM1) manifestieren. Im Rahmen dieser Dissertation wurden zwei Strategien zur Modifikation des prä-mRNA cis-Spleißens zur *DYSF* Genkorrektur etabliert, das (i) Spleißosom-vermittelte prä-mRNA trans-Spleißen (engl. Spliceosome-mediated pre-mRNA trans-splicing, SmaRT) durch ein technisiertes prä-mRNA trans-Spleißmolekül (engl. pre-mRNA trans-splicing molecule, PTM) und (ii) das Antisense-Oligonukleotid (AON)-induzierte Ausschneiden des *DYSF* exons 32 aus der *DYSF* prä-mRNA .

SmaRT mittels eines PTMs erlaubt das Ersetzen von umfagreichen Abschnitten der prä-mRNA und die Erhaltung des kompletten mRNA-Transkripts eines Gens. Dieser Ansatz eignet sich besonders zur Korrektur des *DYSF* Gens, da krankheitserregende Mutationen innerhalb des gesamten Leserahmens des Gens identifiziert worden sind und die Gen-Ersatz-Therapie durch Expression eines verkürzten Mini-Dysferlin Proteins die Muskeldegeneration nicht lindert. Fuer die Entwicklung einer effizienten SmaRT-Strategie ist der cis-Spleißprozess von Introns der *DYSF* prä-mRNA, die unterschiedlich starke Spleißsignale aufweisen und sich in ihrer Länge unterscheiden durch PTMs in humanen Dysferlin-defizienten Myoblasten angezielt worden. Diese Introns wurden durch PTMs mit unterschiedlichen prä-mRNA Bindedomänen angegriffen, um das PTM entweder in die Nähe des Intron internen 5'Spleißsignals zu bringen, oder um das Intron interne 3'Spleißsignal zu maskieren. Eine Modifikation des cis-Spleißens durch ein PTM war in Introns, die schwache Spleißsignale kodieren, jedoch nicht in Introns, die durch starke Spleißsignale definiert sind, mittels eines PTMs, welches durch seine Bindedomäne in der Nähe des 5' Spleißsignals und damit in der Nähe des im Spleißprozess aktivierten U1 snRNPs lokalisiert, am effizientesten. Das Trans-Spleißen von zwei der angezielten *DYSF* prä-mRNA Introns fuehrte zu einer Wiederherstellung der Translation des Dysferlin Proteins im *DYSF-/-* Mausmodell. Eine Wiederherstellung des Dysferlin Proteins konnte jedoch nur in moderatem Mass detektiert werden, was an die geringe Effizienz von SmaRT-Strategien, die bereits für andere Gene entwickelt worden sind, erinnert. Allerdings konnten übereinstimmende Eigenschaften zwischen effizient angezielten *DYSF* Introns und Introns, die in zuvor entwickelten Strategien angezielten wurden, identifiziert werden, die eine systematische Auswahl der Zielintrons in zukünftigen SmaRT-Strategien erlauben könnten.

Die Strategie des AON-vermittelten Ausschneidens des *DYSF* Exons 32 aus der prä-mRNA wurde vor dem Hintergrund entwickelt, dass ein natürlich vorkommendes Ausschneiden des *DYSF* exons 32 in der prä-mRNA einer Patientin zu einer milden Gliedergürteldystrophie des Typs 2B und Gehfähigkeit bis zu einem hohen Alter geführt hat. Es wurden AONs mit einem tricyclo-DNA-Rückgrat angewendet, welche durch die zwei zusätzlichen Kohlenstoffringeinheiten im einzelnen

Nukleosid weniger elastisch sind und eine höhere Bindeaffinität als DNA gegenber RNA-Molekülen zeigen. Die in vitro und in vivo Anwendung der entwickelten AON-Sequenzen haben Ergebnisse voriger Studien bestätigt, in denen gezeigt wurde, dass das Ausschneiden von bestimmten Exons am effizientesten durch Maskierung Exon interner Spleißverstärkender Sequenzen (engl. exon splicing enhancer, ESE) erreicht werden kann. Zwei der entwickelten Exon intern bindenden AONs haben zur Wiederherstellung der Translation des Dysferlin Proteins in humanen Dysferlin defizienten Myoblasten geführt.

7 Supplementary Figures

A

	hE26	Intron 26	
WT	...CG<u>GAGAAGAC</u>GTGAGTCGTGGGC...		MaxEnt 9.22
IM DYSF4	...CG<u>GAGAAGAC</u>GAGAGTCGTGGGC...		MaxEnt 1.03
	hE25	hE27	
	...<u>GCTGAAACC</u>	TC<u>TGCTCCATGACATGGA</u>...	

Figure 7.1: The c.2810+2T>A mutation in IM DYSF4 assumably results in a STOP codon by exon 26 exclusion due to the 5'splice site mutation in intron 26. No dysferlin protein is expressed in IM DYSF4. Underscores depict every second triplet of the in-frame triplet code. MaxEnt scores for endogenous 5'SS and for the strongest cryptic 5'SS within 200 nucleotides downstream of the endogenous 5'SS were calculated using the MaxEntScan::score5ss algorithm.
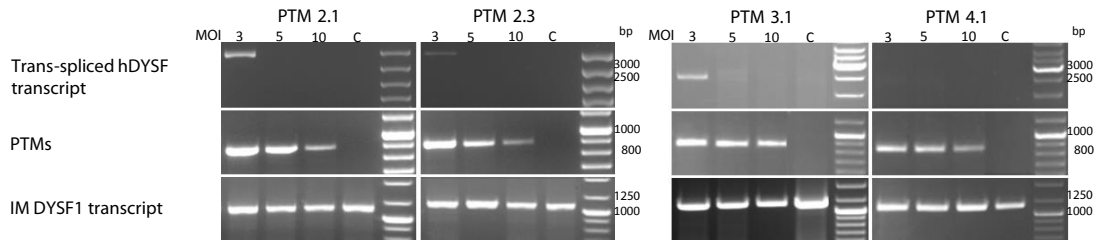
Figure 7.2: *Trans*-splicing in IM DYSF1 was detectable after transduction at the MOI of 3. *Trans*-spliced hDYSF transcripts, hPTM transcripts and IM DYSF1 dysferlin transcripts in transductions at MOIs of 3; 5 and 10. Transcript detection was performed as described for Fig.2.
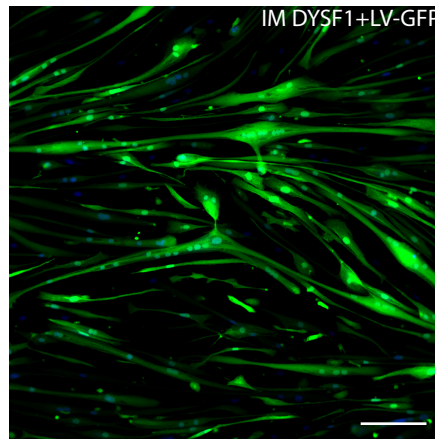
Figure 7.3: LV-GFP transduced IM DYSF1 myoblasts at differentiation day 14.
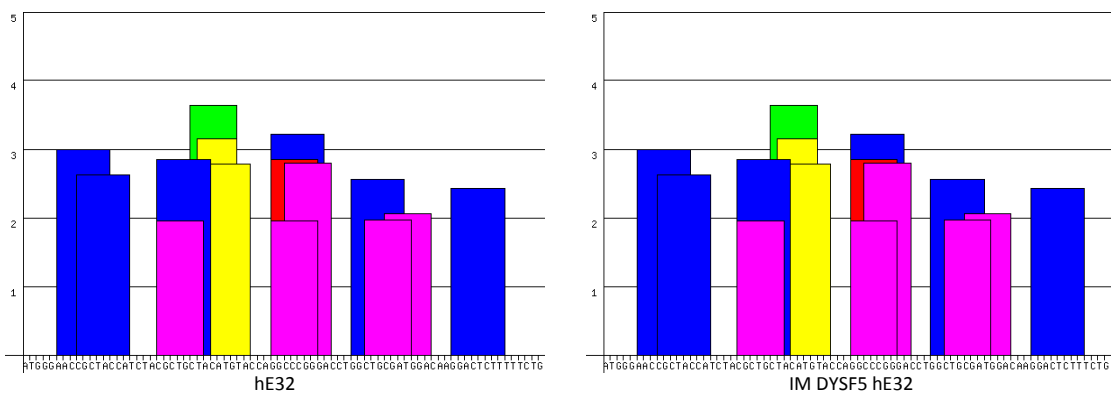
Figure 7.4: Prediction of high-score ESE motifs for human dysferlin exon 32 is unaltered in IM DYSF5. (A) Unmutated human dysferlin exon 32. (B) Mutated human dysferlin exon 32 in IM DYSF5 (delTT c.3516_3517).

A

```
                              hE4              Intron 4
WT          ...GCCCACAGGGGTAAGTGCCCATC...    MaxEnt 9.65

IM DYSF5    ...GCCCACAGGGATAAGTGCCCATC...    MaxEnt 1.47

                   hE3                    hE5
           ...GAGGAACAG GCCTCGCTGGTCCTGCAG ... GATGTAGTG
```

B

```
WT
             hE4                    Intron 4
...GCCCACAGGGGTAAGTGCCCATCAGCCTCTGCCAGGTTAAGG...  MaxEnt 3.60


IM DYSF5
                  hE4cryptic                        hE5
...GCCCACAGGGATAAGTGCCCATCAGCCTCTGCCAG GCCTCG...CCTGACCTG...
```

Figure 7.5: The c.342+1G>A mutation in IM DYSF5 results in a STOP codon either by (**A**) exon 4 exclusion or (**B**) possible cryptic 5'SS recognition. No dysferlin protein is expressed in IM DYSF5. Underscores depict every second triplet of the triplet in-frame code. MaxEnt scores for endogenous 5'SS and for the strongest cryptic 5'SS within 200 nucleotides downstream of the endogenous 5'SS were calculated using the MaxEntScan::score5ss algorithm.


Figure 7.6: The FΔ508 mutation in human exon 10 causes the deletion of a putative ESE sequence indicating a possible weakening of the exon 10 definition by the mutation. Graphic depiction of the ESE analysis showing high-score values of putative ESE exceeding default thresholds set be the ESE finder 3.0 software (Cartegni et al., 2003)

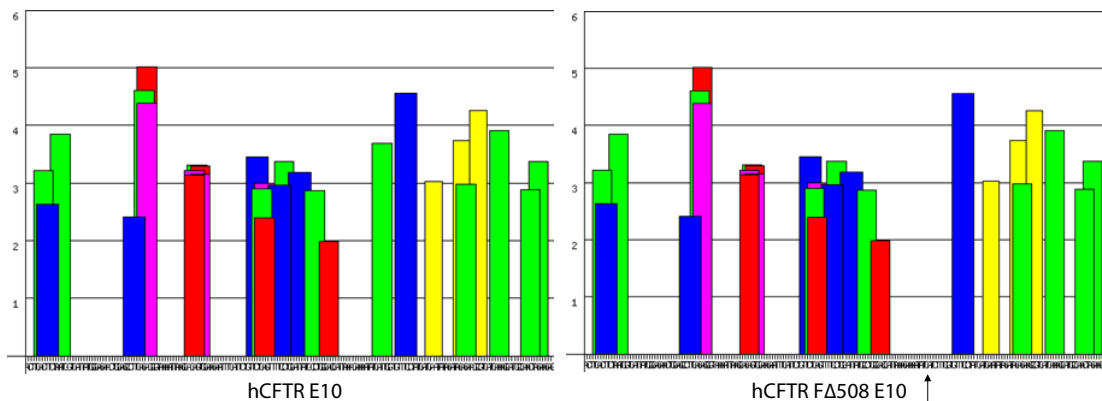|	Gene	TI	Size	3'Splice Site	MaxEnt	exon downstream of TI	antisense binding position
	hDYSF	31	551 bp	UGUUUUUCCCUUGGUGAAGaug	4.44	unmutated	5'SS proximity
	hDYSF	35	1247 bp	AUCCCAUGGCUGUGGGCCAGgug	4.57	unmutated	5'SS proximity
	mDYSF	31	551 bp	CUGUUUCCUCCUGAGUGAAGaug	0.29	unmutated	5'SS proximity
	mDYSF	35	1236 bp	CUGGAUGUGGCCCAUCACAGaug	4.24	unmutated	5'SS proximity
Puttaraju M, 1999	hGC6	1	352 bp	AAGCAGUGUCCUUGUCCCAGggg	3.30	unmutated	3'SS proximity; masking bp
Lorain S, 2010 and 2013*	mDMD	22	913 bp	AACUUCUAUUUAAUUUUGAGgcu	1.94	unmutated in *mdx4Cv* and wt, nonsense in *mdx*	5'SS proximity
Monjaret F, 2014	hDYSF	48	269 bp	AGAGUGAUACCUUUCCCCAGguu	5.67	unmutated	3'SS and 5'SS proximity masking ppt and bp
Liu X, 2002&2005	hCFTR	9	10640 bp	AUGAUGGGUUUUAUUUCCAGacu	6.56	ΔF508 c.1521_1523delCTT	3'SS proximity
Rodriguez T, 2005 and 2009;Avale ME, 2013*	htau	9	13645 bp	CUUUUUCUGGCUACCAAAGgug	5.70	excessively ΔE10-causing in *htau*	3'SS proximity; masking bp
Chao H, 2003*	mF8	15	2706 bp	GGAUUUUUUUCCUCUCUUCAGgua	10.76	neomycin insertion(E16+17) in *F8E16*	3'SS proximity; masking 3'SS
Coady T, 2007*, 2008* and 2010*	hSMN2	6	5769 bp	UUCCUUUAUUUUCCUUACAGggu	10.92	ΔE7-causing *mSMN-/-;hSMN2*	3'SS proximity; masking bp and ppt

Figure 7.7: Qualities of target introns (TIs) succesfully *trans*-spliced on endogenous pre-mRNA in this work and in previous studies. 3'SSs were analysed by MaxEntScan::score3ss software (Yeo G, 2004). In publications marked with * the protein translated from the *trans*-spliced transcript was shown.

8 Appendix

8.1 Primer sequences

8.1.1 Dysferlin *trans*-splicing

8.1.1.1 pre-mRNA *trans*-splicing molecule constructs

pSMD2 Synthesis

Kpn1-Xho1-EcoR5-3'SS-hDYSF-E36-F *GGGGTACCCTCGAGCCGGATATCTTTTTTTTTTTTTTTTTT-TAATTAACAGGTGCAGGAGACATCAAGGATC*

Kpn1-Xho1-EcoR5-3'SS-hDYSF-E37-F *GGGGTACCCTCGAGCCGGATATCTTTTTTTTTTTTTTTTTT-TAATTAACAGTCTGAGGACACAGACCTGCC*

Kpn1-Xho1-EcoR5-3'SS-hDYSF-E32-F *GGGGTACCCTCGAGCGGGATATCTTTTTTTTTTTTTTTTTT-TAATTAACAGATGGGAACCGCTACCATCTAC*

Kpn1-Xho1-EcoR5-3'SS-hDYSF-E31-F *GGGGTACCCTCGAGCGGGATATCTTTTTTTTTTTTTTTTTT-TAATTAACAGGGCGGCGTGATGGATGACAA*

EcoR1-HAtag-hDYSF-E55-R *CGGAATTCAAGCGTAATCTGGAACATCGTATGGGTAGCT-GAAGGGC*
TTCACCAGCTTC

TI30-AS1-F *CCGCTCGAGCACACAGCTGGCTTCACATG*

TI30-AS1-R *GAAGGCCTAGTTAGTATTCGAGCAACGTTATAATAATGTTCCGCGGGGCGCGC-CGTACTGGCACACAGCCAGTC*

TI30-AS2-F *CCGCTCGAGCTGGAGACACGAAGCTGGTTATG*

TI30-AS2-R *GAAGGCCTAGTTAGTATTCGAGCAACGTTATAATAATGTTCCGCGGGGCGCGC-CGAGCTCCCCAGAATGAAATTAG*

TI35-AS1-F *CCGCTCGAGGAGGTCTTGGTAAGAACAATTC*

TI35-AS1-R *GAAGGCCTAGTTAGTATTCGAGCAACGTTATAATAATGTTCCGCGGGGCGCGC-CGAGTCCTACTTCAAGCCCAC*

TI35-AS2-F *CCGCTCGAGCTGGCCCACAGCCATGGGATG*

TI35-AS2-R *GAAGGCCTAGTTAGTATTCGAGCAACGTTATAATAATGTTCCGCGGGGCGCGC-CGTGGTTTCTGTTGGCTCCTC*

TI36-AS1-F *CCGCTCGAGCTAATGGCAGGAAGTGGCTGC*

TI36-AS1-R *GAAGGCCTAGTTAGTATTCGAGCAACGTTATAATAATGTTCCGCGGGGCGCGC-CGGAGGAGAGATGCACGTTCC*

mTI31-mAS1-F *CCGCTCGAGGACAGATCCTAGCTCAGAAGCAG*

mTI31-mAS1-R *GAAGGCCTAGTTAGTATTCGAGCAACGTTATAATAATGTTCCGCGGGGCGCGC-CGAGATGTGTGCATTCAAGTTCCTG*

mTI31-mAS3-F *CCGCTCGAGGAATATCCAGCACTCACAGAAGATG*

mTI31-mAS3-R *GAAGGCCTAGTTAGTATTCGAGCAACGTTATAATAATGTTCCGCGGGGCGCGC-CCTGGTAGGTGGGAGAAGGAGAG*

mTI35-mAS1-F *CCGCTCGAGCAGAGGTTGTGATGACACTTG*

mTI35-mAS1-R *GAAGGCCTAGTTAGTATTCGAGCAACGTTATAATAATGTTCCGCGGGGCGCGC-CGAGTTCCAGACTGCAGAGAG*

mTI35-AS2-F *CCGCTCGAGCTGTGATGGGCCACATCCAG*

mTI35-mAS2-R *GAAGGCCTAGTTAGTATTCGAGCAACGTTATAATAATGTTCCGCGGGGCGCGC-CGGGTGCCATCTCTGTCTCAGTG*

pRRL synthesis

CMV-F1-Xba1 *TCTAGAAAGACACCGGGACCGATCC*

PSMD2-R7-Xba1 *TCTAGAGGCAGCCTGC*

Xba1-Mlu1-EcoR5-3'SS-hDYSF-E32-F *GCTCTAGAACGCGTCGGGATATCTTTTTTTTTTTTTTTTTT-TAATTAACAGATGGGAACCGCTACCATCTA*

Xba1-EcoR1-HaTag-E55R *GCTCTAGAGAATTCAAGCGTAATCTGGAACATCGTATGGGTAGCT-GAAGGGCTTCACCAGCT*

I31-AS1-F *CGACGCGTTTAACATGTCCTTGGGCCAGC*

I31-AS1-R *CGACGCGTAGTTAGTATTCGAGCAACGTTATAATAATGTTCCGCGGGGCGCGC-CCAAATCTGAGATCAGGCATTTAAGG*

I31-AS2-F *CGACGCGTCATCTTCACCAAGGGAAAAAACAG*

I31-AS2-R *CGACGCGTAGTTAGTATTCGAGCAACGTTATAATAATGTTCCGCGGGGCGCGC-CGCCCTTTCTAGGGACAGACTCCAC*

I31-AS3-F *CGACGCGTGAAGCCACAGGACCCTGGTGAC*

I31-AS3-R *CGACGCGTAGTTAGTATTCGAGCAACGTTATAATAATGTTCCGCGGGGCGCGC-CCTGGTAGGTGGGAGAGAGGCAG*

Excision HA-tag

Xba1-EcoR1-noHaTag-E55-R *GCTCTAGAGAATTCAGCTGAAGGGCTTCACCAGCTTCATG-GCAG*

Excision AS

Kpn1-Xho1-deltaAS-F *GGTACCCTCGAGGTTGCTCGAATACTAACTAGG*

8.1.1.2   Dysferlin *trans*-splicing detection and sequencing

Trans-splicing detection hDYSF

hE37R *GTGGTGGGTAGGGCAGG*

hE30F *GGAAGTTCCACCTCGAGTAC*

hE35F *CCACCATATTCCTGGTTTTGAG*

HA-tagR *CGTAATCTGGAACATCGTATG*

E48F *GGACCTCCCTTCAACATCAC*

hE40R *CATCGACATTGATGACAAGG*

Trans-splicing detection mDYSF

HemiF *TTGCTCGAATACTAACTAGGATC*

mE30F *GGAGTATGCCTCTCTCTTCG*

mE40R *TGGACAGGAATGAGAGGCTC*

E48F *GGACCTCCCTTCAACATCAC*

hE54R *GATGATGAAGAGGATGATGG*

mE30Fi *GAGTACCGCAAGACAGATGC*

hE37R *GTGGTGGGTAGGGCAGG*

hE40R *CATCGACATTGATGACAAGG*

m18SF *ACCTGGTTGATCCTGCCAGTAG*

m18SR *TTAATGAGCCATTCGCAGTTTC*

Sequencing *trans*-splicing mDYSF

mE31F *GTGGATGACAAGAGCGAAGAC*

mE34F *GCTCTATGACCACGACACC*

hE37R *GTGGTGGGTAGGGCAGG*

Sequencing *trans*-splicing hDYSF

hE30Fi *CATGGAGCCACTGGAGAAG*

hE34F *TGCATCTGTCAACCGAGTC*

hE33R *TACAGCTCCACCACAATGC*

hE38R *GGTGCAGATGTCAAAGTTG*

8.1.2 Dysferlin exon 32-skipping detection, sequencing and quantification

Detection *hDYSF* exon 32 excision

    hE30F *GGAAGTTCCACCTCGAGTAC*

    hE30Fi *CATGGAGCCACTGGAGAAG*

    hE38R *GGTAACTCTTCATGTTCCGCA*

    hE40R *GACTGAGTAGGCTCACATCG*

Detection *mDYSF* exon 32 excision

    mE30F *GGAGTATGCCTCTCTCTTCG*

mE30Fi *GAGTACCGCAAGACAGATGC*

mE39R *CAATAGGTGGACAGTAGAGGTC*

mE40R *GGCTGAGTAAGCTCACATC*

Sequencing human Δ32-dysferlin transcript

hE30Fi *CATGGAGCCACTGGAGAAG*

hE37R GTGGTGGGTAGGGCAGG

Sequencing murine Δ32-dysferlin transcript

mE31F *GTGGATGACAAGAGCGAAGAC*

m39R *CAATAGGTGGACAGTAGAGGTC*

Quantification Δ32-dysferlin transcript

mE31F *TGGATGACAAGAGCGAAGAC*

mE31_33R *GAGACGATGGCGTAGGGATAGT*

mE31_32R *GATGGTAGCGGTTCCCATAGT*

m18SF *ACCTGGTTGATCCTGCCAGTAG*

m18SR *TTAATGAGCCATTCGCAGTTTC*

9   Abbreviations

AAV	adeno-associated virus
A	adenosine
AON	antisense-oligonucleotide
AS	antisense sequence of the pre-mRNA *trans*-splicing molecule binding domain
ATP	adenosine triphosphate
bp	base pair
BP	branch point
BSA	bovine serum albumin
C	cytidine
˚C	degree celcius
C2	second constant sequence found in classical protein kinase C isoform
CaCl$_2$	calcium chloride
cdk-4	cyclin-dependent kinase 4
CK	creatine kinase
CMV	cytomegalovirus
c-terminus	carboxyl-terminus
Cy3	cyanine dye 3
cPPT	optimized polypurine tract
DGC	dystrophin-associated glycoprotein complex
DMD	Duchenne muscular dystrophy
DNA	deoxyribonucleic acid
DYSF	dysferlin
EDTA	Ethylenediaminetetraacetic acid
ESE	exonic spice enhancer
ESS	exonic spice silencer
G	guanosine
HEPES	2-[4-(2-hydroxyethyl)piperazin-1-yl]ethanesulfonic acid
HIV-1	human immunodeficiency virus 1
hnRNP	heterogenous nuclear ribonucleoprotein
hTERT	human telomerase reverse transcriptase
IM DYSF	immortalized human myoblasts taken from a patient biopsy

CHAPTER 9. ABBREVIATIONS

IM WT	immortalized human myoblasts taken from a healthy individual
kb	kilobase
KCl	potassium chloride
LGMD2B	limb girdle muscular dystrophy type 2B
LV	lentivirus vector
mAON	antisense-oligonucleotide complementary to murine genomic sequence
MAPK/ERK	mitogen-activated protein kinase/extracellular signal-regulated kinases
MaxEnt	maximum entropy model score of splice sites
mBBP	mammalian branch point bridging protein
MCS	multiple cloning site
MD	muscular dystrophy
$MgCl_2$	magnesium chloride
MHC	myosin heavy chain (slow)
mM	millimolar
MMD1	Miyoshi Myopathy 1
MOI	multiplicity of infection
mPTM	pre-mRNA *trans*-splicing molecule comprising murine antisense sequence
mRNA	messenger ribonucleic acid
mW	milliwatt
Na	sodium
NaCl	sodium chloride
NaF	sodium fluoride
nt	nucleotide
n-terminus	amino-terminus
PBS	phosphate-buffered saline
PCR	polymerase chain reaction
PD	population doublings
PGK-1	phosphoglycerate kinase-1
pH	pH-value, decimal logarithm of the reciprocal of the hydrogen ion activity in a solution
PPT	poly-pyrimidine tract
pre-mRNA	precursor-messenger ribonucleic acid
PTM	pre-mRNA *trans*-splicing molecule
Qua	quadriceps
qPCR	quantitative polymerase chain reaction
rAAV	recombinant adeno-associated virus
RNA	ribonucleic acid
RT	reverse transcription
RT-PCR	reverse transcription polymerase chain reaction
s	seconds
SD	standard deviation
SEM	standard error of the mean

SF1	splicing factor 1
SIN	self-inactivating
SL	spliced leader
SmaRT	spliceosome-mediated pre-mRNA *trans*-splicing
SMN	Survival of Motor Neuron
SMN1	Survival of Motor Neuron 1
SMN2	Survival of Motor Neuron 2
snRNP	small nuclear ribonucleoprotein
SR-protein	serine/arginine-rich protein
SS	splice site
T	thymidine
TA	tibialis anterior
tcDNA	tricyclo-DNA
TI	target intron
U	uridine
U2AF	uridine-rich 2 small nuclear ribonucleoprotein auxiliary factor
U snRNP	uridine-rich small nuclear riboprotein
V	Volt
WPRE	Woodchuck hepatitis virus Posttranscriptional Regulatory Element
WT	wild-type
Y	pyrimidine

CHAPTER 9. ABBREVIATIONS

10   Acknowledgements

Chauveaux, PhD for their joyful presence in- and outside of the lab and for sharing a great time in this crazy city of Paris.

I would like to thank my MyoGrad co-fighters from the first generation of PhD students in this great bilateral graduate programme (which sadly was denied to be continued by the German Research Foundation) Elja Schirwis, PhD; Sonia Relizani, PhD; Antoine Zalc, Joscha Griger, Séverine Kunz and Adeline Bourgois.

I would like to thank Dr.rer.nat. Andreas Marg for sharing his expertise on laser-mediated membrane wounding and teaching me the conductance of this technique and for his scientific advice during my time in the Berlin lab.

I would like to thank Dr.rer.nat. Ute Zacharias for guiding me during the initial period of my thesis and on my work of immortalised myoblasts, and Dr. rer. nat. Katrin Wenzel for her scientific advice during my time in the lab in Berlin.

I would like to thank Stephanie Meyer-Liesener, Séverine Kunz and Dr.med. Verena Schoewel for the joyful atmosphere in the Berlin lab and their organisational support from the Berlin site during my time in Paris.

I would like to thank Dr.rer.nat. Stefanie Grunwald, Dr.ing. Tobias Timmel, Kornelia Gräning, Adrienne Rothe and Stefanie Belz for the friendly atmosphere in the Berlin lab.

I would like to thank Melanie Durand and Maud Casier for being my best french friends, for introducing me to many aspects of their culture, for spending great nights out in Paris, for including me into their circle of friends, even though I was the gringa soon to return to good old Germany.

I would like to thank Florian Rau and Cornelia Schendzielorz and Anne Geib for being my most important persons and supportive and loving always.

I would like to thank my beloved parents for having given me access to this excess of education and being supportive always.

11   Publications

Lorain S, Peccate C, Le Hir M, Griffith G, Philippi S, Precigout G, Mamchaoui K, Jollet A, Voit T, Garcia L (2013). Dystrophin rescue by trans-splicing: a strategy for DMD genotypes not eligible for exon skipping approaches. Nucleic Acids Research. 1-12.

Philippi S, Bigot A, Marg A, Mouly V, Spuler S, Zacharias U (2012). Dysferlin-deficient immortalized human myoblasts and myotubes as a useful tool to study dysferlinopathy. PLoS Currents Muscular Dystrophy. 2;4:RRN1298.

Mamchaoui K, Trollet C, Bigot A, Negroni E, Chaouch S, Wolff A, Kandalla PK, Marie S, Di Santo J, St Guily JL, Muntoni F, Kim J, Philippi S, Spuler S, Levy N, Blumen SC, Voit T, Wright WE, Aamiri A, Butler-Browne G, Mouly V (2011). Immortalized pathological human myoblasts: towards a universal tool for the study of neuromuscular disorders. Skeletal Muscle. 1, 34.

CHAPTER 11. PUBLICATIONS

Bibliography

Aartsma-Rus A, De Winter CL, Janson AAM, Kaman WE, Van Ommen GJB, Den Dunnen JT, Van Deutekom JCT (2005) Functional analysis of 114 exon-internal AONs for targeted DMD exon skipping: indication for steric hindrance of SR protein binding sites. Oligonucleotides 15:284–297.

Abovich N, Liao XC, Rosbash M (1994) The yeast MUD2 protein: an interaction with PRP11 defines a bridge between commitment complexes and U2 snRNP addition. Genes Dev 8:843–854.

Achanzar WE, Ward S (1997) A nematode gene required for sperm vesicle fusion. J Cell Sci 110 (Pt 9):1073–1081.

Ampong BN, Imamura M, Matsumiya T, Yoshida M, Takeda S (2005) Intracellular localization of dysferlin and its association with the dihydropyridine receptor. Acta Myol 24:134–144.

Anderson LV, Davison K, Moss JA, Young C, Cullen MJ, Walsh J, Johnson MA, Bashir R, Britton S, Keers S, Argov Z, Mahjneh I, Fougerousse F, Beckmann JS, Bushby KM (1999) Dysferlin is a plasma membrane protein and is expressed early in human development. Hum Mol Genet 8:855–861.

Andorfer C, Kress Y, Espinoza M, de Silva R, Tucker KL, Barde YA, Duff K, Davies P (2003) Hyperphosphorylation and aggregation of tau in mice expressing normal human tau isoforms. J Neurochem 86:582–590.

Aoki M, Liu J, Richard I, Bashir R, Britton S, Keers SM, Oeltjen J, Brown HE, Marchand S, Bourg N, Beley C, McKenna-Yasek D, Arahata K, Bohlega S, Cupler E, Illa I, Majneh I, Barohn RJ, Urtizberea JA, Fardeau M, Amato A, Angelini C, Bushby K, Beckmann JS, Brown R Jr (2001) Genomic organization of the dysferlin gene and novel mutations in Miyoshi myopathy. Neurology 57:271–278.

Aoki Y, Nakamura A, Yokota T, Saito T, Okazawa H, Nagata T, Takeda S (2010) In-frame dystrophin following exon 51-skipping improves muscle pathology and function in the exon 52-deficient mdx mouse. Mol Ther 18:1995–2005.

Aoki Y, Yokota T, Nagata T, Nakamura A, Tanihata J, Saito T, Duguez SMR, Nagaraju K, Hoffman EP, Partridge T, Takeda S (2012) Bodywide skipping of exons 45-55 in dystrophic mdx52 mice by systemic antisense delivery. Proc Natl Acad Sci U S A 109:13763–13768.

BIBLIOGRAPHY

Arechavala-Gomeza V, Graham IR, Popplewell LJ, Adams AM, Aartsma-Rus A, Kinali M, Morgan JE, van Deutekom JC, Wilton SD, Dickson G, Muntoni F (2007) Comparative analysis of antisense oligonucleotide sequences for targeted skipping of exon 51 during dystrophin pre-mRNA splicing in human muscle. Hum Gene Ther 18:798–810.

Arning S, Grüter P, Bilbe G, Krämer A (1996) Mammalian splicing factor SF1 is encoded by variant cDNAs and binds to RNA. RNA 2:794–810.

Avale ME, Rodríguez-Martín T, Gallo JM (2013) Trans-splicing correction of tau isoform imbalance in a mouse model of tau mis-splicing. Hum Mol Genet 22:2603–2611.

Bansal D, Miyake K, Vogel SS, Groh S, Chen CC, Williamson R, McNeil PL, Campbell KP (2003) Defective membrane repair in dysferlin-deficient muscular dystrophy. Nature 423:168–172.

Bartlett JS, Wilcher R, Samulski RJ (2000) Infectious entry pathway of adeno-associated virus and adeno-associated virus vectors. J Virol 74:2777–2785.

Bashir R, Britton S, Strachan T, Keers S, Vafiadaki E, Lako M, Richard I, Marchand S, Bourg N, Argov Z, Sadeh M, Mahjneh I, Marconi G, Passos-Bueno MR, Moreira EdS, Zatz M, Beckmann JS, Bushby K (1998) A gene related to Caenorhabditis elegans spermatogenesis factor fer-1 is mutated in limb-girdle muscular dystrophy type 2B. Nat Genet 20:37–42.

Belanto JJ, Diaz-Perez SV, Magyar CE, Maxwell MM, Yilmaz Y, Topp K, Boso G, Jamieson CH, Cacalano NA, Jamieson CAM (2010) Dexamethasone induces dysferlin in myoblasts and enhances their myogenic differentiation. Neuromuscul Disord 20:111–121.

Bennett CF, Swayze EE (2010) RNA targeting therapeutics: molecular mechanisms of antisense oligonucleotides as a therapeutic platform. Annu Rev Pharmacol Toxicol 50:259–293.

Berget SM (1995) Exon recognition in vertebrate splicing. J Biol Chem 270:2411–2414.

Berglund JA, Chua K, Abovich N, Reed R, Rosbash M (1997) The splicing factor BBP interacts specifically with the pre-mRNA branchpoint sequence UACUAAC. Cell 89:781–787.

Berns KI, Giraud C (1995) Adenovirus and adeno-associated virus as vectors for gene therapy. Ann N Y Acad Sci 772:95–104.

Béroud C, Tuffery-Giraud S, Matsuo M, Hamroun D, Humbertclaude V, Monnier N, Moizard MP, Voelckel MA, Calemard LM, Boisseau P, Blayau M, Philippe C, Cossée M, Pagès M, Rivier F, Danos O, Garcia L, Claustres M (2007) Multiexon skipping leading to an artificial DMD protein lacking amino acids from exons 45 through 55 could rescue up to 63 Hum Mutat 28:196–202.

Bi L, Lawler AM, Antonarakis SE, High KA, Gearhart JD, Kazazian H Jr (1995) Targeted disruption of the mouse factor VIII gene produces a model of haemophilia A. Nat Genet 10:119–121.

Bigot A, Jacquemin V, Debacq-Chainiaux F, Butler-Browne GS, Toussaint O, Furling D, Mouly V (2008) Replicative aging down-regulates the myogenic regulatory factors in human myoblasts. Biol Cell 100:189–199.

Blankinship MJ, Gregorevic P, Chamberlain JS (2006) Gene therapy strategies for Duchenne muscular dystrophy utilizing recombinant adeno-associated virus vectors. Mol Ther 13:241–249.

Blau HM, Chiu CP, Pavlath GK, Webster C (1985) Muscle gene expression in heterokaryons. Adv Exp Med Biol 182:231–247.

Blumenthal T (2012) Trans-splicing and operons in C. elegans. WormBook pp 1–11.

Bolduc V, Marlow G, Boycott KM, Saleki K, Inoue H, Kroon J, Itakura M, Robitaille Y, Parent L, Baas F, Mizuta K, Kamata N, Richard I, Linssen WHJP, Mahjneh I, de Visser M, Bashir R, Brais B (2010) Recessive mutations in the putative calcium-activated chloride channel Anoctamin 5 cause proximal LGMD2L and distal MMD3 muscular dystrophies. Am J Hum Genet 86:213–221.

Bostick B, Yue Y, Long C, Marschalk N, Fine DM, Chen J, Duan D (2009) Cardiac expression of a mini-dystrophin that normalizes skeletal muscle force only partially restores heart function in aged Mdx mice. Mol Ther 17:253–261.

Branlant C, Krol A, Ebel JP, Lazar E, Haendler B, Jacob M (1982) U2 RNA shares a structural domain with U1, U4, and U5 RNAs. EMBO J 1:1259–1265.

Breen MA, Ashcroft SJ (1997) A truncated isoform of Ca2+/calmodulin-dependent protein kinase II expressed in human islets of Langerhans may result from trans-splicing. FEBS Lett 409:375–379.

Breslauer KJ, Frank R, Blöcker H, Marky LA (1986) Predicting DNA duplex stability from the base sequence. Proc Natl Acad Sci U S A 83:3746–3750.

Bruzik JP, Maniatis T (1992) Spliced leader RNAs from lower eukaryotes are trans-spliced in mammalian cells. Nature 360:692–695.

Burge C, Tuschl T, Sharp P (1999) The RNA world. The RNA World .

Cai C, Masumiya H, Weisleder N, Matsuda N, Nishi M, Hwang M, Ko JK, Lin P, Thornton A, Zhao X, Pan Z, Komazaki S, Brotto M, Takeshima H, Ma J (2009a) MG53 nucleates assembly of cell membrane repair machinery. Nat Cell Biol 11:56–64.

Cai C, Weisleder N, Ko JK, Komazaki S, Sunada Y, Nishi M, Takeshima H, Ma J (2009b) Membrane repair defects in muscular dystrophy are linked to altered interaction between MG53, caveolin-3, and dysferlin. J Biol Chem 284:15894–15902.

Carothers AM, Urlaub G, Grunberger D, Chasin LA (1993) Splicing mutants and their second-site suppressors at the dihydrofolate reductase locus in Chinese hamster ovary cells. Mol Cell Biol 13:5085–5098.

BIBLIOGRAPHY

Cartegni L, Wang J, Zhu Z, Zhang MQ, Krainer AR (2003) ESEfinder: a web resource to identify exonic splicing enhancers. Nucleic acids research 31:3568–3571.

Caudevilla C, Serra D, Miliar A, Codony C, Asins G, Bach M, Hegardt FG (1998) Natural transsplicing in carnitine octanoyltransferase pre-mRNAs in rat liver. Proc Natl Acad Sci U S A 95:12185–12190.

Chan JH, Lim S, Wong W (2006) Antisense oligonucleotides: from design to therapeutic application. Clinical and experimental pharmacology and physiology 33:533–540.

Chao H, Liu Y, Rabinowitz J, Li C, Samulski RJ, Walsh CE (2000) Several log increase in therapeutic transgene delivery by distinct adeno-associated viral serotype vectors. Mol Ther 2:619–623.

Chao H, Mansfield SG, Bartel RC, Hiriyanna S, Mitchell LG, Garcia-Blanco MA, Walsh CE (2003) Phenotype correction of hemophilia A mice by spliceosome-mediated RNA trans-splicing 9:1015–1019.

Chaouch S, Mouly V, Goyenvalle A, Vulin A, Mamchaoui K, Negroni E, Di Santo J, Butler-Browne G, Torrente Y, Garcia L, Furling D (2009) Immortalized skin fibroblasts expressing conditional MyoD as a renewable and reliable source of converted human muscle cells to assess therapeutic strategies for muscular dystrophies: validation of an exon-skipping approach to restore dystrophin in Duchenne muscular dystrophy cells. Hum Gene Ther 20:784–790.

Charrier S, Stockholm D, Seye K, Opolon P, Taveau M, Gross D, Bucher-Laurent S, Delenda C, Vainchenker W, Danos O, et al. (2005) A lentiviral vector encoding the human Wiskott–Aldrich syndrome protein corrects immune and cytoskeletal defects in WASP knockout mice. Gene therapy 12:597–606.

Chirmule N, Xiao W, Truneh A, Schnell MA, Hughes JV, Zoltick P, Wilson JM (2000) Humoral immunity to adeno-associated virus type 2 vectors following administration to murine and nonhuman primate muscle. J Virol 74:2420–2425.

Chiu YH, Hornsey MA, Klinge L, Jørgensen LH, Laval SH, Charlton R, Barresi R, Straub V, Lochmüller H, Bushby K (2009) Attenuated muscle regeneration is a key factor in dysferlin-deficient muscular dystrophy. Hum Mol Genet 18:1976–1989.

Cirak S, Arechavala-Gomeza V, Guglieri M, Feng L, Torelli S, Anthony K, Abbs S, Garralda ME, Bourke J, Wells DJ, Dickson G, Wood MJA, Wilton SD, Straub V, Kole R, Shrewsbury SB, Sewry C, Morgan JE, Bushby K, Muntoni F (2011) Exon skipping and dystrophin restoration in patients with Duchenne muscular dystrophy after systemic phosphorodiamidate morpholino oligomer treatment: an open-label, phase 2, dose-escalation study. Lancet 378:595–605.

Coady TH, Baughan TD, Shababi M, Passini MA, Lorson CL (2008) Development of a single vector system that enhances trans-splicing of SMN2 transcripts 3:–.

110

Coady TH, Lorson CL (2010) Trans-splicing-mediated improvement in a severe mouse model of spinal muscular atrophy 30:126–130.

Coady TH, Shababi M, Tullis GE, Lorson CL (2007) Restoration of SMN function: delivery of a trans-splicing RNA re-directs SMN2 pre-mRNA splicing. Mol Ther 15:1471–1478.

Coffin JM (1990) Molecular mechanisms of nucleic acid integration. J Med Virol 31:43–49.

Conrad R, Lea K, Blumenthal T (1995) SL1 trans-splicing specified by AU-rich synthetic RNA inserted at the 5' end of Caenorhabditis elegans pre-mRNA. RNA 1:164–170.

Covian-Nares JF, Koushik SV, Puhl HL 3rd, Vogel SS (2010) Membrane wounding triggers ATP release and dysferlin-mediated intercellular calcium signaling. J Cell Sci 123:1884–1893.

Crick F (1979) Split genes and RNA splicing. Science 204:264–271.

Cudré-Mauroux C, Occhiodoro T, König S, Salmon P, Bernheim L, Trono D (2003) Lentivector-mediated transfer of Bmi-1 and telomerase in muscle satellite cells yields a duchenne myoblast cell line with long-term genotypic and phenotypic stability. Hum Gene Ther 14:1525–1533.

Davis DB, Doherty KR, Delmonte AJ, McNally EM (2002) Calcium-sensitive phospholipid binding properties of normal and mutant ferlin C2 domains. J Biol Chem 277:22883–22888.

De Angelis FG, Sthandier O, Berarducci B, Toso S, Galluzzi G, Ricci E, Cossu G, Bozzoni I (2002) Chimeric snRNA molecules carrying antisense sequences against the splice junctions of exon 51 of the dystrophin pre-mRNA induce exon skipping and restoration of a dystrophin synthesis in Delta 48-50 DMD cells. Proc Natl Acad Sci U S A 99:9456–9461.

De Luna N, Díaz-Manera J, Paradas C, Iturriaga C, Rojas-García R, Araque J, Genebriera M, Gich I, Illa I, Gallardo E (2012) 1α,25(OH)(2)-Vitamin D3 increases dysferlin expression in vitro and in a human clinical trial. Mol Ther 20:1988–1997.

De Luna N, Gallardo E, Illa I (2004) In vivo and in vitro dysferlin expression in human muscle satellite cells 63:1104–1113.

De Luna N, Gallardo E, Soriano M, Dominguez-Perles R, de la Torre C, Rojas-García R, García-Verdugo JM, Illa I (2006) Absence of dysferlin alters myogenin expression and delays human muscle differentiation "in vitro". J Biol Chem 281:17092–17098.

De Morrée A, Flix B, Bagaric I, Wang J, van den Boogaard M, Grand Moursel L, Frants RR, Illa I, Gallardo E, Toes R, van der Maarel SM (2013) Dysferlin regulates cell adhesion in human monocytes. J Biol Chem 288:14147–14157.

Demonbreun AR, Fahrenbach JP, Deveaux K, Earley JU, Pytel P, McNally EM (2011) Impaired muscle growth and response to insulin-like growth factor 1 in dysferlin-mediated muscular dystrophy. Hum Mol Genet 20:779–789.

BIBLIOGRAPHY

Denti MA, Rosa A, D'Antona G, Sthandier O, De Angelis FG, Nicoletti C, Allocca M, Pansarasa O, Parente V, Musarò A, Auricchio A, Bottinelli R, Bozzoni I (2006) Chimeric adeno-associated virus/antisense U1 small nuclear RNA effectively rescues dystrophin synthesis and muscle function by local treatment of mdx mice. Hum Gene Ther 17:565–574.

Ding W, Zhang L, Yan Z, Engelhardt JF (2005) Intracellular trafficking of adeno-associated viral vectors. Gene Ther 12:873–880.

Djikeng A, Ferreira L, D'Angelo M, Dolezal P, Lamb T, Murta S, Triggs V, Ulbert S, Villarino A, Renzi S, Ullu E, Tschudi C (2001) Characterization of a candidate Trypanosoma brucei U1 small nuclear RNA gene. Mol Biochem Parasitol 113:109–115.

Doherty KR, Cave A, Davis DB, Delmonte AJ, Posey A, Earley JU, Hadhazy M, McNally EM (2005) Normal myoblast fusion requires myoferlin. Development 132:5565–5575.

Doherty KR, Demonbreun AR, Wallace GQ, Cave A, Posey AD, Heretis K, Pytel P, McNally EM (2008) The endocytic recycling protein EHD2 interacts with myoferlin to regulate myoblast fusion. J Biol Chem 283:20252–20260.

Dönmez G, Hartmuth K, Kastner B, Will CL, Lührmann R (2007) The 5' end of U2 snRNA is in close proximity to U1 and functional sites of the pre-mRNA in early spliceosomal complexes. Mol Cell 25:399–411.

Douar AM, Poulard K, Stockholm D, Danos O (2001) Intracellular trafficking of adeno-associated virus vectors: routing to the late endosomal compartment and proteasome degradation. J Virol 75:1824–1833.

Dye MJ, Proudfoot NJ (1999) Terminal exon definition occurs cotranscriptionally and promotes termination of RNA polymerase II. Mol Cell 3:371–378.

Fairbrother WG, Yeo GW, Yeh R, Goldstein P, Mawson M, Sharp PA, Burge CB (2004) RESCUE-ESE identifies candidate exonic splicing enhancers in vertebrate exons. Nucleic Acids Res 32:W187–W190.

Follenzi A, Ailles LE, Bakovic S, Geuna M, Naldini L (2000) Gene transfer by lentiviral vectors is limited by nuclear translocation and rescued by HIV1 pol sequences. Nature genetics 25:217–222.

Freier SM, Kierzek R, Jaeger JA, Sugimoto N, Caruthers MH, Neilson T, Turner DH (1986) Improved free-energy parameters for predictions of RNA duplex stability. Proc Natl Acad Sci U S A 83:9373–9377.

Fuson K, Rice A, Mahling R, Snow A, Nayak K, Shanbhogue P, Meyer AG, Redpath GMI, Hinderliter A, Cooper ST, Sutton RB (2014) Alternate splicing of dysferlin C2A confers Ca^{2+}-dependent and Ca^{2+}-independent binding for membrane repair. Structure 22:104–115.

Gallardo E, Rojas-García R, de Luna N, Pou A, Brown R Jr, Illa I (2001) Inflammation in dysferlin myopathy: immunohistochemical characterization of 13 patients. Neurology 57:2136–2138.

112

Gazzerro E, Sotgia F, Bruno C, Lisanti MP, Minetti C (2010) Caveolinopathies: from the biology of caveolin-3 to human diseases. Eur J Hum Genet 18:137–145.

Glover L, Brown RH Jr (2007) Dysferlin in membrane trafficking and patch repair. Traffic 8:785–794.

Glover LE, Newton K, Krishnan G, Bronson R, Boyle A, Krivickas LS, Brown J Robert H (2010) Dysferlin overexpression in skeletal muscle produces a progressive myopathy 67:384–393.

Goemans NM, Tulinius M, van den Akker JT, Burm BE, Ekhart PF, Heuvelmans N, Holling T, Janson AA, Platenburg GJ, Sipkens JA, Sitsen JMA, Aartsma-Rus A, van Ommen GJB, Buyse G, Darin N, Verschuuren JJ, Campion GV, de Kimpe SJ, van Deutekom JC (2011) Systemic administration of PRO051 in Duchenne's muscular dystrophy. N Engl J Med 364:1513–1522.

Gorman L, Suter D, Emerick V, Schümperli D, Kole R (1998) Stable alteration of pre-mRNA splicing patterns by modified U7 small nuclear RNAs. Proc Natl Acad Sci U S A 95:4929–4934.

Goyenvalle A, Babbs A, van Ommen GJB, Garcia L, Davies KE (2009) Enhanced exon-skipping induced by U7 snRNA carrying a splicing silencer sequence: Promising tool for DMD therapy. Mol Ther 17:1234–1240.

Goyenvalle A, Vulin A, Fougerousse F, Leturcq F, Kaplan JC, Garcia L, Danos O (2004) Rescue of dystrophic muscle through U7 snRNA-mediated exon skipping. Science 306:1796–1799.

Graveley BR, Hertel KJ, Maniatis T (2001) The role of U2AF35 and U2AF65 in enhancer-dependent splicing. RNA 7:806–818.

Grieger JC, Samulski RJ (2005) Packaging capacity of adeno-associated virus serotypes: impact of larger genomes on infectivity and postentry steps. J Virol 79:9933–9944.

Guglieri M, Magri F, D'Angelo MG, Prelle A, Morandi L, Rodolico C, Cagliani R, Mora M, Fortunato F, Bordoni A, Del Bo R, Ghezzi S, Pagliarani S, Lucchiari S, Salani S, Zecca C, Lamperti C, Ronchi D, Aguennouz M, Ciscato P, Di Blasi C, Ruggieri A, Moroni I, Turconi A, Toscano A, Moggio M, Bresolin N, Comi GP (2008a) Clinical, molecular, and protein correlations in a large sample of genetically diagnosed Italian limb girdle muscular dystrophy patients. Hum Mutat 29:258–266.

Guglieri M, Straub V, Bushby K, Lochmüller H (2008b) Limb-girdle muscular dystrophies. Curr Opin Neurol 21:576–584.

Han R (2011) Muscle membrane repair and inflammatory attack in dysferlinopathy. Skelet Muscle 1:10.

Han R, Frett EM, Levy JR, Rader EP, Lueck JD, Bansal D, Moore SA, Ng R, Beltrán-Valero de Bernabé D, Faulkner JA, Campbell KP (2010) Genetic ablation of complement C3 attenuates muscle pathology in dysferlin-deficient mice. J Clin Invest 120:4366–4374.

BIBLIOGRAPHY

Hernández-Deviez DJ, Martin S, Laval SH, Lo HP, Cooper ST, North KN, Bushby K, Parton RG (2006) Aberrant dysferlin trafficking in cells lacking caveolin or expressing dystrophy mutants of caveolin-3. Hum Mol Genet 15:129–142.

Ho M, Gallardo E, McKenna-Yasek D, De Luna N, Illa I, Brown Jr RH (2002) A novel, blood-based diagnostic assay for limb girdle muscular dystrophy 2B and Miyoshi myopathy. Ann Neurol 51:129–133.

Hofacker IL (2003) Vienna RNA secondary structure server. Nucleic acids research 31:3429–3431.

Hoffman EP, Brown R Jr, Kunkel LM (1987) Dystrophin: the protein product of the Duchenne muscular dystrophy locus. Cell 51:919–928.

Humphrey GW, Mekhedov E, Blank PS, de Morree A, Pekkurnaz G, Nagaraju K, Zimmerberg J (2012) GREG cells, a dysferlin-deficient myogenic mouse cell line. Exp Cell Res 318:127–135.

Illa I, Serrano-Munuera C, Gallardo E, Lasa A, Rojas-García R, Palmer J, Gallano P, Baiget M, Matsuda C, Brown RH (2001) Distal anterior compartment myopathy: a dysferlin mutation causing a new muscular dystrophy phenotype. Ann Neurol 49:130–134.

Illarioshkin SN, Ivanova-Smolenskaya IA, Greenberg CR, Nylen E, Sukhorukov VS, Poleshchuk VV, Markova ED, Wrogemann K (2000) Identical dysferlin mutation in limb-girdle muscular dystrophy type 2B and distal myopathy. Neurology 55:1931–1933.

Inagaki K, Lewis SM, Wu X, Ma C, Munroe DJ, Fuess S, Storm TA, Kay MA, Nakai H (2007) DNA palindromes with a modest arm length of greater, similar 20 base pairs are a significant target for recombinant adeno-associated virus vector integration in the liver, muscles, and heart in mice. J Virol 81:11290–11303.

Jaiswal JK, Marlow G, Summerill G, Mahjneh I, Mueller S, Hill M, Miyake K, Haase H, Anderson LVB, Richard I, Kiuru-Enari S, McNeil PL, Simon SM, Bashir R (2007) Patients with a non-dysferlin Miyoshi myopathy have a novel membrane repair defect. Traffic 8:77–88.

Kashima T, Manley JL (2003) A negative element in SMN2 exon 7 inhibits splicing in spinal muscular atrophy. Nat Genet 34:460–463.

Kashima T, Rao N, David CJ, Manley JL (2007) hnRNP A1 functions with specificity in repression of SMN2 exon 7 splicing. Hum Mol Genet 16:3149–3159.

Kent OA, MacMillan AM (2002) Early organization of pre-mRNA during spliceosome assembly. Nat Struct Biol 9:576–581.

Kikumori T, Cote GJ, Gagel RF (2001) Promiscuity of pre-mRNA spliceosome-mediated trans splicing: a problem for gene therapy? Hum Gene Ther 12:1429–1441.

Klinge L, Dean AF, Kress W, Dixon P, Charlton R, Müller JS, Anderson LV, Straub V, Barresi R, Lochmüller H, Bushby K (2008) Late onset in dysferlinopathy widens the clinical spectrum. Neuromuscul Disord 18:288–290.

114

Klinge L, Harris J, Sewry C, Charlton R, Anderson L, Laval S, Chiu YH, Hornsey M, Straub V, Barresi R, Lochmüller H, Bushby K (2010) Dysferlin associates with the developing T-tubule system in rodent and human skeletal muscle. Muscle Nerve 41:166–173.

Klinge L, Laval S, Keers S, Haldane F, Straub V, Barresi R, Bushby K (2007) From T-tubule to sarcolemma: damage-induced dysferlin translocation in early myogenesis. FASEB J 21:1768–1776.

Koenig M, Hoffman EP, Bertelson CJ, Monaco AP, Feener C, Kunkel LM (1987) Complete cloning of the Duchenne muscular dystrophy (DMD) cDNA and preliminary genomic organization of the DMD gene in normal and affected individuals. Cell 50:509–517.

Konarska MM, Padgett RA, Sharp PA (1985) Trans splicing of mRNA precursors in vitro. Cell 42:165–171.

Kotin RM, Siniscalco M, Samulski RJ, Zhu XD, Hunter L, Laughlin CA, McLaughlin S, Muzyczka N, Rocchi M, Berns KI (1990) Site-specific integration by adeno-associated virus. Proc Natl Acad Sci U S A 87:2211–2215.

Krahn M, Béroud C, Labelle V, Nguyen K, Bernard R, Bassez G, Figarella-Branger D, Fernandez C, Bouvenot J, Richard I, Ollagnon-Roman E, Bevilacqua JA, Salvo E, Attarian S, Chapon F, Pellissier JF, Pouget J, Hammouda EH, Laforêt P, Urtizberea JA, Eymard B, Leturcq F, Lévy N (2009) Analysis of the DYSF mutational spectrum in a large cohort of patients. Hum Mutat 30:E345–E375.

Krahn M, Labelle V, Borges A, Bartoli M, Lévy N (2010a) Exclusion of mutations in the dysferlin alternative exons 1 of DYSF-v1, 5a, and 40a in a cohort of 26 patients. Genet Test Mol Biomarkers 14:153–154.

Krahn M, Wein N, Bartoli M, Lostal W, Courrier S, Bourg-Alibert N, Nguyen K, Vial C, Streichenberger N, Labelle V, DePetris D, Pécheux C, Leturcq F, Cau P, Richard I, Lévy N (2010b) A naturally occurring human minidysferlin protein repairs sarcolemmal lesions in a mouse model of dysferlinopathy. Sci Transl Med 2:50ra69.

Kuru S, Yasuma F, Wakayama T, Kimura S, Konagaya M, Aoki M, Tanabe M, Takahashi T (2004) [A patient with limb girdle muscular dystrophy type 2B (LGMD2B) manifesting cardiomyopathy]. Rinsho Shinkeigaku 44:375–378.

Lasda EL, Blumenthal T (2011) Trans-splicing 2:417–434.

Le Hir M, Goyenvalle A, Peccate C, Précigout G, Davies KE, Voit T, Garcia L, Lorain S (2013) AAV genome loss from dystrophic mouse muscles during AAV-U7 snRNA-mediated exon-skipping therapy. Mol Ther 21:1551–1558.

Lefebvre S, Bürglen L, Reboullet S, Clermont O, Burlet P, Viollet L, Benichou B, Cruaud C, Millasseau P, Zeviani M (1995) Identification and characterization of a spinal muscular atrophy-determining gene. Cell 80:155–165.

BIBLIOGRAPHY

Lek A, Evesson FJ, Lemckert FA, Redpath GMI, Lueders AK, Turnbull L, Whitchurch CB, North KN, Cooper ST (2013) Calpains, cleaved mini-dysferlinC72, and L-type channels underpin calcium-dependent muscle membrane repair. J Neurosci 33:5085–5094.

Lek A, Lek M, North KN, Cooper ST (2010) Phylogenetic analysis of ferlin genes reveals ancient eukaryotic origins 10:–.

Lennon NJ, Kho A, Bacskai BJ, Perlmutter SL, Hyman BT, Brown RH Jr (2003) Dysferlin interacts with annexins A1 and A2 and mediates sarcolemmal wound-healing. J Biol Chem 278:50466–50473.

Lerner MR, Steitz JA (1979) Antibodies to small nuclear RNAs complexed with proteins are produced by patients with systemic lupus erythematosus. Proc Natl Acad Sci U S A 76:5495–5499.

Liu J, Aoki M, Illa I, Wu C, Fardeau M, Angelini C, Serrano C, Urtizberea JA, Hentati F, Hamida MB, Bohlega S, Culper EJ, Amato AA, Bossie K, Oeltjen J, Bejaoui K, McKenna-Yasek D, Hosler BA, Schurr E, Arahata K, de Jong PJ, Brown R Jr (1998) Dysferlin, a novel skeletal muscle gene, is mutated in Miyoshi myopathy and limb girdle muscular dystrophy. Nat Genet 20:31–36.

Liu X, Jiang Q, Mansfield SG, Puttaraju M, Zhang Y, Zhou W, Cohn JA, Garcia-Blanco MA, Mitchell LG, Engelhardt JF (2002) Partial correction of endogenous DeltaF508 CFTR in human cystic fibrosis airway epithelia by spliceosome-mediated RNA trans-splicing 20:47–52.

Liu X, Luo M, Zhang LN, Yan Z, Zak R, Ding W, Mansfield SG, Mitchell LG, Engelhardt JF (2005) Spliceosome-mediated RNA trans-splicing with recombinant adeno-associated virus partially restores cystic fibrosis transmembrane conductance regulator function to polarized human cystic fibrosis airway epithelial cells 16:1116–1123.

Lo HP, Cooper ST, Evesson FJ, Seto JT, Chiotis M, Tay V, Compton AG, Cairns AG, Corbett A, MacArthur DG, Yang N, Reardon K, North KN (2008) Limb-girdle muscular dystrophy: diagnostic evaluation, frequency and clues to pathogenesis. Neuromuscul Disord 18:34–44.

Lorain S, Gross DA, Goyenvalle A, Danos O, Davoust J, Garcia L (2008) Transient immunomodulation allows repeated injections of AAV1 and correction of muscular dystrophy in multiple muscles 16:541–547.

Lorain S, Peccate C, Le Hir M, Garcia L (2010) Exon exchange approach to repair Duchenne dystrophin transcripts. PLoS One 5:e10894.

Lorain S, Peccate C, Le Hir M, Griffith G, Philippi S, Précigout G, Mamchaoui K, Jollet A, Voit T, Garcia L (2013) Dystrophin rescue by trans-splicing: a strategy for DMD genotypes not eligible for exon skipping approaches. Nucleic Acids Res 41:8391–8402.

Lorusso A, Covino C, Priori G, Bachi A, Meldolesi J, Chieregatti E (2006) Annexin2 coating the surface of enlargeosomes is needed for their regulated exocytosis. EMBO J 25:5443–5456.

Lostal W, Bartoli M, Bourg N, Roudaut C, BentaÃ¯b A, Miyake K, Guerchet N, Fougerousse F, McNeil P, Richard I (2010) Efficient recovery of dysferlin deficiency by dual adeno-associated vector-mediated gene transfer 19:1897–1907.

Lostal W, Bartoli M, Roudaut C, Bourg N, Krahn M, Pryadkina M, Borel P, Suel L, Roche JA, Stockholm D, Bloch RJ, Levy N, Bashir R, Richard I (2012) Lack of correlation between outcomes of membrane repair assay and correction of dystrophic changes in experimental therapeutic strategy in dysferlinopathy. PLoS One 7:e38036.

Lu QL, Mann CJ, Lou F, Bou-Gharios G, Morris GE, Xue Sa, Fletcher S, Partridge TA, Wilton SD (2003) Functional amounts of dystrophin produced by skipping the mutated exon in the mdx dystrophic mouse. Nat Med 9:1009–1014.

Mahjneh I, Passos-Bueno MR, Zatz M, Vainzof M, Marconi G, Nashef L, Bashir R, Bushby K (1996) The phenotype of chromosome 2p-linked limb-girdle muscular dystrophy. Neuromuscul Disord 6:483–490.

Mamchaoui K, Trollet C, Bigot A, Negroni E, Chaouch S, Wolff A, Kandalla PK, Marie S, Di Santo J, St Guily JL, et al. (2011) Immortalized pathological human myoblasts: towards a universal tool for the study of neuromuscular disorders. Skeletal muscle 1:1–11.

Mann CJ, Honeyman K, Cheng AJ, Ly T, Lloyd F, Fletcher S, Morgan JE, Partridge TA, Wilton SD (2001) Antisense-induced exon skipping and synthesis of dystrophin in the mdx mouse. Proc Natl Acad Sci U S A 98:42–47.

Mansfield SG, Clark RH, Puttaraju M, Kole J, Cohn JA, Mitchell LG, Garcia-Blanco MA (2003) 5' exon replacement and repair by spliceosome-mediated RNA trans-splicing 9:1290–1297.

Mansfield SG, Kole J, Puttaraju M, Yang CC, Garcia-Blanco MA, Cohn JA, Mitchell LG (2000) Repair of CFTR mRNA by spliceosome-mediated RNA trans-splicing 7:1885–1895.

Marg A, Schoewel V, Timmel T, Schulze A, Shah C, Daumke O, Spuler S (2012) Sarcolemmal repair is a slow process and includes EHD2. Traffic 13:1286–1294.

Matoulkova E, Michalova E, Vojtesek B, Hrstka R (2012) The role of the 3' untranslated region in post-transcriptional regulation of protein expression in mammalian cells. RNA Biol 9:563–576.

Matsuda C, Hayashi YK, Ogawa M, Aoki M, Murayama K, Nishino I, Nonaka I, Arahata K, Brown J R H (2001) The sarcolemmal proteins dysferlin and caveolin-3 interact in skeletal muscle 10:1761–1766.

Matsuda C, Miyake K, Kameyama K, Keduka E, Takeshima H, Imamura T, Araki N, Nishino I, Hayashi Y (2012) The C2A domain in dysferlin is important for association with MG53 (TRIM72). PLoS Curr 4:e5035add8caff4.

McLaughlin SK, Collis P, Hermonat PL, Muzyczka N (1988) Adeno-associated virus general transduction vectors: analysis of proviral structures. J Virol 62:1963–1973.

BIBLIOGRAPHY

McNeil AK, Rescher U, Gerke V, McNeil PL (2006) Requirement for annexin A1 in plasma membrane repair. J Biol Chem 281:35202–35207.

McNeil PL, Miyake K, Vogel SS (2003) The endomembrane requirement for cell surface repair. Proc Natl Acad Sci U S A 100:4592–4597.

McNeil PL, Steinhardt RA (2003) Plasma membrane disruption: repair, prevention, adaptation. Annu Rev Cell Dev Biol 19:697–731.

Mellgren RL, Miyake K, Kramerova I, Spencer MJ, Bourg N, Bartoli M, Richard I, Greer PA, McNeil PL (2009) Calcium-dependent plasma membrane repair requires m- or mu-calpain, but not calpain-3, the proteasome, or caspases. Biochim Biophys Acta 1793:1886–1893.

Minetti C, Sotgia F, Bruno C, Scartezzini P, Broda P, Bado M, Masetti E, Mazzocco M, Egeo A, Donati MA, Volonte D, Galbiati F, Cordone G, Bricarelli FD, Lisanti MP, Zara F (1998) Mutations in the caveolin-3 gene cause autosomal dominant limb-girdle muscular dystrophy. Nat Genet 18:365–368.

Miyoshi K, Kawai H, Iwasa M, Kusaka K, Nishino H (1986) Autosomal recessive distal muscular dystrophy as a new type of progressive muscular dystrophy. Seventeen cases in eight families including an autopsied case. Brain 109 (Pt 1):31–54.

Monani UR, Sendtner M, Coovert DD, Parsons DW, Andreassi C, Le TT, Jablonka S, Schrank B, Rossoll W, Rossol W, Prior TW, Morris GE, Burghes AH (2000) The human centromeric survival motor neuron gene (SMN2) rescues embryonic lethality in SMN(-/-) mice and results in a mouse with spinal muscular atrophy. Hum Mol Genet 9:333–339.

Monjaret F, Bourg N, Suel L, Roudaut C, Le Roy F, Richard I, Charton K (2014) Cis-splicing and translation of the pre-trans-splicing molecule combine with efficiency in spliceosome-mediated RNA trans-splicing. Mol Ther 22:1176–1187.

Mount SM, Pettersson I, Hinterberger M, Karmas A, Steitz JA (1983) The U1 small nuclear RNA-protein complex selectively binds a 5' splice site in vitro. Cell 33:509–518.

Mourkioti F, Kustan J, Kraft P, Day JW, Zhao MM, Kost-Alimova M, Protopopov A, DePinho RA, Bernstein D, Meeker AK, Blau HM (2013) Role of telomere dysfunction in cardiac failure in Duchenne muscular dystrophy. Nat Cell Biol 15:895–904.

Muzyczka N (1992) Use of adeno-associated virus as a general transduction vector for mammalian cells. Curr Top Microbiol Immunol 158:97–129.

Nagaraju K, Rawat R, Veszelovszky E, Thapliyal R, Kesari A, Sparks S, Raben N, Plotz P, Hoffman EP (2008) Dysferlin deficiency enhances monocyte phagocytosis: a model for the inflammatory onset of limb-girdle muscular dystrophy 2B. Am J Pathol 172:774–785.

Nakai K, Sakamoto H (1994) Construction of a novel database containing aberrant splicing mutations of mammalian genes. Gene 141:171–177.

118

Nguyen K, Bassez G, Krahn M, Bernard R, Laforêt P, Labelle V, Urtizberea JA, Figarella-Branger D, Romero N, Attarian S, Leturcq F, Pouget J, Lévy N, Eymard B (2007) Phenotypic study in 40 patients with dysferlin gene mutations: high frequency of atypical phenotypes. Arch Neurol 64:1176–1182.

Okahashi S, Ogawa G, Suzuki M, Ogata K, Nishino I, Kawai M (2008) Asymptomatic sporadic dysferlinopathy presenting with elevation of serum creatine kinase. Typical distribution of muscle involvement shown by MRI but not by CT. Intern Med 47:305–307.

Padgett RA, Konarska MM, Grabowski PJ, Hardy SF, Sharp PA (1984) Lariat RNA's as intermediates and products in the splicing of messenger RNA precursors. Science 225:898–903.

Park JI, Venteicher AS, Hong JY, Choi J, Jun S, Shkreli M, Chang W, Meng Z, Cheung P, Ji H, McLaughlin M, Veenstra TD, Nusse R, McCrea PD, Artandi SE (2009) Telomerase modulates Wnt signalling by association with target gene chromatin. Nature 460:66–72.

Parker R, Siliciano PG, Guthrie C (1987) Recognition of the TACTAAC box during mRNA splicing in yeast involves base pairing to the U2-like snRNA. Cell 49:229–239.

Patel AA, Steitz JA (2003) Splicing double: insights from the second spliceosome. Nat Rev Mol Cell Biol 4:960–970.

Penaud-Budloo M, Le Guiner C, Nowrouzi A, Toromanoff A, Chérel Y, Chenuaud P, Schmidt M, von Kalle C, Rolling F, Moullier P, Snyder RO (2008) Adeno-associated virus vector genomes persist as episomal chromatin in primate muscle. J Virol 82:7875–7885.

Petrof BJ, Shrager JB, Stedman HH, Kelly AM, Sweeney HL (1993) Dystrophin protects the sarcolemma from stresses developed during muscle contraction. Proc Natl Acad Sci U S A 90:3710–3714.

Philippi S, Bigot A, Marg A, Mouly V, Spuler S, Zacharias U (2012) Dysferlin-deficient immortalized human myoblasts and myotubes as a useful tool to study dysferlinopathy. PLoS currents 4.

Piccolo F, Moore SA, Ford GC, Campbell KP (2000) Intracellular accumulation and reduced sarcolemmal expression of dysferlin in limb–girdle muscular dystrophies. Ann Neurol 48:902–912.

Posey J Avery D, Pytel P, Gardikiotes K, Demonbreun AR, Rainey M, George M, Band H, McNally EM (2011) Endocytic recycling proteins EHD1 and EHD2 interact with fer-1-like-5 (Fer1L5) and mediate myoblast fusion 286:7379–7388.

Pramono ZAD, Lai PS, Tan CL, Takeda S, Yee WC (2006) Identification and characterization of a novel human dysferlin transcript: dysferlin v1. Hum Genet 120:410–419.

BIBLIOGRAPHY

Pramono ZAD, Tan CL, Seah IAL, See JSL, Kam SY, Lai PS, Yee WC (2009) Identification and characterisation of human dysferlin transcript variants: implications for dysferlin mutational screening and isoforms. Hum Genet 125:413–420.

Preußer C, Jaé N, Bindereif A (2012) mRNA splicing in trypanosomes. Int J Med Microbiol 302:221–224.

Proudfoot NJ (2011) Ending the message: poly(A) signals then and now. Genes Dev 25:1770–1782.

Puttaraju M, Jamison SF, Mansfield SG, Garcia-Blanco MA, Mitchell LG (1999) Spliceosome-mediated RNA trans-splicing as a tool for gene therapy 17:246–252.

Rabinowitz JE, Rolling F, Li C, Conrath H, Xiao W, Xiao X, Samulski RJ (2002) Cross-packaging of a single adeno-associated virus (AAV) type 2 vector genome into multiple AAV serotypes enables transduction with broad specificity. J Virol 76:791–801.

Rahimov F, Kunkel LM (2013) The cell biology of disease: cellular and molecular mechanisms underlying muscular dystrophy. J Cell Biol 201:499–510.

Ramirez RD, Herbert BS, Vaughan MB, Zou Y, Gandia K, Morales CP, Wright WE, Shay JW (2003) Bypass of telomere-dependent replicative senescence (M1) upon overexpression of Cdk4 in normal human epithelial cells. Oncogene 22:433–444.

Reed R (1996) Initial splice-site recognition and pairing during pre-mRNA splicing. Curr Opin Genet Dev 6:215–220.

Renneberg D, Bouliong E, Reber U, Schümperli D, Leumann CJ (2002) Antisense properties of tricyclo-DNA. Nucleic Acids Res 30:2751–2757.

Renneberg D, Leumann CJ (2002a) Watson-Crick base-pairing properties of tricyclo-DNA. Journal of the American Chemical Society 124:5993–6002.

Renneberg D, Leumann CJ (2002b) Watson-Crick base-pairing properties of tricyclo-DNA. J Am Chem Soc 124:5993–6002.

Richard I, Broux O, Allamand V, Fougerousse F, Chiannilkulchai N, Bourg N, Brenguier L, Devaud C, Pasturaud P, Roudaut C (1995) Mutations in the proteolytic enzyme calpain 3 cause limb-girdle muscular dystrophy type 2A. Cell 81:27–40.

Rivera VM, Gao Gp, Grant RL, Schnell MA, Zoltick PW, Rozamus LW, Clackson T, Wilson JM (2005) Long-term pharmacologically regulated expression of erythropoietin in primates following AAV-mediated gene transfer. Blood 105:1424–1430.

Riviere C, Danos O, Douar A (2006) Long-term expression and repeated administration of AAV type 1, 2 and 5 vectors in skeletal muscle of immunocompetent adult mice. Gene therapy 13:1300–1308.

Rodriguez-Martin T, Anthony K, Garcia-Blanco MA, Mansfield SG, Anderton BH, Gallo JM (2009) Correction of tau mis-splicing caused by FTDP-17 MAPT mutations by spliceosome-mediated RNA trans-splicing 18:3266–3273.

Rodriguez-Martin T, Garcia-Blanco MA, Mansfield SG, Grover AC, Hutton M, Yu Q, Zhou J, Anderton BH, Gallo JM (2005) Reprogramming of tau alternative splicing by spliceosome-mediated RNA trans-splicing: implications for tauopathies 102:15659–15664.

Roostalu U, Strähle U (2012) In vivo imaging of molecular interactions at damaged sarcolemma. Dev Cell 22:515–529.

Roux I, Safieddine S, Nouvian R, Grati M, Simmler MC, Bahloul A, Perfettini I, Le Gall M, Rostaing P, Hamard G, Triller A, Avan P, Moser T, Petit C (2006) Otoferlin, defective in a human deafness form, is essential for exocytosis at the auditory ribbon synapse. Cell 127:277–289.

Rutledge EA, Halbert CL, Russell DW (1998) Infectious clones and vectors derived from adeno-associated virus (AAV) serotypes other than AAV type 2. J Virol 72:309–319.

Sacco A, Mourkioti F, Tran R, Choi J, Llewellyn M, Kraft P, Shkreli M, Delp S, Pomerantz JH, Artandi SE, Blau HM (2010) Short telomeres and stem cell exhaustion model Duchenne muscular dystrophy in mdx/mTR mice. Cell 143:1059–1071.

Samulski RJ, Zhu X, Xiao X, Brook JD, Housman DE, Epstein N, Hunter LA (1991) Targeted integration of adeno-associated virus (AAV) into human chromosome 19. EMBO J 10:3941–3950.

Schmidt M, Voutetakis A, Afione S, Zheng C, Mandikian D, Chiorini JA (2008) Adeno-associated virus type 12 (AAV12): a novel AAV serotype with sialic acid- and heparan sulfate proteoglycan-independent transduction activity. J Virol 82:1399–1406.

Schmittgen TD, Livak KJ (2008) Analyzing real-time PCR data by the comparative CT method. Nature protocols 3:1101–1108.

Schnepp BC, Clark KR, Klemanski DL, Pacak CA, Johnson PR (2003) Genetic fate of recombinant adeno-associated virus vector genomes in muscle. J Virol 77:3495–3504.

Schoewel V, Marg A, Kunz S, Overkamp T, Carrazedo RS, Zacharias U, Daniel PT, Spuler S (2012) Dysferlin-peptides reallocate mutated dysferlin thereby restoring function. PLoS One 7:e49603.

Schultz BR, Chamberlain JS (2008) Recombinant adeno-associated virus transduction and integration. Mol Ther 16:1189–1199.

Schwartz SH, Silva J, Burstein D, Pupko T, Eyras E, Ast G (2008) Large-scale comparative analysis of splicing signals and their corresponding splicing factors in eukaryotes. Genome Res 18:88–103.

BIBLIOGRAPHY

Seisenberger G, Ried MU, Endress T, Büning H, Hallek M, Bräuchle C (2001) Real-time single-molecule imaging of the infection pathway of an adeno-associated virus. Science 294:1929–1932.

Selcen D, Stilling G, Engel AG (2001) The earliest pathologic alterations in dysferlinopathy. Neurology 56:1472–1481.

Shimizu A, Honjo T (1993) Synthesis and regulation of trans-mRNA encoding the immunoglobulin epsilon heavy chain. FASEB J 7:149–154.

Singh RK, Cooper TA (2012) Pre-mRNA splicing in disease and therapeutics 18:472–482.

Sinnreich M, Therrien C, Karpati G (2006) Lariat branch point mutation in the dysferlin gene with mild limb-girdle muscular dystrophy. Neurology 66:1114–1116.

Smith CW, Valcárcel J (2000) Alternative pre-mRNA splicing: the logic of combinatorial control. Trends Biochem Sci 25:381–388.

Smith LL, Coller HA, Roberts JM (2003) Telomerase modulates expression of growth-controlling genes and enhances cell proliferation. Nat Cell Biol 5:474–479.

Smith PJ, Zhang C, Wang J, Chew SL, Zhang MQ, Krainer AR (2006) An increased specificity score matrix for the prediction of SF2/ASF-specific exonic splicing enhancers. Human molecular genetics 15:2490–2508.

Snyder RO, Spratt SK, Lagarde C, Bohl D, Kaspar B, Sloan B, Cohen LK, Danos O (1997) Efficient and stable adeno-associated virus-mediated transduction in the skeletal muscle of adult immunocompetent mice. Human gene therapy 8:1891–1900.

Solnick D (1985) Trans splicing of mRNA precursors. Cell 42:157–164.

Spuler S, Engel AG (1998) Unexpected sarcolemmal complement membrane attack complex deposits on nonnecrotic muscle fibers in muscular dystrophies. Neurology 50:41–46.

Stadler G, Chen JC, Wagner K, Robin JD, Shay JW, Emerson CP Jr, Wright WE (2011) Establishment of clonal myogenic cell lines from severely affected dystrophic muscles - CDK4 maintains the myogenic population. Skelet Muscle 1:12.

Staknis D, Reed R (1994) SR proteins promote the first specific recognition of Pre-mRNA and are present together with the U1 small nuclear ribonucleoprotein particle in a general splicing enhancer complex. Mol Cell Biol 14:7670–7682.

Steffens R, Leumann C (1997) Nucleid-acid analogs with constraint conformational flexibility in the sugar-phosphate backbone 'Tricyclo-DNA'. PART 1. Preparation of (5'R, 6'R)-2'-deoxy-3', 5'-ethano-5', 6'-methane-beta-D-ribofuranosylthymine and -adenine, and the corresponding phosphoramidites for oligonucleotide synthesis. Helvetica chimica acta 80:2426–2439.

Sterner DA, Berget SM (1993) In vivo recognition of a vertebrate mini-exon as an exon-intron-exon unit. Mol Cell Biol 13:2677–2687.

Stewart SA, Hahn WC, O'Connor BF, Banner EN, Lundberg AS, Modha P, Mizuno H, Brooks MW, Fleming M, Zimonjic DB, Popescu NC, Weinberg RA (2002) Telomerase contributes to tumorigenesis by a telomere length-independent mechanism. Proc Natl Acad Sci U S A 99:12606–12611.

Südhof TC, Rizo J (1996) Synaptotagmins: C2-domain proteins that regulate membrane traffic. Neuron 17:379–388.

Takahashi T, Aoki M, Tateyama M, Kondo E, Mizuno T, Onodera Y, Takano R, Kawai H, Kamakura K, Mochizuki H, Shizuka-Ikeda M, Nakagawa M, Yoshida Y, Akanuma J, Hoshino K, Saito H, Nishizawa M, Kato S, Saito K, Miyachi T, Yamashita H, Kawai M, Matsumura T, Kuzuhara S, Ibi T, Sahashi K, Nakai H, Kohnosu T, Nonaka I, Arahata K, Brown R Jr, Saito H, Itoyama Y (2003) Dysferlin mutations in Japanese Miyoshi myopathy: relationship to phenotype. Neurology 60:1799–1804.

Tange TO, Damgaard CK, Guth S, Valcárcel J, Kjems J (2001) The hnRNP A1 protein regulates HIV-1 tat splicing via a novel intron silencer element. EMBO J 20:5748–5758.

Tarköy M, Bolli M, Schweizer B, Leumann C (1993) Nucleic-Acid Analogues with Constraint Conformational Flexibility in the Sugar-Phosphate Backbone (Bicyclo-DNA). Part 1. Preparation of (3S, 5 R)-2 -Deoxy-3 , 5 -ethano-$\alpha\beta$-D-ribonucleosides (Bicyclonucleosides). Helvetica chimica acta 76:481–510.

Tarn WY, Steitz JA (1997) Pre-mRNA splicing: the discovery of a new spliceosome doubles the challenge. Trends Biochem Sci 22:132–137.

Therrien C, Dodig D, Karpati G, Sinnreich M (2006) Mutation impact on dysferlin inferred from database analysis and computer-based structural predictions. J Neurol Sci 250:71–78.

Tschudi C, Ullu E (1990) Destruction of U2, U4, or U6 small nuclear RNA blocks trans splicing in trypanosome cells. Cell 61:459–466.

Tsukahara T, Casciato C, Helfman DM (1994) Alternative splicing of beta-tropomyosin pre-mRNA: multiple cis-elements can contribute to the use of the 5'- and 3'-splice sites of the nonmuscle/smooth muscle exon 6. Nucleic Acids Res 22:2318–2325.

Vafiadaki E, Reis A, Keers S, Harrison R, Anderson LV, Raffelsberger T, Ivanova S, Hoger H, Bittner RE, Bushby K, Bashir R (2001) Cloning of the mouse dysferlin gene and genomic characterization of the SJL-Dysf mutation. Neuroreport 12:625–629.

Vandenberghe LH, Wang L, Somanathan S, Zhi Y, Figueredo J, Calcedo R, Sanmiguel J, Desai RA, Chen CS, Johnston J, Grant RL, Gao G, Wilson JM (2006) Heparin binding directs activation of T cells against adeno-associated virus serotype 2 capsid. Nat Med 12:967–971.

Vandré DD, Ackerman WE 4th, Kniss DA, Tewari AK, Mori M, Takizawa T, Robinson JM (2007) Dysferlin is expressed in human placenta but does not associate with caveolin. Biol Reprod 77:533–542.

Vasileva A, Jessberger R (2005) Precise hit: adeno-associated virus in gene targeting. Nat Rev Microbiol 3:837–847.

Vellard M, Sureau A, Soret J, Martinerie C, Perbal B (1992) A potential splicing factor is encoded by the opposite strand of the trans-spliced c-myb exon. Proc Natl Acad Sci U S A 89:2511–2515.

von Maltzahn J, Chang NC, Bentzinger CF, Rudnicki MA (2012) Wnt signaling in myogenesis. Trends Cell Biol 22:602–609.

Wahl MC, Will CL, Lührmann R (2009) The spliceosome: design principles of a dynamic RNP machine. Cell 136:701–718.

Wang Z, Tapscott SJ, Chamberlain JS, Storb R (2011) Immunity and AAV-Mediated Gene Therapy for Muscular Dystrophies in Large Animal Models and Human Trials. Front Microbiol 2:201.

Wang Z, Zhu T, Qiao C, Zhou L, Wang B, Zhang J, Chen C, Li J, Xiao X (2005) Adeno-associated virus serotype 8 efficiently delivers genes to muscle and heart. Nat Biotechnol 23:321–328.

Weiler T, Bashir R, Anderson LV, Davison K, Moss JA, Britton S, Nylen E, Keers S, Vafiadaki E, Greenberg CR, Bushby CR, Wrogemann K (1999) Identical mutation in patients with limb girdle muscular dystrophy type 2B or Miyoshi myopathy suggests a role for modifier gene(s). Hum Mol Genet 8:871–877.

Wein N, Avril A, Bartoli M, Beley C, Chaouch S, Laforet P, Behin A, Butler-Browne G, Mouly V, Krahn M, Garcia L, Levy N (2010) Efficient bypass of mutations in dysferlin deficient patient cells by antisense-induced exon skipping 31:136–142.

Wenzel K, Carl M, Perrot A, Zabojszcza J, Assadi M, Ebeling M, Geier C, Robinson PN, Kress W, Osterziel KJ, et al. (2006) Novel sequence variants in dysferlin-deficient muscular dystrophy leading to mRNA decay and possible C2-domain misfolding. Human mutation 27:599–600.

Wenzel K, Geier C, Qadri F, Hubner N, Schulz H, Erdmann B, Gross V, Bauer D, Dechend R, Dietz R, Osterziel KJ, Spuler S, Ozcelik C (2007) Dysfunction of dysferlin-deficient hearts. J Mol Med (Berl) 85:1203–1214.

Wenzel K, Zabojszcza J, Carl M, Taubert S, Lass A, Harris CL, Ho M, Schulz H, Hummel O, Hubner N, Osterziel KJ, Spuler S (2005) Increased susceptibility to complement attack due to down-regulation of decay-accelerating factor/CD55 in dysferlin-deficient muscular dystrophy. J Immunol 175:6219–6225.

Wolf JR, Hirschhorn RR, Steiner SM (1992) Growth factor responsiveness: role of MyoD and myogenin. Exp Cell Res 202:105–112.

Worton R (1995) Muscular dystrophies: diseases of the dystrophin-glycoprotein complex. Science 270:755–756.

Wu B, Benrashid E, Lu P, Cloer C, Zillmer A, Shaban M, Lu QL (2011) Targeted skipping of human dystrophin exons in transgenic mouse model systemically for antisense drug development. PLoS One 6:e19906.

Wu S, Romfo CM, Nilsen TW, Green MR (1999) Functional recognition of the 3' splice site AG by the splicing factor U2AF35. Nature 402:832–835.

Wu Z, Miller E, Agbandje-McKenna M, Samulski RJ (2006) Alpha2,3 and alpha2,6 N-linked sialic acids facilitate efficient binding and transduction by adeno-associated virus types 1 and 6. J Virol 80:9093–9103.

Xiao W, Chirmule N, Berta SC, McCullough B, Gao G, Wilson JM (1999a) Gene therapy vectors based on adeno-associated virus type 1. J Virol 73:3994–4003.

Xiao W, Chirmule N, Berta SC, McCullough B, Gao G, Wilson JM (1999b) Gene therapy vectors based on adeno-associated virus type 1. J Virol 73:3994–4003.

Xiao X, Li J, Samulski RJ (1998) Production of high-titer recombinant adeno-associated virus vectors in the absence of helper adenovirus. Journal of virology 72:2224–2232.

Yasunaga S, Grati M, Cohen-Salmon M, El-Amraoui A, Mustapha M, Salem N, El-Zir E, Loiselet J, Petit C (1999) A mutation in OTOF, encoding otoferlin, a FER-1-like protein, causes DFNB9, a nonsyndromic form of deafness. Nat Genet 21:363–369.

Yeo G, Burge CB (2004) Maximum entropy modeling of short sequence motifs with applications to RNA splicing signals. Journal of Computational Biology 11:377–394.

Zamore PD, Patton JG, Green MR (1992) Cloning and domain structure of the mammalian splicing factor U2AF. Nature 355:609–614.

Zhu CH, Mouly V, Cooper RN, Mamchaoui K, Bigot A, Shay JW, Di Santo JP, Butler-Browne GS, Wright WE (2007) Cellular senescence in human myoblasts is overcome by human telomerase reverse transcriptase and cyclin-dependent kinase 4: consequences in aging muscle and therapeutic strategies for muscular dystrophies. Aging cell 6:515–523.

Zhuang YA, Goldstein AM, Weiner AM (1989) UACUAAC is the preferred branch site for mammalian mRNA splicing. Proc Natl Acad Sci U S A 86:2752–2756.

Zielenski J, Tsui L (1995) Cystic fibrosis: genotypic and phenotypic variations. Annual review of genetics 29:777–807.

Zufferey R, Dull T, Mandel RJ, Bukovsky A, Quiroz D, Naldini L, Trono D (1998) Self-inactivating lentivirus vector for safe and efficient in vivo gene delivery. Journal of virology 72:9873–9880.